Numerical investigation of the robustness of extended stiffened end-plate bolted beam-to-column joints subjected to column removal

Candidate Name: Joseph Romeo M. Diño

Supervisor: Prof. Ph.D. Raffaele Landolfo, Assist. Prof. Ph.D. Mario D'Aniello
Co-Supervisor: Eng. Roberto Tartaglia

University of Naples Federico II

Thesis submitted in partial fulfilment of the requirements For the Degree of Master of Science in Construction of Steel and Composite Structures European Erasmus Mundus Masters Course Sustainable Construction Under Natural Hazards and Catastrophic Events

Naples, ITALY
Date: 14th February 2017

Numerical investigation of the robustness of extended stiffened end-plate bolted beam-to-column joints subjected to column removal

Author: Joseph Romeo M. Diño

Supervisor: Prof. Ph.D. Raffaele Landolfo, Assist. Prof. Ph.D. Mario D'Aniello
Co-Supervisor: Eng. Roberto Tartaglia

University of Naples Federico II

STATEMENT OF THESIS APPROVAL

This thesis prepared by **Joseph Romeo M. Diño** entitled **'Numerical investigation of the robustness of extended stiffened end-plate bolted beam-to-column joints subjected to column removal'** is approved in partial fulfillment of the requirements for the degree of Master of Science by the following faculty members served as the supervisory committee chair and members.

_____,Chair _____
Date Approved

_____,Member _____
Date Approved

_____,Member _____
Date Approved

Student's signature _____

Date of Submission _____

ACKNOWLEDGEMENT

While this dissertation is officially under my name, I can never take the credit on my own, as a number of people contributed a lot for the completion of this work. I would like to express my gratitude to my adviser, Assistant Professor Ph.D. Mario D'ANIELLO, for the inputs – may it be technical or organizational – that he contributed in this thesis work. I am also deeply grateful to my co-adviser, Engr. Roberto TARTAGLIA, for his patience and guidance right from the start in learning ABAQUS, to the very critical parts of running my model, up to the end in extracting and interpreting the results. I am also grateful for Engr. Mariana ZIMBRU, who gave supplementary materials to accelerate my learning curve in ABAQUS.

I would also like to thank Professor Raffaele LANDOLFO for welcoming us in the Department of Structures for Engineering and Architecture with ease, allowing me and my colleagues to work and use the facility of the Department. Same appreciation is also given to the academic staff in the Department who offered help even on the littlest things for our adjustment in the University and in Naples itself.

Special thanks to Professor František WALD, Professor Luis Simões DA SILVA, Professor Raffaele LANDOLFO, and the rest of the coordinators involved in SUSCOS_M Program. All the professors who imparted their knowledge for every subject in this master's course, it is an honour for me to be part of your class. This is one great opportunity that I will forever be grateful of. Special mention to Miss Barbora Skálová and Miss Věra Klátová for their professionalism in providing administrative support and immediate help when we need it.

I would also like to acknowledge the European Commission – Education, Audiovisual and Culture Executive Agency (EACEA), since everything in this valuable experience will not be existent without the scholarship grant they gave me.

To my colleagues in the SUSCOS_M Batch 2015-2017, it is a pleasure of meeting every one of you. I will be always grateful to meet people from literally all over the world and to have an amazing experience of cultural diversity.

Lastly, I would like to honour my family for being an inspiration throughout this journey. Their moral support and motivation keeps me upbeat to pursue this master's program in spite the distance and time difference.

ABSTRACT

Emphasis on the study of robustness of structures have gained attention after the famous collapse of infrastructures over the years. After the 9/11 World Trade Center incident, a drastic increase on researches on progressive collapse and the role of catenary action have occurred, indicating the urgency of focusing the efforts of engineers on designing blast-resistant buildings. Aside from terror attacks, robustness of structures is deemed significant for designing structures against natural catastrophes. In this study, the joints are given focus in designing moment-resisting steel frames. It is the aim of this study to analyse the robustness of steel joints using a typology that was typically used for regions with high seismicity. Hence, the use of MRF and larger column sizes. This was done by simulating a local joint under sudden loss of the middle column in ABAQUS.

Nine (9) finite element models were done, using joint typologies for equal, full, and partial-strength joints, with three (3) different column sizes – HEB 340, HEB 500, and HEB 650. These typologies were taken from a study by [1] regarding the seismic design of extended stiffened end-plates. Hence, this is a continuity on the improvement of the typical joint used for seismic zones by focusing also on robustness, where post-earthquake accidents can happen. Numerical results were validated from previous experimental studies and found that the model is adequate.

Symmetry on the left and right part of the joint were evident on all models, confirming more valid outputs. Results show that for all examined joints arching effect develops before catenary action at small rotations under column loss. All nine models showed a trend that a more elaborate arching effect leads to a lesser catenary action. All ES3 models have greater compression forces at small displacements compared with their counterparts, and ended having lesser axial catenary load. Consequently, the full-strength joints, showing the least arching effect among the models, also performed well in terms of axial capacity at larger rotations. Moment capacity curves show a similar pattern for all models, only magnifying in strength as the column size is increased.

Plastic dissipation energy ratios showed expected results for all models, except for ES3-P. Equal-strength joints have approximately close contribution for the beam and the connection. Full-strength joints have way higher contribution from the beam than the rest of the components while partial-strength joints have more contribution on the plasticity of the connection than the beams. Convergence problems were encountered with ES3-P, which could have been the source of discrepancy on that part of the results.

The influence of the secondary beams on the joint performance under column loss scenario was also investigated by running separate models in ABAQUS where the secondary beams are deactivated. Results showed very little difference in the moment capacity between the models with and without the secondary beams. Further investigations were done by plotting the moment capacity of the secondary beams with the primary beams. It presented that the moment capacity of the secondary beams is almost negligible when compared with the primary beams. It is also found that the secondary beams have the same shear forces on the beam tip, the angular plates, and the secondary bolts. PEEQ values indicate high plasticity on the angular plates, disabling the component to transfer the loads to the secondary beams. This validated that the forces are not transferred on the secondary beam, leading to a negligible influence on the joint. Higher stiffness and strength of the connections must be done to investigate more on this matter.

It is recommended by the author for further studies to conduct a numerical study for pure bending only to determine if the capacity of the joint is indeed increasing when catenary action is in effect. A higher forced displacement at the middle column is also suggested since a 500-mm displacement does not cover rotations larger than 0.09 rad for some models. Lastly, the stiffness and strength of the connection to the secondary beams must be increased to be able to optimize the influence of secondary beams under column loss scenario.

TABLE OF CONTENTS

1. INTRODUCTION

1.1 Overview

Natural catastrophes, such as earthquakes, are one of the major causes of destruction and losses—especially in terms of costs and fatalities—when it comes to natural disasters. Various studies have been conducted to verify the performance of buildings and to further improve their efficiency against seismic events. However, one major aspect must also be focused on is the accidental loss of one part of a building (i.e. column, beam) after such a disaster.

Investigations about loss of a structural part of a building are not only useful for post-earthquake effects but also for general enhancement of a structure's robustness. Robustness assessment is of increasing interest in structural design. Aside from post-earthquake effects, the robustness of a structure is deemed significant due to the increase of terrorism over the past decades. A more robust structure will lead to less damage during damage from terror attacks, ensuring enhanced strength against progressive collapse.

Robustness, per **Eurocode EN 1991-1-7:2006** [2] is defined as the ability of a structure to withstand events like fire, explosions, impact or the consequences of human error, without being damaged to an extent disproportionate to the original cause. Hence, robustness is a specific factor that must be generally considered in designing buildings, since structures must have adequate robustness to resist localized failure from abnormal/accidental loads (e.g. fire, explosion, impact, collision, or a combination of loads) [3].

Figure 1.1 Ronan Point explosion [a] (left), World Trade Center aircraft attacks [b] (right)

Study on robustness gained an increasing interest after the gas explosion in the recently-opened Ronan Point building in England (Figure 1.1), way back 1968. The explosion caused a series of failures (hence, the term "progressive collapse"), destroying an entire corner of the building. More recently, the 9/11 aircraft

[a] The Daily Telegraph, 1968
[b] Spencer Platt/GettyImages, 2001

attacks triggered engineers from all over the world to conduct more thorough researches on the said topic. In fact, **El-Tawil** [4] compiled statistics of published studies over the years regarding progressive collapse as seen on Figure 1.2. The rate of published papers increased in a considerable amount succeeding the 9/11 historical event.

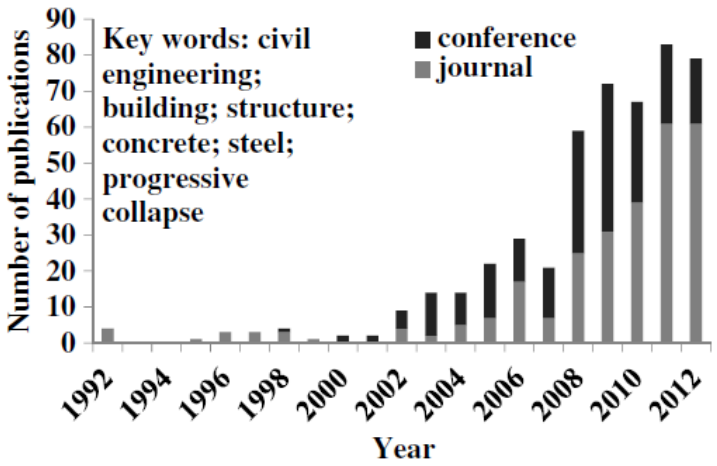

Figure 1.2. Statistics on the number of published studies on progressive collapse by El-Tawil et al [4]

1.2 Robustness – the concept of progressive collapse and catenary action

Blockley et al [5] indicated in their study that a robust structure should be attained by (a) preventing the action or reducing it to an acceptable probability, (b) protecting the building, and (c) reducing the building sensitivity to disproportionate collapse. Designers must be able to prove that removal of any structural building component must not generate complete collapse of the structure. Local damage must be controlled within the storeys above and below the part where the element is removed. This case has significant uncertainties in the problem formulation and appropriate assessment of its robustness must be accounted for.

Formisano et al [6] defined the concept of **progressive collapse** for structures which is usually the process that happens when a structure is not robust. It is of great interest in assessing robustness since removal of any element could lead to a progressive collapse. It is when the final failure state is excessively larger than the initial one that caused it. Simply put, **ASCE** [7] defined it as "the spread of an initial local failure from element to element resulting, eventually, in the collapse of an entire structure or a disproportionately large part of it." Thus, the "domino effect" scenario describes this phenomenon.

Development of **catenary action** plays a significant part as well in the robustness of structures. It ensures enough ductility and redistribution capability of the structure after sudden column removal situation. To demonstrate, it happens when a vertical load P is resisted by a tensile internal force T (Figure 1.3) after the beam experiences a deflection Δ.

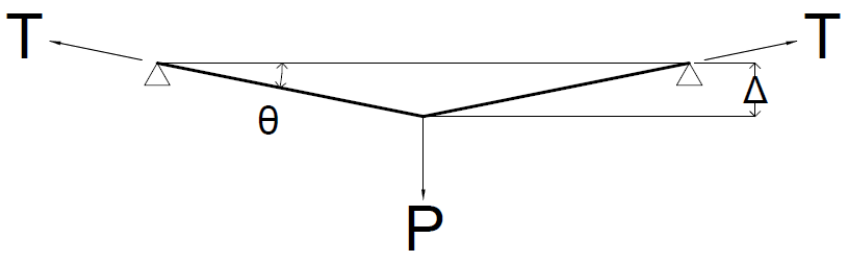

Figure 1.3. Catenary action

While the idea of catenary action is not new in general, it is of great interest in recent studies on designing infrastructures against blast and fire. It has two very interesting design implications which gives it a good potential against such scenarios described by **Yin and Wang** [8]:

1. When catenary action is in effect, the beam's resistance is not entirely limited by its material properties, but is related to its deflection. Hence, a beam with reduced material capacity (e.g. due to fire or blast attack) can still resist the load applied, merely by deflecting the beam.
2. Under situations when an axially restrained beam is experiencing temperature that is above its regular limit for pure flexural bending, it will always develop catenary actions.

From these reasons, one can conclude that taking advantage of catenary action is important in designing robust structures in terms of safety and cost optimization. It is evident in such cases that the bolts of the beam-column joint are critical in this state. They are exposed to huge amount of forces (e.g. axial forces, shear forces, and bending moment), which is caused by the secondary effects and catenary action that is growing into the structure.

Joints such as stiffened extended end plates are typically used in steel structures for connecting beams and columns. However, information on such joints subjected to column removal under catenary actions are not as comprehensive as seismic scenario. **Dinu et al** [3] mentioned in their study that design standards for robustness are rather generic and do not account specific cases (e.g. construction type, explosion from external factors). Hence, emphasis on their behaviour under this kind of action must be done on a more thorough approach.

1.2.1 Local failure: column loss and the role of connections

Robustness is a very broad topic due to the vast amount of cases that must be considered. A structure can be enhanced for robustness against explosion (that eventually can cause fire), seismic, impact, and even a combination of various causes. That is why it is also advantageous to consider the result of the action on local failure situations, rather than determining the load impact on the whole structure. For building, specifically, local failure is usually due to the extreme impairment of a structural member (say, the column or the beam). This study therefore focused on the case when a column is lost in the local part of a typical structure (rectangular, multi-storey) after a specific scenario (i.e. earthquake, blast).

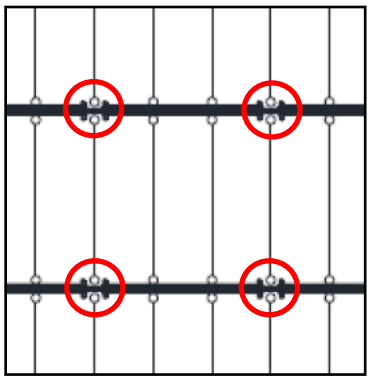

Figure 1.4. Middle column loss scenario in a structure

More precisely, the case in which a middle internal column (an example shown in Figure 1.4) was studied in this analysis. The catenary action was analysed, taking a significant look on the behaviour of the connections during this scenario. Depending on its strength, ductility, and stiffness, the load transfer could be successful, allowing the catenary action to mobilize.

A structure is then said to be robust if its structural integrity is not completely lost in such events. Considering the robustness of a structure, especially its connections, is also vital for testing and analysis in

an earthquake or terror attack scenario. Therefore, designing structures for robustness is of equal importance and conducting further studies on such matter is essential.

1.3 Objectives

The objectives of this study are relevant to the study conducted by **D'Aniello et al** [1]. However, instead of analysing an extended stiffened end plate's behaviour under seismic load, this study focuses on the behaviour of such joints under middle-column loss scenario. The study therefore aims to investigate the robustness of moment-resisting steel joints when the middle-column of a local internal connection is impaired. Specific typologies of the said joint are incorporated in the project as shown in Figure 1.5. The joint is further improved by reinforcing rib stiffeners on the endplate of the connection.

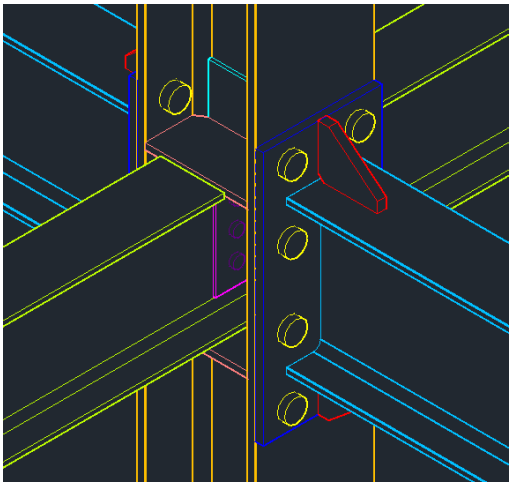

Figure 1.5. Typology of the extended local joint

This study started from the idea of further enhancing extended end plate connections since it is a common joint used for steel and composite structure. Moreover, studies on such typology regarding its seismic behaviour have been established already. Hence, it is reasonable to begin this study on the idea of **improving both the seismic and robust behaviour of these joints**. It is also the interest of this study to test deep columns (i.e. columns with larger cross-sectional heights) since several studies [9, 10, 11, 12]-[13], show that deep columns can tend to be more economical for regions with high seismicity. **Shen et al** [9] mentioned in their report that today's design engineers find it more economical for many projects to use columns deeper than W14 sections (356 mm height). More common in the US, there has been a strong economic incentive to use deep columns in Special Moment Frames (SMF) to meet storey drift requirements.

An investigation study of equal, partial, and full strength joints will be utilized in the project. Its results would help identify the differences from each typology, specifically in terms of its strength, stiffness, and ductility. The project could provide support in improving the present standards in the Eurocode especially for robustness design. The main objectives of the thesis are listed as follows:

1) To examine and identify previous studies and experiments relating to seismic behaviour and robustness analysis of steel joints.
2) To describe the typologies and parameters of the steel joint implemented in the study.
3) The validation of the finite element model (FE) against experimental results.
4) To generate FE models and run the analysis for robustness action.
5) To extract and interpret results from the FEA.
6) To provide sound investigation via analysis and conclusion from the numerical analysis.

2. LITERATURE REVIEW

Major losses (especially in terms of costs and fatalities) are attributed to catastrophic activities like earthquakes and terror attacks. Various studies have been conducted regarding the behaviour of steel structures during seismic activities. Bolted end plate joints have become a typical type of connection for steel structures. Substantial amount of analytical, experimental, and numerical models was already available to be able to support succeeding studies about it.

Studies on robustness, as previously mentioned, are still not as comprehensive compared with seismic analysis of bolted end plate connections, let alone robustness studies on deep columns. That is why in this study, a more in-depth understanding of such type of joints was shown and its viability to be also used for increasing robustness. The focus of this study was how bolted end plated connections can be used not just for seismic endurance but also for column loss scenario during a catastrophe. A link between seismic and robustness, through previous literature, was also shown since both catastrophic cases are evidently related.

The role of joints in the structure greatly affect its performance—overall behaviour, failure mechanism—during such disasters. The final typology used in this study was supported from previous studies on bolted end plate connections. Three approaches are typically used over the years in developing studies in joint behaviour:

1) **Numerical method** – the advancement of software for finite element analysis greatly increased over the years. Steel joints can be numerically modelled in such software, providing easy and accurate results depending on the mesh used. Local behaviour of steel joints is better understood with numerical analysis since they are difficult to measure experimentally [14]**.** This type of analysis supports experimental tests especially in validating its results. It also reduces the amount of time needed for generating results without compromising its accuracy as long as the parameters in the model are carefully selected.

2) **Experimental method** – conducting actual results simulates the real behaviour of the steel joint. This method constitutes not just more time but also costs. However, numerical analysis can only be qualified if its results are validated from the experimental results. This type of analysis also allows improvement of the current numerical methods since it projects a more realistic behaviour and parameters during the action.

3) **Analytical method** – design methods presented in the Eurocode provide a more standardized solution for analysis of steel joints. However, such methods are found to be tedious if used for preliminary joint design in a typical scenario. Improving current methods as well as simplifying analytical approach are deemed to be significant when conducting such analyses.

The focus of this study is by using the numerical method and validate it with numerical and experimental results from previous literature.

2.1 Use of deep columns

Shen et al [9] conducted a study on the use of deep columns in special moment frames (SMF). To avoid confusion, AISC [15] distinguishes moment frames as ordinary (O), intermediate (I), and special (S), increasing the ability to dissipate energy in plastic mechanisms. Hence, SMFs are moment resisting frames with the highest ductility and is therefore used in regions with high seismicity. Shen et al [9] highlighted that the typical design requirement that governs is the stiffness to control the drift, making deep columns more economical. The downside, however, is that there is a limited amount of information on the cyclic

behaviour of such typologies. Deep columns essentially have larger moment of inertia than smaller sections, which means they have increased stiffness *EI*. Comparatively, larger *EI* results in larger global stiffness of the frame, helping the structure to reduce drift and damage.

In their study, they used two prototype SMFs: one with W14 (356mm) and one with W27 (686mm). They conducted inelastic time history analysis and nonlinear finite element analysis to check the effect of deep columns to the performance of a reduced beam section (RBS) connections. Results of their research showed that (1) the use of deep columns are found to be satisfactory for use in moment frames, including SMFs; (2) their investigation showed that deep column connections should be able to provide vital strength, especially for rotational ductility in excess of the requirement in FEMA-350 for pre-qualified connections; (3) presence of composite slab reduces the twisting of the column, which is a major concern in using deep columns; (4) cyclic behaviour of RBS connections with W27 columns were analogous to that of W14 columns; (5) the use of deep columns in moment frames satisfy the drift limit requirement, with less steel tonnage, making it more economical; and (6) further studies must be done on RBS connection to a deep column with composite slab.

Zhang et al [11] did analytical work regarding welded connections of deep column-to-RBS-beam. Since the RBS region is prone to local buckling and out-of-plane beam movement, the connection subjects the column to torsion, negatively affecting its performance. They conducted nonlinear FEA to see the effect on the deep column with regards to the inelastic behaviour of the connection. Results of their test demonstrate that under seismic inelastic loading, the connection could satisfactorily perform if the beam is effectively laterally braced.

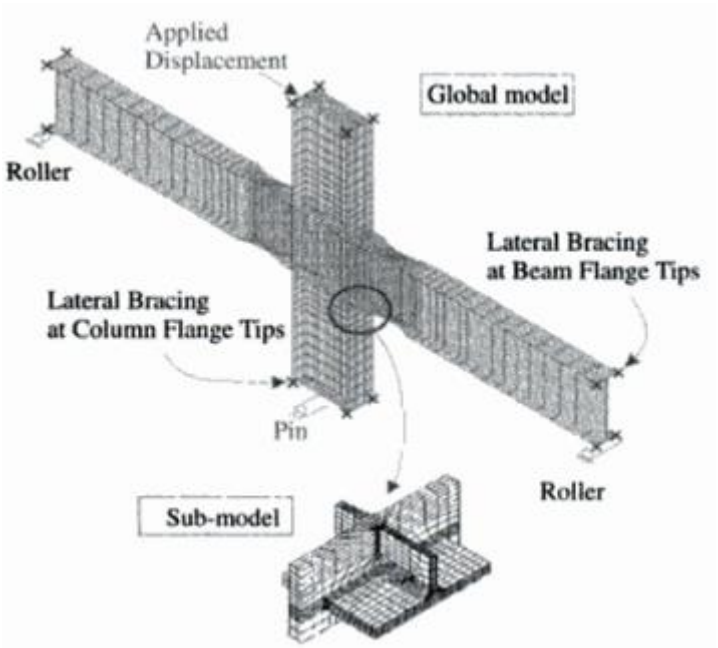

Figure 2.1. Global model and sub-model of the FEA by [11]

On a subsequent related study by **Zhang and Ricles** [10], experimental tests on six full-scale specimens are done on the same geometry in [11]. This is to validate as well the numerical results with the experimental findings. Summary of the test results are seen on Table 2.1. Results showed similar outcomes as the restraint from the concrete composite floor slab reduced the lateral movement on the beam, minimizing the column twist. It reduced the strength deterioration from the lateral buckling of the beam's flanges which results to possibly torque on the column. Moreover, the connections of the specimens (with or without the floor slab, and a lateral brace at the RBS region) were able to pass the criteria of AISC seismic provisions [15], qualifying connection for SMF seismic resistant designs.

Specimen	SPEC-1	SPEC-2	SPEC-3	SPEC-4	SPEC-5	SPEC-6
Maximum story drift (% rad)[a], θ_{max}	4.0	4.0	5.0	4.0	5.0	4.0
Maximum inelastic story drift (% rad)[a], $\theta_{p,max}$	3.1	2.8	4.0	3.0	3.9	2.6
Maximum panel zone inelastic story drift (% rad)[a], $\theta_{p,max}^{pz}$	0.6	1.3	0.4	0.4	1.3	1.9
Maximum beam inelastic story drift (% rad)[a], $\theta_{p,max}^{bm}$	2.5	1.4	3.7	2.7	2.6	0.6
Maximum column inelastic story drift (% rad)[a], $\theta_{p,max}^{col}$	0.2	0.2	0.2	0.1	0.2	0.2
Column twist at 4% story drift (rad), ϕ_{max}	0.016	0.025	0.006	0.037	0.007	0.004
Beam bottom flange out-of-plane movement in RBS at 4% story drift (mm), ϕ_{flg}	35	34	35	38	26	5
Maximum beam moment at column face, $M_{f,exp}/M_{pn}$	1.03	1.13	1.15	1.11	1.20	1.00
Maximum beam moment at center of RBS, $M_{RBS,exp}/M_{pn,RBS}$	1.34	1.48	1.50	1.44	1.56	1.29
Location of fracture (all fractures occurred in the RBS except SPEC-6)	Beam bottom flanges	Beam top flanges	Beam bottom flange	Beam bottom flange	Beam bottom flange	Beam bottom flange HAZ

[a]Values for story drift and drift components are the maximum prior to the occurrence of either fracture or strength deterioration to below 80% of specimen nominal capacity.

Table 2.1. Summary of test results by [10]

Elkady and Lignos [12] conducted a study on the collapse assessment of steel moment resisting frames designed with deep members. They investigated three deep column sizes typically used for SMFs using FEA. Attention is focused on the effect of the slenderness of the section and the axis load level on the cyclic decline in terms of stiffness and strength of deep columns because their performance is related to collapse potential of SMFs in seismic areas. Results of the simulations indicate that columns with huge web slenderness have a larger rate of cyclic deterioration in terms of axial shortening and strength because of severe web local buckling, even amplified when axial loads are higher. Hence, in a seismic point of view, the major issue of using deep columns is the fact that it is prone to buckling. Further studies about this specific issue is needed as recommended by previous researchers. **Uang** [13] also did numerical and experimental testing on deep columns, for which he indicated that criteria to limit the local buckling, ensuring sufficient column rotation capacities, are currently in the works. The effect of column shortening on the vulnerability to collapse of a multi-storey steel moment frame buildings has also been evaluated.

2.2 Typology of the joint for seismic design

2.2.1 Extended end plates

Sumner et al [16] conducted an experimental study on the use of extended end plates for moment connections subjected to cyclic loading. Six specimens of steel beam-to-column connections and one composite slab beam-to-column connection were created in their investigation. These specimens include stiffened and unstiffened end plates (Figure 2.2). They varied the size of the beams and columns for each specimen. The steel grade of the beams and columns are ASTM A572 Grade 50 except for the composite slab's column, which is ASTM A36. The end plates, stiffeners, continuity plates and additional web plates were ASTM A36 steel as well and they used 32mm bolts ASTM 1490 or ASTM A325.

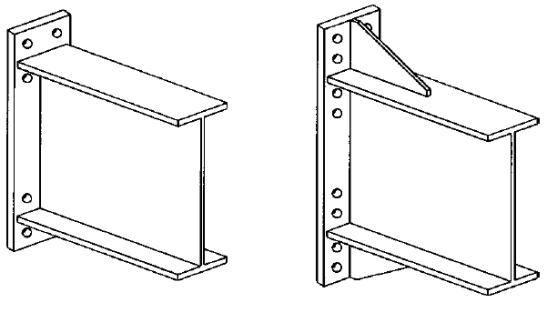

a) Four Bolt Unstiffened b) Eight Bolt Stiffened

Figure 2.2. Unstiffened and stiffened extended end plate setup by Sumner et al.

Results indicate that extended end plate moment connections could be designed in such a way that its strength, stiffness, and ductility requirements are satisfactory for use in seismic force resisting moment frames. The connections must be designed to be stronger than the connecting beam (i.e. strong plate connection). In their study, this is done by designing the connection to develop 110% of the expected nominal plastic moment strength M_{pe} of the connecting beam. This is to enable beam flange and web local buckling (which is a ductile and reliable limit state), to limit the strength of the beam-to-column connection assembly.

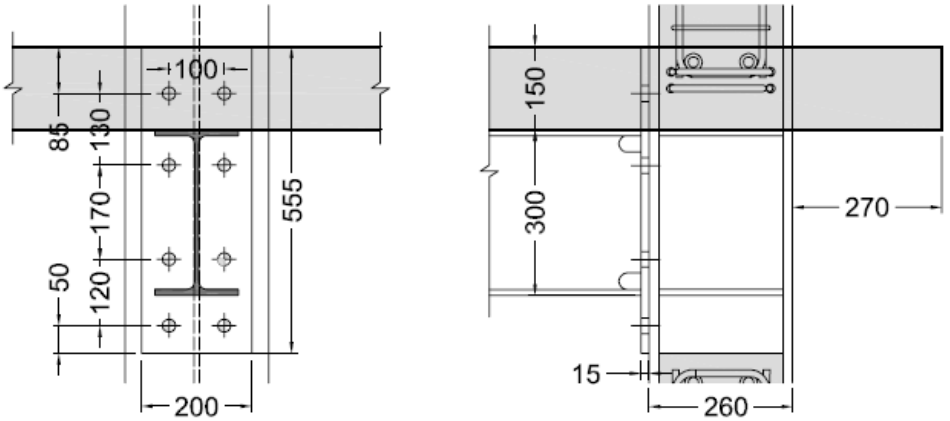

Figure 2.3. Exterior joint

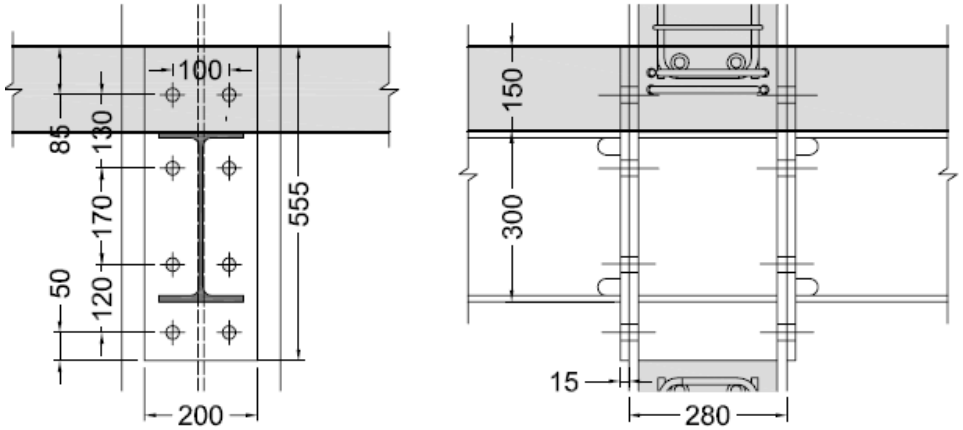

Figure 2.4. Interior joint

Gracia et al [17] conducted experimental tests on semi-rigid composite joint with a double-sided extended end plate to determine its seismic performance. They performed tests for both interior and exterior joints (Figure 2.3 and Figure 2.4).

They performed monotonic tests to evaluate the resistance and the rotation capacity of the joint, and cyclic tests to assess the energy dissipation capacity and characterize the degradation in terms of stiffness and resistance. They also used IPE 300 steel profile for the beams and HEB 260 and HEB 280 partially encased columns for the exterior and interior joints, respectively.

Results show for the exterior joints that all the specimens have very good ductile behaviour. Similar behaviour was observed for interior joints. The behaviour of the panel zone allowed high plastic rotation at the joint. Though this is good for the energy dissipation and ductility of the structure during an earthquake, it could still affect the overall stability of the structure, allowing large lateral displacements and P-Δ effects. Hence, it should still be evaluated by nonlinear analyses to check if it complies with the limits set in the code.

Moreover, the contribution to the overall performance of the left and right connections is relatively smaller than that of the exterior joint specimens, with limited amount of energy dissipated. Cyclic tests showed that both interior and exterior joints provided uniform gradual degradation of the resistance and stiffness, as well as plastic deformation.

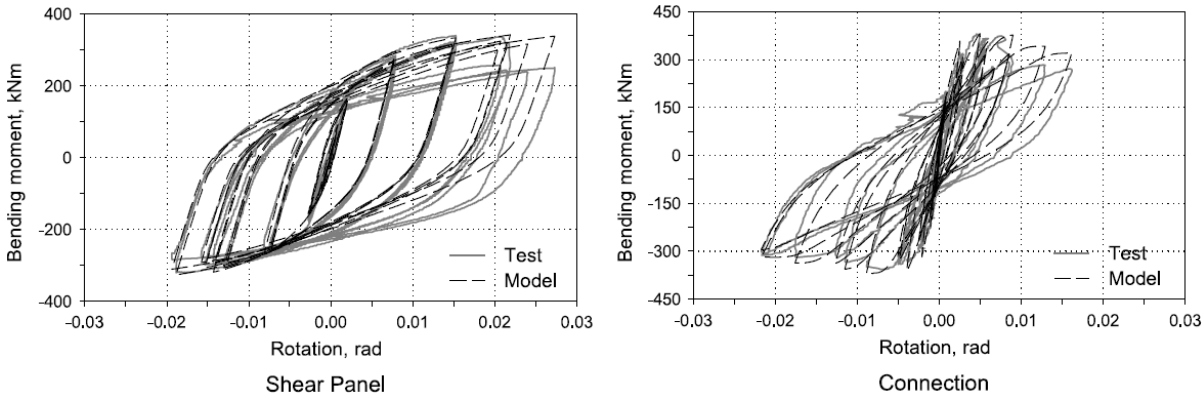

Figure 2.5. Calibration of the exterior joint

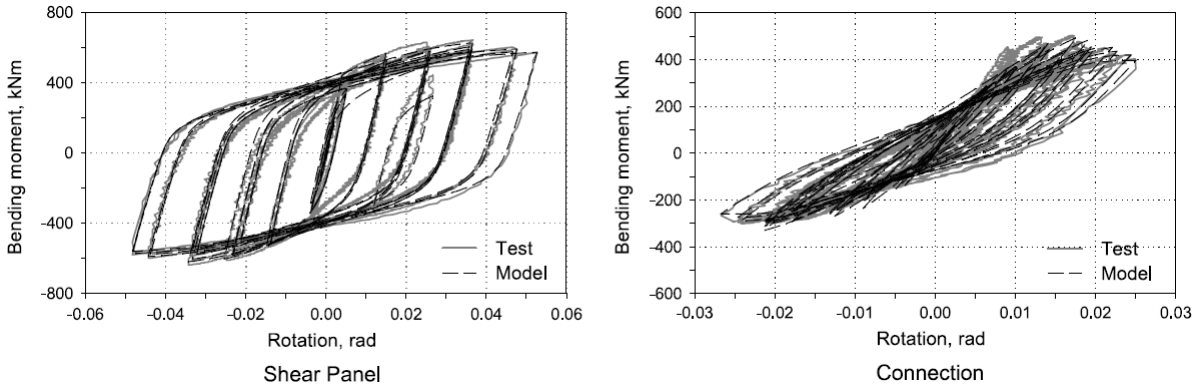

Figure 2.6. Calibration of the interior joint

To validate their results, they also conducted numerical tests using the software IDARC 2D. The numerical models are calibrated with the experimental results, as seen on Figure 2.5 and Figure 2.6, showing sufficiently good matching behaviour between the two. In here, it can be observed that the use of both experimental and numerical tests is deemed vital for calibrating the results. A double sided extended end plate system is found to be useful in seismic design for composite joints.

2.2.2 Rib stiffeners: stiffening the end plates

The usefulness of stiffening the end plate was the focus of the study of **Guo et al** [18]. They compared the hysteretic behaviour, stiffness, and strength of stiffened and unstiffened extended end plate connections of beam-column joints. Six specimens were experimented and the end plate thickness, end plate stiffeners, and column web stiffeners were varied from one specimen to another. Three of the specimens have end plate stiffeners, the thicknesses of the end plates varied from 12 to 25 mm, and five specimens have column web stiffener.

Results show that stiffeners have a remarkable influence on the hysteretic behaviour of joints albeit increasing the fabrication costs and sophistication of connection details. From the specimens observed, stiffened connections have increased load carrying and energy dissipation capacities due to the ability of such to change the mechanism of load transmission and upgrade the restriction conditions. Specimens 3 and 5, which are stiffened generated the best hysteretic behaviour as seen on Figure 2.7. Lastly, they

suggested that while increasing the thicknesses of the end plate and column web would generally enhance the load carrying capacity and rigidity of extended end plate connections, the more viable approach is to just set rib stiffeners on them. In the end, they were able to cover some significant part of the behaviour of the connection but they also recommended to conduct further study on other parameters such as exploring on wider range of beam-column configurations to cover both low-rise and high-rise structures.

Specimen	End-plate thickness (mm)	End-plate stiffeners	Column web stiffeners
S-1	12	Haven't	Have
S-2	12	Have	Have
S-3	15	Have	Have
S-4	18	Haven't	Haven't
S-5	18	Have	Have
S-6	25	Haven't	Have

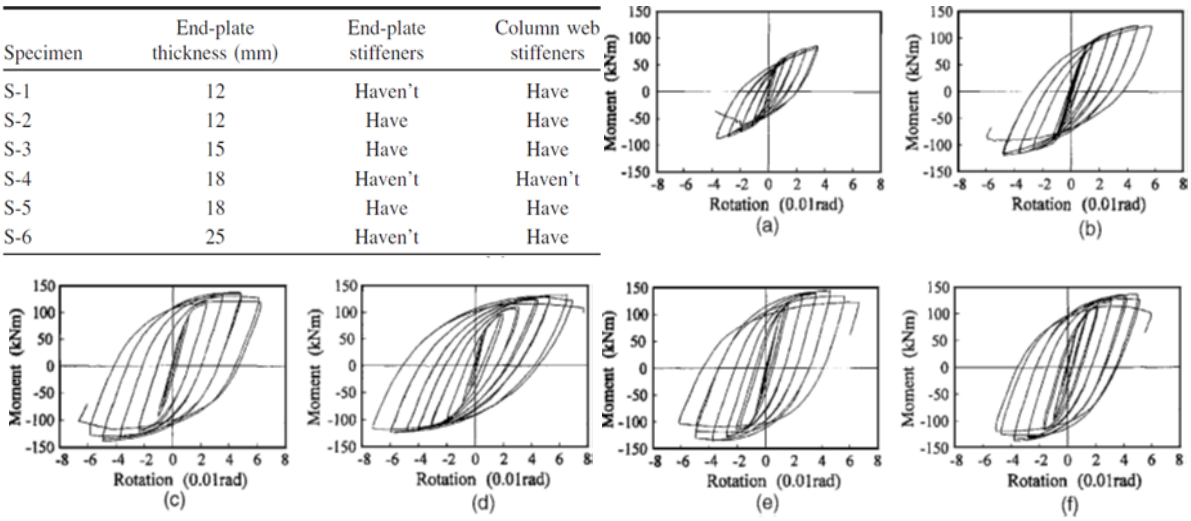

Figure 2.7. Configuration of the specimens used in the study of Guo et al [18] and their respective hysteretic behaviour.

In another study by **Abidelah et al** [19], they also concentrated on the experimental and analytical behaviour of bolted end plate beam-beam and beam-column connections with and without stiffeners. They generated eight specimens, the first half of it is unstiffened, while the other half is stiffened. Moreover, for each set, they also variated the use of extended and flush end plates. The location of the stiffeners was also varied as shown in Figure 2.8.

Results show similarity with the study conducted by **Guo et al** [18]. In their study, the ductility was measured as the length of the yield plateau of the M-Φ curve as shown in Figure 2.9. This is quantified by means of the index ψ_j that relates the rotation Φ_u, corresponding to the ultimate moment M_u, to the rotation Φ_p, corresponding to the plastic moment M_p. Hence, $\psi_j = \Phi_u / \Phi_p$. As seen on the figure, the plastic moment M_p and the initial stiffness $S_{j,ini}$ are larger for BC4, which is the joint stiffened on both sides. However, as also seen on the figure, ductility greatly decreased for BC4 compared to BC1, which has the unstiffened end plates.

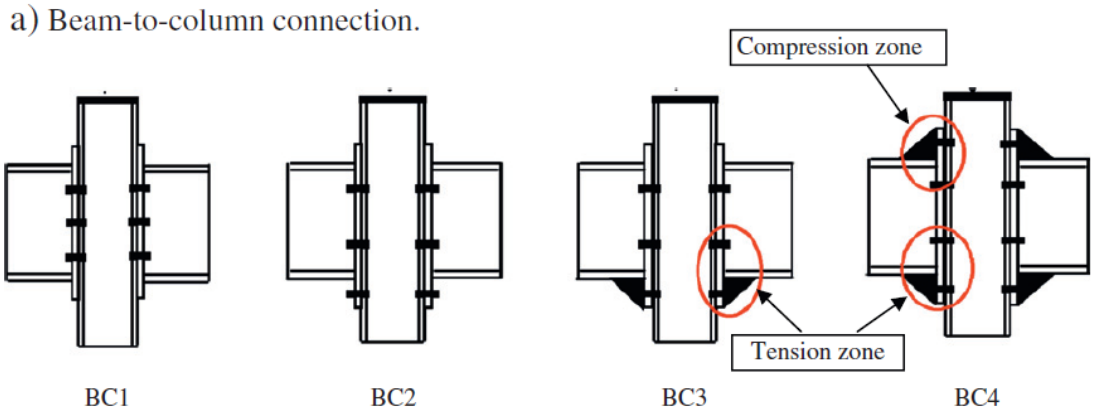

Figure 2.8. Part of the configuration of the specimens used by Abidelah et al [19].

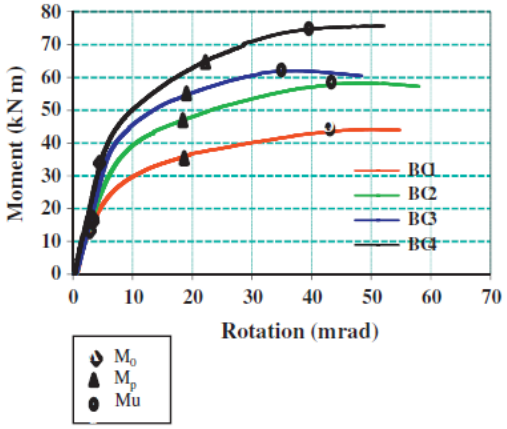

Main parameters of the experimental moment–rotation curves.

Specimen	Strength (kN m)			Stiffness (kN m/ mrad)		Rotation (mrad)				Ductility
	M_0	M_p	M_u	$S_{j,ini}$	Φ_0	Φ_p	Φ_{xd}	Φ_u	Φ_f	Ψ_j
BC1	14	34	44	8.1	0.3	5	16	46	55	9.2
BC2	16	47	58	8.7	0.6	6	18	36	59	6
BC3	17	53	63	9.5	0.6	6.6	19	36	49	5.5
BC4	34	65	75	10.1	0.7	9.2	23	45	62	4.8
BB1	20	65	75	29.8	0.6	1.9	3.5	5.8	6.1	3.2
BB2	22	95	107	40.8	0.5	2.4	4.4	6.3	7.2	3.0
BB3	29	105	115	42.4	0.6	2.5	4.0	5.7	6.2	2.5
BB4	39	123	134	44.9	0.8	2.9	5.6	6.2	7.0	2.4

Figure 2.9. Moment curve and tabulated results for the beam-column connection by Abidelah et al [19].

Moreover, the stiffening of the extended end plate in BC3 and BC4 modified the distribution of the forces in the tension bolts in contrast to the unstiffened connection BC2 (Figure 2.10). In BC2, the first bolt row above the beam tension flange has a higher force than the bolt row outside of it. On the other hand, the measured values of the forces are almost identical for values of moment lower than M_p. Per **Abidelah et al** [19], this is because the stiffeners ensure continuity to the beam web. Stiffening of the extended part of the end plate provides better equal distribution of the rigidity between both sides of the beam tension flange.

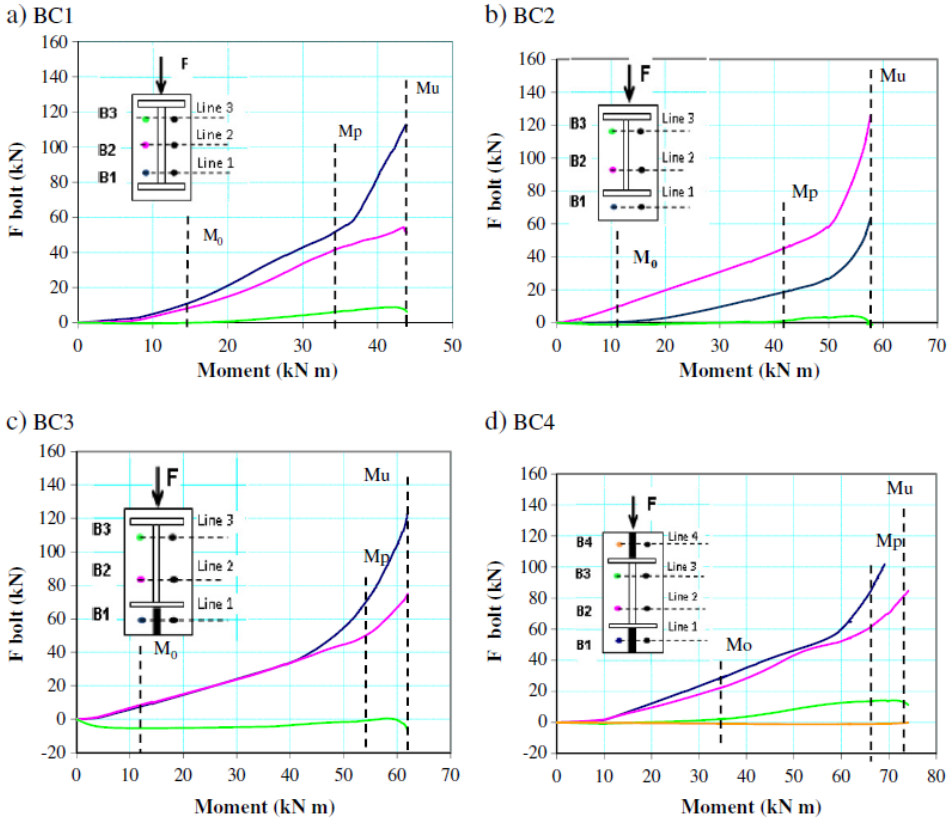

Figure 2.10. Bolt forces vs the applied moment in the beam-column connections [19].

D'Aniello et al [1] conducted a comprehensive study regarding the seismic design of extended stiffened end plate joints. The study is for the advancement of the framework of Eurocodes since they provided a new approach on designing steel bolted connections. Part of the said study also emphasised on the significance of stiffening the connection with ribs (See Figure 2.11).

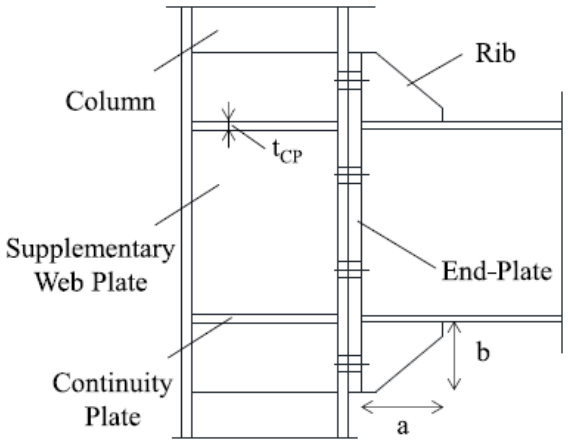

Figure 2.11. Geometry of the connection on D'Aniello et al's study [1].

The sizes of the beam and column were varied to determine its effect on the local behaviour of the connection. ES1 (extended stiffened) and E1 (extended unstiffened) models represent IPE 360 Beam – HEB 280 Column, ES2 and E2 are IPE 450 Beam – HEB 340 Column, and ES3 and E3 are IPE 600 Beam – HEB 500 Column. Results of their study show that the presence of the rib stiffeners significantly increases the stiffness and strength of the joint by 8% to 42% and 14% to 83%, respectively, as shown in Figure 2.12. It is also worth noting that on all models, all full-strength ES joints behave in the elastic range, while the unstiffened extended joints exhibit plastic behaviour and even lower for equal (*E*) and partial (*P*) strength unstiffened joints. Lastly, using rib stiffeners improve a joint's low-cyclic fatigue capacity due to a more efficient yield line pattern (provided that full welds are used).

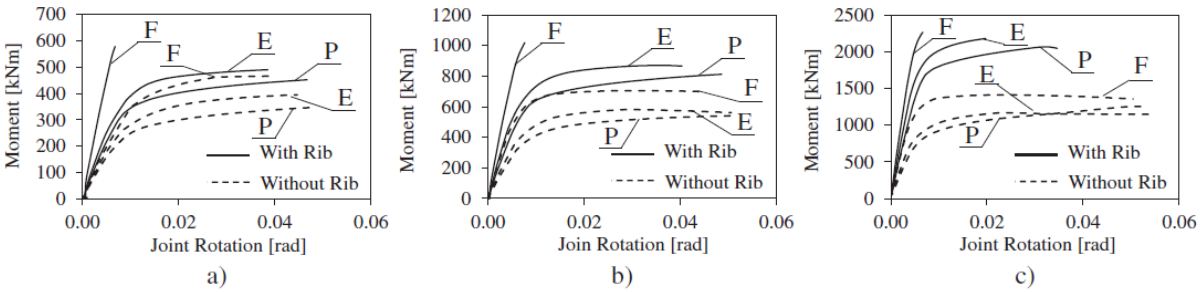

Figure 2.12. Influence of the rib stiffener on moment-joint rotation response curve for (a) ES1 vs E1, (b) ES2 vs E2, and (c) ES3 vs E3 [1].

2.2.3 Continuity plates

Ghobarah et al [20] concluded in their study that extended end plate connections are suitable for moment resisting frames for areas with high level of seismicity. Specifically, they also pointed out that joints with unstiffened columns showed very bad performance compared with those that were stiffened on a seismic point of view. Figure 2.13 shows the joint geometry implemented in their experiment.

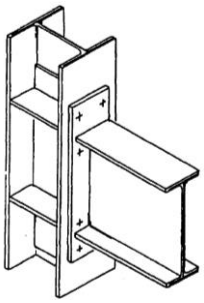

Figure 2.13. Extended end plate connection from Ghoborah et al's experiment

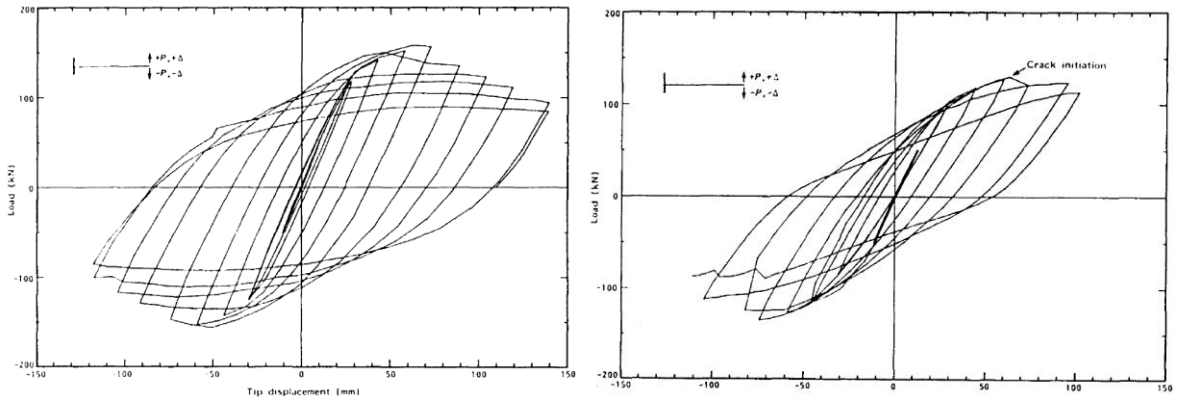

Figure 2.14. Beam load vs beam-tip displacement hysteretic curves for stiffened (left) and unstiffened (right) column flange [20].

Figure 2.14 shows results of their test from specimens with stiffened and unstiffened column flange. Furthermore, pre-tension forces in all the bolts showed degradation with repeated load cycles. The authors suggested that the bolts must be designed to sustain a force corresponding to a beam moment of $1.3M_p$ so that the bolts won't lose their pre-tension forces significantly even during moderate earthquake excitation.

2.2.4 End plate thickness and steel grade

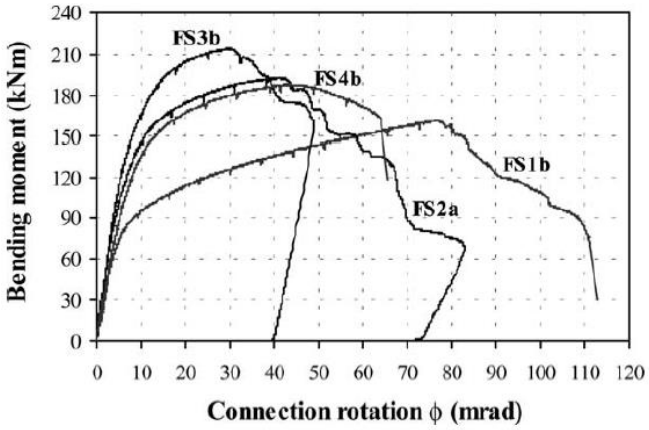

Figure 2.15. Comparison of the specimens' moment-rotation curve in Girão Coelho et al's study [21].

Girão Coelho et al [21] focused their experimental investigation on the end plate thickness and steel grade of statically loaded extended end plate moment connections. The specimens used in the study were design to ensure failure to the end plate and/or bolts without developing full plastic moment capacity of the beam. They accentuated that the lack thereof on the available specifications on the rotation capacity of structural joints is of priority to be further improved especially under seismic conditions. They also indicated that while the Eurocode 3 provides safe criteria for rotation capacity, these standards are perhaps too conservative.

Their study indicated that increasing the end plate thickness and yield stress lead to an increase of its moment resistance. The joint initial rotational stiffness also increases along with the end plate thickness but the steel grade has slight influence, if there's any, on this property. The joint's post rotational stiffness is identical for all specimens. Thus, increasing the thickness and steel grade has little significance. However, as seen on Figure 2.15, the rotation capacity of the joint (i.e. ductility), decreases significantly when the end plate's thickness and steel grade is increased.

2.2.5 Supplementary web plates

The same study by **D'Aniello** [1] also emphasised the use of supplementary web plates for full and equal strength joints. This is due to the criticisms they mentioned in their study regarding the present form of EN 1993:1-8. According to the Eurocode, the shear strength of the column web panel should be calculated as the sum of the section strength ($V_{wp,Rd}$) and the overstrength ($V_{wp,add,Rd}$) due to the formation of local links in column flanges, if continuity plates are used. However, allowing web panel to develop $V_{wp,add,Rd}$ could lead to a substantial post-quake residual deformations, with considerable out-of-plumb for deep columns, therefore corresponding to large costs for repair. Moreover, large costs for repair means that the damage is significantly huge, which makes it an imposed requisite as an added measure to prevent global collapse. From this, the authors agreed that the web column should be strengthened by means of an additional steel plate, where the thickness should be lesser or equal to the column's web thickness. Specifically, D'Aniello et al's study neglected the $V_{wp,add,Rd}$ for full and equal strength joints. Consequently, additional web plate is required to satisfy the strength requirement given in EN 1993-1-8.

A study by **Ciutina and Dubina** [22] shows that the shear area can be amplified by the total section of the supplementary web plates. Their study focused on testing various specimens of connections with one-sided or two-sided stiffeners on the column web, varying the size of the stiffeners. They found that a web panel strengthened by an additional web plate is verified to be very stable with good ductility and rotation (>0.035 rad). Figure 2.16 shows the result of each specimen. It can be observed that the connection reinforced with two doubler plates and distanced from the fillet portion of the welded column web (CP-IIPD) resulted the most effective resistance and an enhanced deformation capacity.

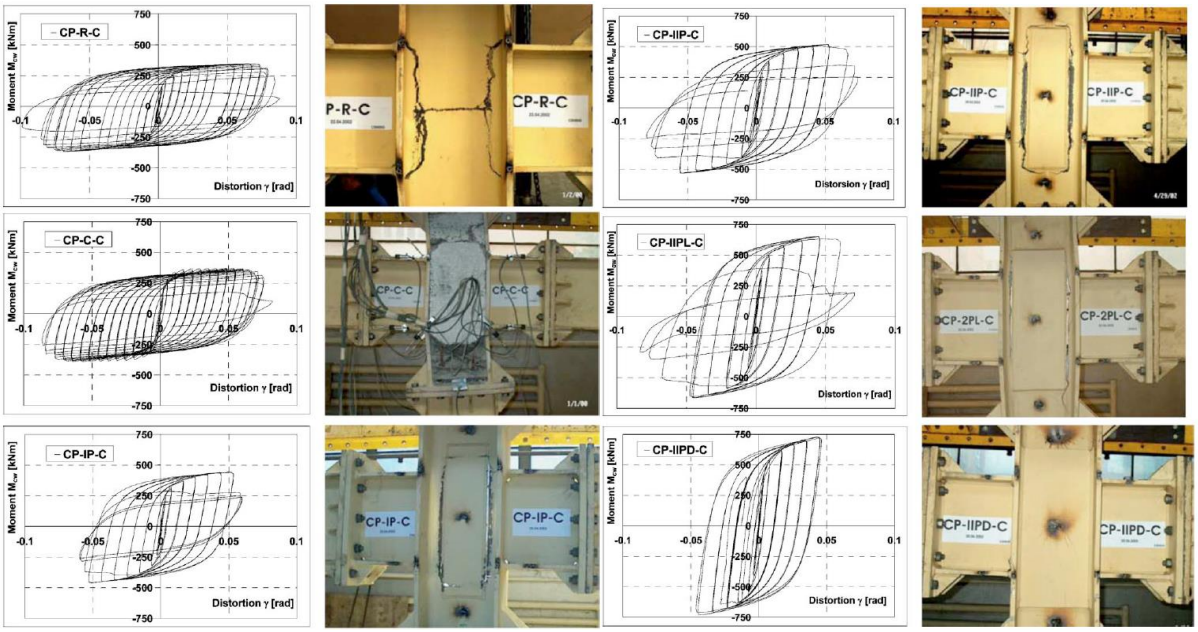

Figure 2.16. Cyclic behavior and failure mode of cyclic specimens [22].

2.3 Moment-rotation response of stiffened extended end-plate joints

2.3.1 Standard details of extended stiffened connections from test results

Tsai and Popov [23] emphasised as well the use of stronger bolts and rib stiffeners since results showed that they can significantly scale up the behaviour of end plate connections under large cyclic loadings. Furthermore, they concluded that the extended end plate moment connections can be designed to develop

the full plastic moment capacity of the beam under cyclic loading, and the use of the end plate stiffener can decrease the effect of prying force.

From the previous tests discussed in Section 2.1, various researchers were able to come up with a typical detail for an end plate connection on a seismic point of view. **Shi et al** [24] summarised their test results and other relevant research results which are as follows:

1. End plate to be used must extend on both sides
2. Column flange and end plate are stiffened
3. Thickness of the column flange stiffener must be no less than the thickness of the beam flange
4. Thickness of the end plate extension stiffener should be no less than the thickness of the beam web
5. Thickness of the column flange is equal to the end plate, within the range of 100 mm above and below the extension edge of the end plate

Shi et al's [24] experimental setup on the extended end plate joint is shown in Figure 2.17. They tested five specimens, varying the end plate thickness and bolt diameter and subjected it to a cyclic load. The beams and the column are welded built up profiles. Full penetration end plate-to-beam welds were used and fillet welds with depth equal to 8mm were used for the rest.

Table 2.2 shows the thickness of the end-plates and the diameter of the bolts implemented by Shi et al [24] in their study for their parametric analysis. On the other hand, Table 2.3 shows the material properties of the joint assemblies in their experiment.

Specimen number	End-plate thickness (mm)	Bolt diameter (mm)
EPC-1	20	20
EPC-2	25	20
EPC-3	20	24
EPC-4	25	24
EPC-5	16	20

Table 2.2. End-plate thickness and bolt diameter used by [24]

Material	Measured yield strength (MPa)	Measured tensile strength (MPa)	Measured elastic modulus (MPa)	Design value of bolt pre-tension force (kN)	Measured bolt average pre-tension force (kN)
Steel (thickness $\leq$ 16 mm)	391	559	190 707	–	–
Steel (thickness $>$ 16 mm)	363	537	204 228	–	–
Bolts (M20)	995	1160	–	155	185
Bolts (M24)	975	1188	–	225	251

Table 2.3. Material properties of the joint elements tested by [24]

Their experimental results were then compared with the results from their proposed analytical model. It is shown that the experimental results coincide well with the analytical model for the M-φ curves, M-φ_s curves, and the joint initial rotational stiffness, given that the actual material properties were applied.

The definition of the rotation of the joint, divided into two as seen on Figure 2.18, is also explained in their research. The shearing rotation φ_s is the contribution of the panel zone of the column while the gap rotation φ_{ep} is cause by the relative deformation of the end-plate and the column flange, which includes the bending deformation of the end-plate and the column flange and the extension of the bolts. These two curves are attained and then superimposed. The curves from the experiment are denoted as the function of φ_s and φ_{ep} so they can be compared to the analytical curves.

Results of their comparison are shown in Figure 2.19 and the test results are seen on Table 2.4. The authors further discussed that the contributions of the joint rotational deformation of each component (i.e. shear

deformation of panel zone, bolt extension, bending deformation of the end plate and column flange, etc.) is provided in their study. With their work, an extensive information on analysing the detailed rotational behaviour of end plate connections had been laid out for future researches.

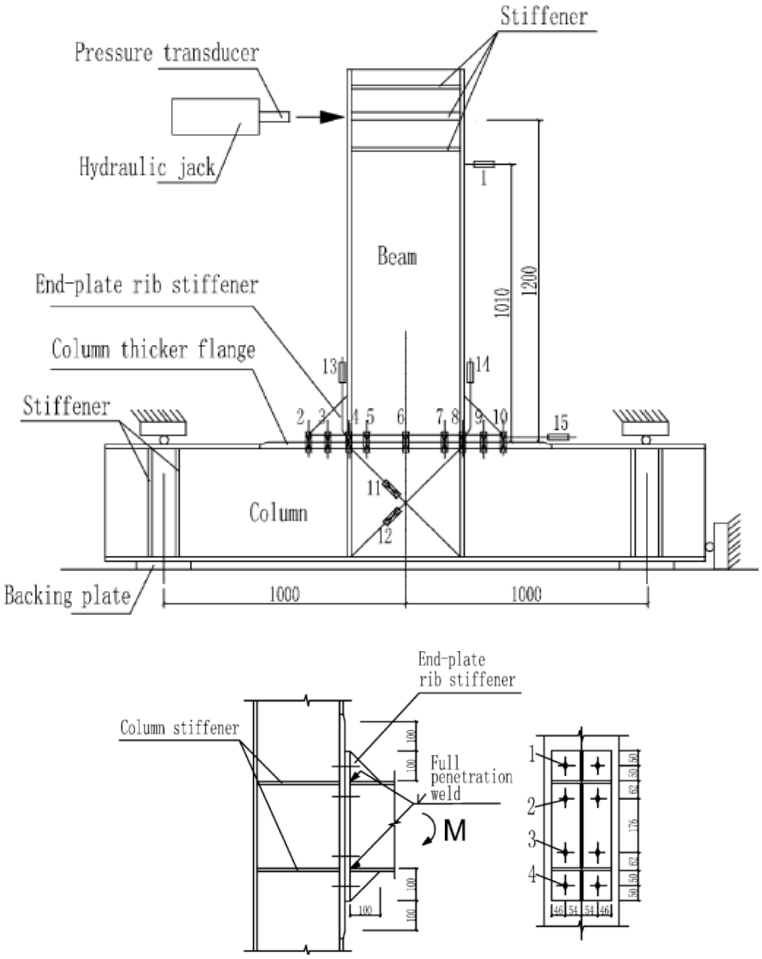

Figure 2.17. Test specimen and loading arrangement of Shi et al's [24] experiment (top), and connection geometry (bottom)

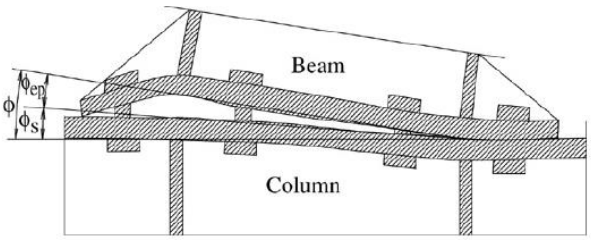

Figure 2.18. Definition of joint rotation according to [24].

Specimen number	Loading capacity (kN)	Moment resistance (kN m)	Moment resistance change compared with EPC-1 (%)	Initial rotational stiffness $S_{j,ini}$ (kN m/rad)	Initial rotational stiffness change compared with EPC-1 (%)	Failure mode
EPC-1	286.4	343.7	0.0	52 276	–	Bolt fracture
EPC-2	268.4	322.1	−6.3	46 094	−11.8	Bolt fracture
EPC-3	325.3	390.3	13.6	46 066	−11.9	Buckling of beam flange and web in compression
EPC-4	342.3	410.8	19.5	47 469	−9.2	Buckling of beam flange and web in compression
EPC-5	296.1	355.4	3.4	41 634	−20.4	Bolt fracture and buckling of end-plate rib stiffener in compression

Table 2.4. Test results of the experiment by [24]

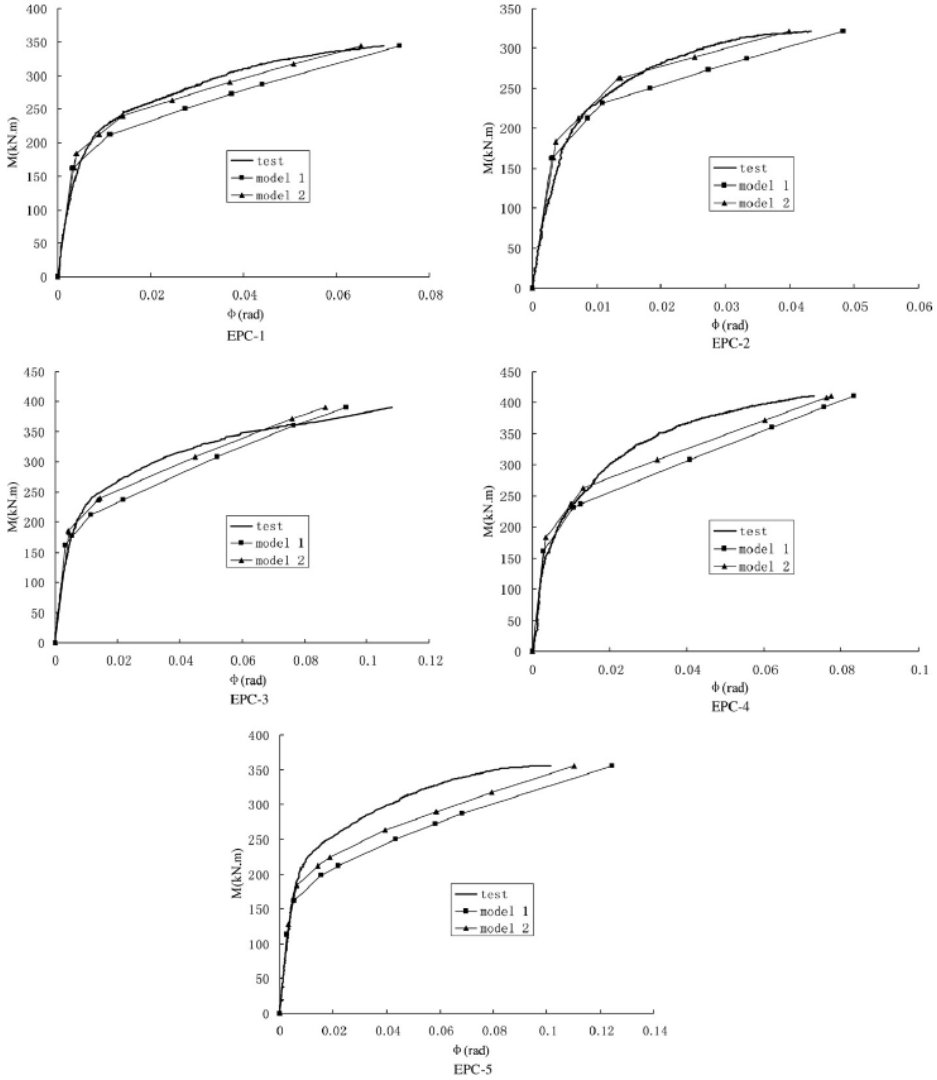

Figure 2.19. Comparison of the M-phi curves from analytical model and experimental tests [24].

2.3.2 Full, equal, and partial strength joints

Continuing from the study by **D'Aniello et al** [1], a numerical analysis was done to test the performance of the extended stiffened end plate bolted connections. They modelled three different types of connection – full strength (*F*), equal strength (*E*), and partial strength (*P*) joints. In case of *F* joints, it must be designed to ensure the formation of all plastic hinges in the beam, being consistent to Eurocode 8 (strong column – weak beam system). For *E* and *P* joints, the plastic behaviour is concentrated on the connection itself. *E* joints are theoretically characterized by the contemporary yielding of all macro-components (i.e. connection, web panel, and beam). *P* joints are just focused on the plastic deformation development only in the joint.

Moreover, *P* joints could have sufficient monotonic rotation capacity if designed to enforce plastic deformations into its components that can provide high ductility (e.g. end plate in bending) whilst the brittle components (e.g. bolts and welds) are in an elastic behaviour. *F* and *E* joints are intended for applications in moment resisting frames (MRF), it just depends on the ductility of the component. If a *P* joint is to be used, further considerations must be done. However, to support the use of *P* joints, using rib

stiffeners is a viable solution. For seismic designs (i.e. use of MRF), *P* joints are deemed workable to increase the stiffness of the MRF spans.

The capacity design standard to obtain the required joint behaviour can be guaranteed using the inequality:

$$M_{wp,Rd} \geq M_{j,Rd} \geq M_{j,Ed} = \alpha \cdot \left(M_{B,Rd} + V_{B,Ed} \cdot s_h \right)$$

where:

$M_{wp,Rd}$ is the flexural resistance corresponding to the strength of the column web panel;

$M_{j,Rd}$ is the flexural strength of the connection;

$M_{j,Ed}$ is the design bending moment at the column face

α is dependent on the design performance level of the joint:

- For *F* joints, it is just equal to $\gamma_{ov} \cdot \gamma_{sh}$ where γ_{ov} is the overstrength factor due to the material randomness and γ_{sh} is the strain hardening factor corresponding to the ration of the ultimate and plastic moment of the beam
- For *E* joints, α is equal to 1
- For *P* joints, it is less than 1. In their study, they used a value of α = 0.8 to limit the lower bound of the value to avoid damage concentration in the connection zone, in accordance to **AISC341-10** [15];

$M_{B,Rd}$ is the plastic flexural strength of the connected beam;

s_h is the distance between the column face and the tip of the rib stiffener;

$V_{B,Ed}$ is the shear force corresponding to the occurring of the plastic hinge in the connected beam, given by:

$$V_{B,Ed} = V_{B,Ed,M} + V_{B,Ed,G}$$

where:

- $V_{B,Ed,M}$ is the shear force due to the formation of plastic hinges at both beam ends, spaced by the length L_h, calculated as:

$$V_{B,Ed,M} = \frac{2 \cdot M_{B,Rd}}{L_h}$$

- $V_{B,Ed,G}$ is the contribution due to the gravity loads

The authors stressed out that the present form of the Eurocode does not predict the rotation capacities of the joints. The case of *E* joints is not also part of the present Eurocode, which D'Aniello et al are proposing in their work as an intermediate performance level. A parametric study of these joints was also done on the same study. They also provided a ductility criterion which has three modes (Figure 2.20), where the third mode must be avoided using two ductility criteria:

Level 1: $\beta \leq 1$, this condition imposes either a failure mode I or failure mode II (but very close to mode I), which provide very high ductility

Level 2: $\beta > 2$ and $\eta \leq 0.95$, this condition imposes a failure mode II with limited ductility, but avoiding brittle failure.

The authors suggested that larger ductility must be enforces for *E* and *P* joints, and less for *F* joints.

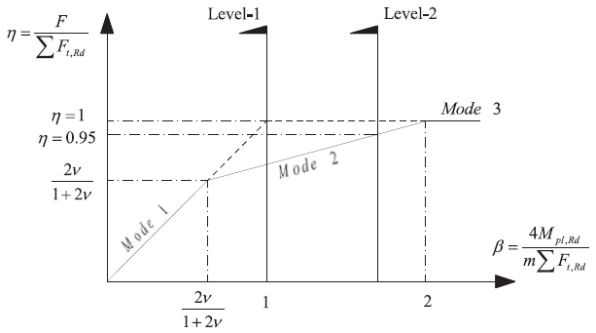

Figure 2.20. T-stub resistance and corresponding failure mechanism

They implemented the analysis through the use of ABAQUS software. Several modelling procedures from their study were implemented by the author of this present research as a continuation of their elaborate analysis. The procedure discussed in Section 2.3.1 is similar to what D'Aniello, et al did in their research. The validation of their numerical analysis was done by comparing it with their experimental analysis from a separate research from **Landolfo et al** [25]. Response is fully consistent with that of the experiment as seen on Figure 2.21. It can be observed that the joint moment rotation curve (Figure 2.21a) and the failure mode of the experiment (Figure 2.21b) and finite element analysis (Figure 2.21c) are very analogous.

Results of their analyses show that the cyclic behaviour of *F* joints is substantially affected by beam degradation, whereas *E* and *P* joints are influenced mostly by the connection response. Moreover, *P* joints dissipate more energy than *E* joints due to the plastic deformation that occurs into the end plate is bended in Mode I. *E* joints are characterized by Mode II, where the plastic demand is found in the bolts. Figure 2.22 shows the monotonic vs hysteretic response of ES3 joints.

They also concluded that the contribution of bolt rows below the horizontal axis of symmetry is negligible and does not affect the strength calculation for seismic design. In addition, they suggested that considering the actual position of the centre of compression is advantageous for the column web panel design, as lower design shear forces can be conservatively taken.

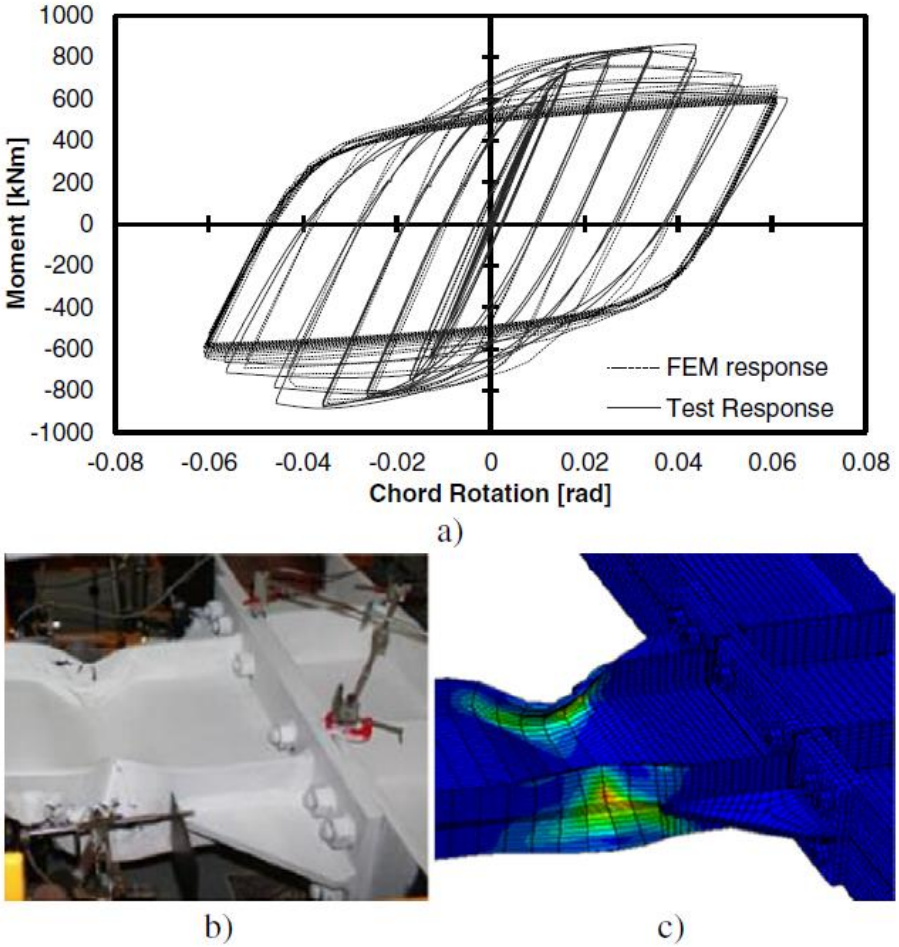

Figure 2.21. Validation of numerical results with experimental results [1]

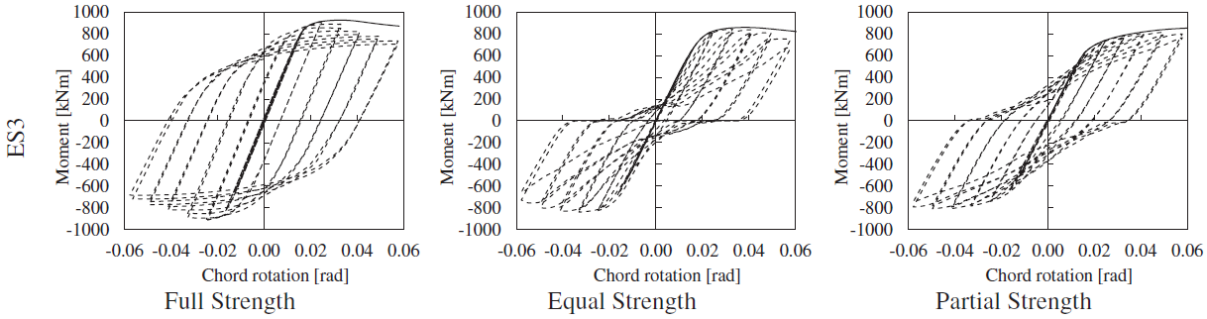

Figure 2.22. Monotonic vs hysteretic response of ES3 joints [1]

2.4 Robustness and catenary action

Robustness is characterized as the insensitivity of a structure to local failure [26]. Specifically, it is connected to events which people did not foresee or have full control (e.g. earthquake, blast action, car crash). It is often connected to progressive collapse analysis of a structure which typically comprises a chain reaction that is "activated" when one member or component failed, leading to redistribution of internal forces. It is a dynamic process in which a collapsing system would repeatedly pursue alternative load paths to survive. **El-Tawil** [27] listed three (3) mechanisms that could contribute to the ability of such systems to sustain collapse:

1) Catenary action of slab and beams allowing gravity load to span adjacent elements;
2) Vierendeel action from the moment frame above a damaged column; and
3) Gravity load support provided by non-structural elements such as partitions and infills

Global collapse will occur once the equilibrium of the structure is not achieved through any of the above mechanisms. From the list, the catenary action (1) is the final line of defence against collapse because it is only triggered once large deformations have occurred. It is the ability of the beams to sustain vertical loads via the formation of a string-like mechanism.

The following researches are studies conducted over the years regarding structural robustness. All of them mentioned the importance of the catenary action in analysing such behaviour:

2.4.1 Tests on different types of connections against column removal

Yang and Tan [28] focused their study on experimental and numerical tests of different types of bolted steel beam-column joints when a column is removed from the system. They indicated that failure typically begins from beam-column joints when subjected to abnormal loads. They presented an experiment for seven (7) specimens with various bolted steel beam-column connections. Four (4) of them are for nominally pinned joints while the other three (3), which includes the use of flush and extended end plates, are for semi-rigid joints. These connections are subjected to a central-column-removal scenario. Figure 2.23 shows the experimental setup implemented in their study.

In their study, the joint is located above the storey where an internal column was removed. As shown in Figure 2.23, only half of the beam span is simulated using pin conditions since the inflection point is at the middle of the beam span during the deflection process. Their experimental setup was compared with numerical models. The simplified model was deemed as an appropriate representation that could produce equivalent performance to a sub-frame test. They highlighted that though the vertical deflection capacities are different from a simplified test to that of sub-frame test, the rotation angles and internal forces at the connections are identical. For the semi-rigid connections, moment resistance values were also recorded.

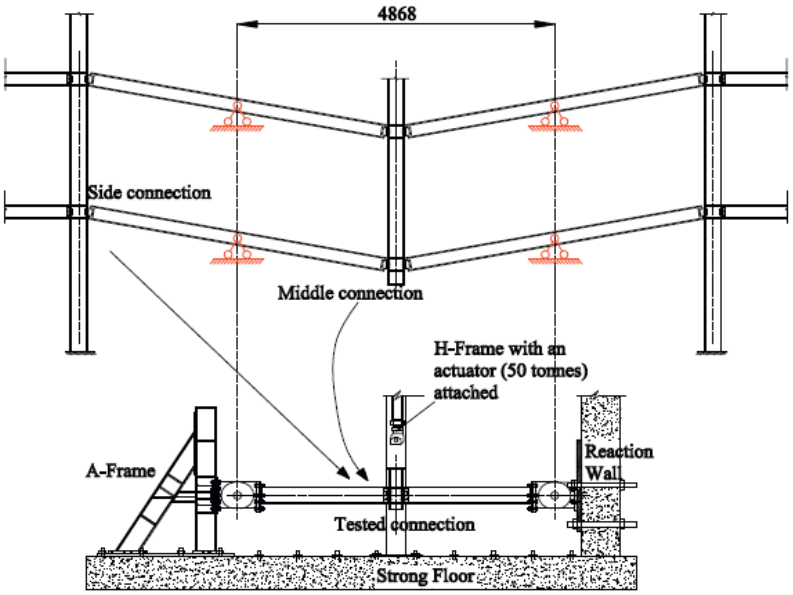

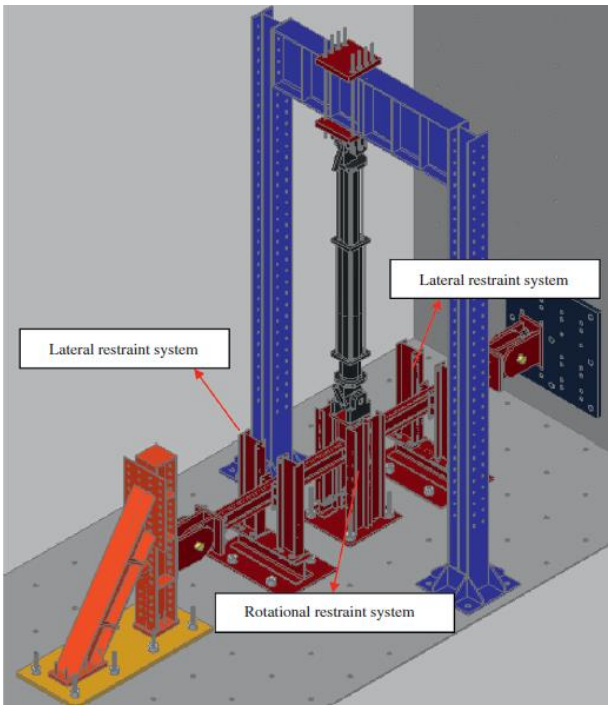

Figure 2.23. Experimental prototype of the beam-column joint [28].

In their experiment, the force-displacement history was split into two stages: flexural and catenary action. Test results show for the flush end plate that once the local buckling occurred at the left beam's top flange, flexural moment greatly decreased while initially, vertical load is sustained due to its high flexural stiffness. Catenary action was activated and resisted the vertical load after the said buckling occurred and could not resist higher vertical loads anymore (Figure 2.24). Figure 2.25 shows the displacement over the span of the setup, showing the catenary action. Straight line profiles start to show after the 69.9 kN load, indicating the formation of the plastic hinges on the beam-column connections.

Figure 2.24. Failure mode of the flush end plate connection [28].

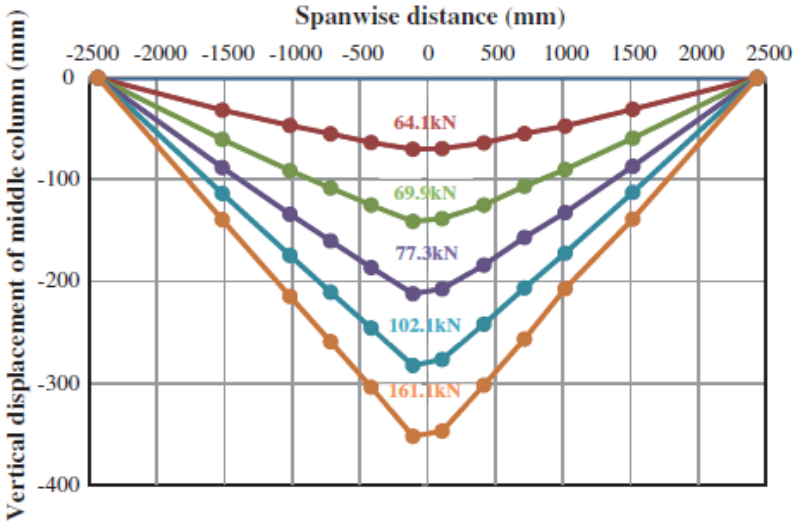

Figure 2.25. Middle column displacement profiles of beams corresponding to indicated vertical forces for flush end plate [28].

On the other hand, the extended end plate connection showed a different behaviour. It has the greatest flexural stiffness and moment strength compared with the other six specimens. Under normal loads, the top beam flange is in tension while the bottom is in compression. However, once the sudden column removal is applied in the system, the signs changed. The partial-strength weld at the right connection sustained a large tensile force and fractures first. Then, there was an abrupt drop of the load until it ultimately failed due to bolt thread stripping failure (See Figure 2.26). The extended connection indeed resisted considerable bending moment at the initial loading stage. However, when displacements became so large, there was no extra increase of loading for catenary action to kick in, unlike the previous specimen.

Figure 2.26. Failure mode of the extended end plate connection [28].

From their results, they highlighted that if flexural action is the only parameter being considered, the extended end plate endured the largest vertical applied load. However, catenary action has slight influence on this type of typology. Flush end plate performed way better than the extended plate when the sudden column removal was applied. Brittle failure was experienced by the extend end plate connection, which contributed a lot on it having very limited catenary action. They also emphasised that tensile forces usually dominate the behaviour and the failure modes for joints which could develop well the catenary action. Hence, enhancing the tensile resistances of such joints during large rotations is a vital way to improve a structure's robustness.

A further study by **Yang and Tan** [29] was conducted to numerically model other type of connection configurations (e.g. bolt number and beam cross-section). They were validated by the experimental tests conducted in their previous study [28]. In the numerical simulation, they had various types of connection (e.g. fin plate, flush end plate, TSWA, etc.). However, for the purpose of this project, the discussion will only be limited for the flush and extended end plate.

They conducted both static and dynamic explicit solver in ABAQUS. In some simulations, the dynamic explicit solver was used due to the significant amount of effort that is required to make the system converge for static solver especially for the fracture simulations. In this way, dynamic explicit solver can overcome these difficulties and allows easy pre-processing. The con, however, is that it requires huge computational resources. C3D8R elements were used in the model since it's able to represent large deformations, geometric and material nonlinearities, and fracture simulations.

Results of the flush end plate numerical simulation matched well with the experimental results, as seen on Figure 2.27 and Figure 2.28. It could be observed as well that the explicit dynamic solver projected a slightly lesser elastic stiffness and larger peak load than the other two parameters shown in the graph.

For the extended end plate, on the other hand, failed by weld fracture as shown in Yang and Tan's experimental study [28]. In the numerical simulation, however, the static solver was not able to simulate the weld fracture due to convergence issues (Figure 2.29) unlike in the dynamic explicit solver. Some discrepancies were observed among the three. Moreover, the static solver predicted the behaviour seen on the experimental results much better than the dynamic explicit solver after experiencing 40mm displacement on the column. Due to these discrepancies, the authors focused their study more on the flush end plate connection rather than the extended end plate.

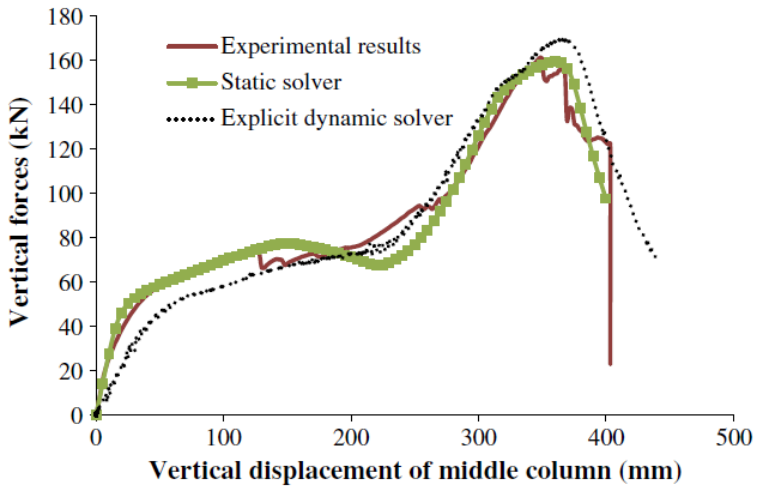

Figure 2.27. Comparison of numerical and experimental testing for flush end plate [28].

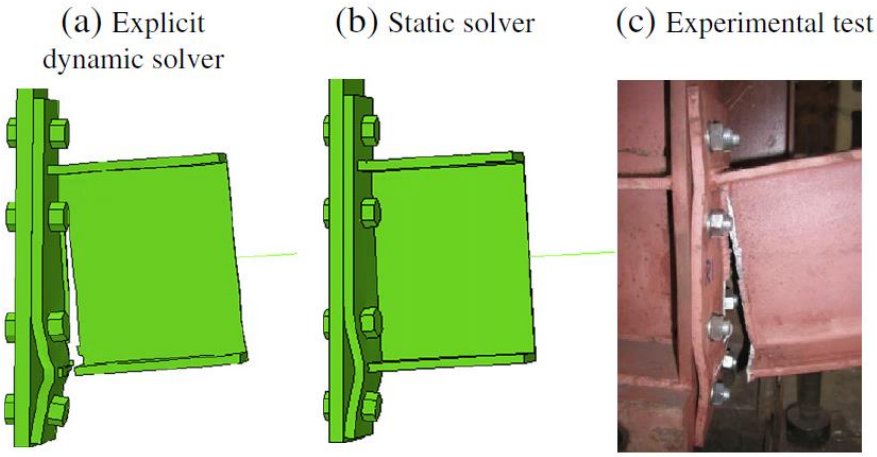

Figure 2.28. Mode failure for extended end plate connection for the numerical and experimental tests

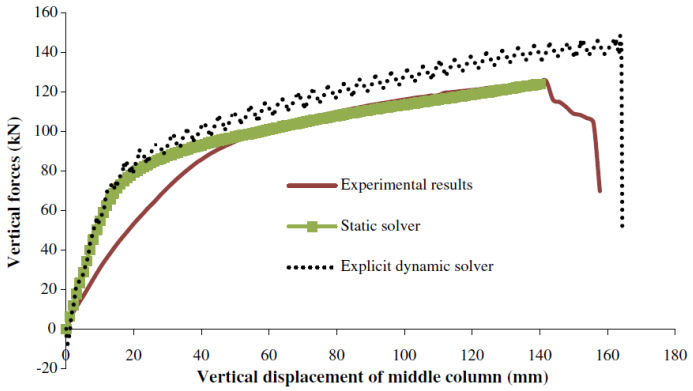

Figure 2.29. Comparison of numerical and experimental results for extended end plate connection [28].

In testing the other configurations of the connection for flush end plate, they modified their original model in two ways: (1) increased the number of bolt rows, and (2) moved the bolts 20mm towards the beam flange and another one by moving 20mm towards the beam centroid. Results show (as seen on Figure 2.30), as bolt rows were increased, the increase of the first peak load is because of the improved flexural resistance. However, the model with the three (3) bolt rows had a larger increase in peak load at the state of larger deformations (e.g. catenary action) than the one with four (4) rows. This is due to the greater rotational capacity of the 3-bolt row connection than the ones with four.

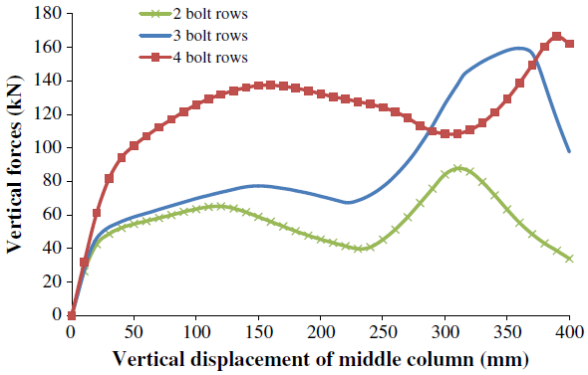

Figure 2.30. Effect of number of bolt rows in the flush end plate connection [28].

Moreover, as seen on Figure 2.31, configuring the bolts closer to the beam centroid increases its load capacity during the catenary action compared with the standard one and the one whose located 20mm

towards the beam flanges. This implies that orienting the bolts to the beam centroid produces a more ductile connection, hence, a stronger connection for large deformations.

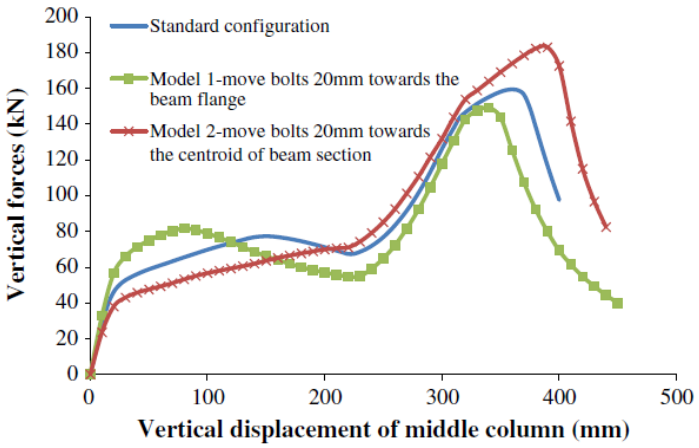

Figure 2.31. Effect of modifying the bolt configuration in the flush end plate connection [28].

Thus, they concluded that during a middle column removal scenario, the number of bolt rows is proportional to the load-carrying capacity and rotation stiffness. However, the connection ductility is also affected as the number of bolt rows is increased, so it is a double-edged effect. Similar case when bolts are moved closer to the beam centroid, it improves its load-carrying capacity but the moment capacity is reduced. Lastly, the also reiterated that similar to the experimental results, the flexural action dominates the applied load at the initial stage. However, as rotation of the joint becomes larger, catenary effect is activated, and the flexural action decreases significantly.

2.4.2 Focus on use of extended end plate connections

Cassiano et al [30] studied the influence of seismic design rules on the robustness of steel moment resisting frames. In their study, they considered MRF structures one designed for wind actions per Eurocode 1 and another one designed for seismic actions in accordance to Eurocode 8. They investigated various parameters (i.e. number of storeys, inter-storey height, span length, building plan layout, column less scenario) to determine their effects on arresting progressive collapse.

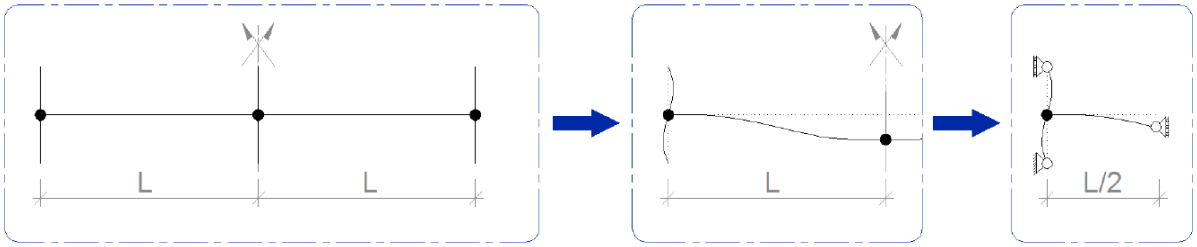

Figure 2.32. Selection of substructure for joint modelling validation

They also conducted numerical investigations for their study. One of the concerns they highlighted is the joint typology. To verify their assumptions for the joints for the global numerical model in SAP 2000, they conducted finite element analysis of the local joint in ABAQUS. Sub-structuring done in the finite element analysis is shown in Figure 2.32. In the model, they considered bolted joints with extended end plates, rib stiffeners, and additional column web panel configurations for the MRF. Meanwhile, flush end plate beam-to-column joints were assumed for the secondary structure. MRF joints are modelled as full-strength rigid joints while gravity designed beams were taken as perfectly pinned at both ends. In the finite element

model, contact phenomena were introduced, considering the general contact algorithm of a Coulomb friction model.

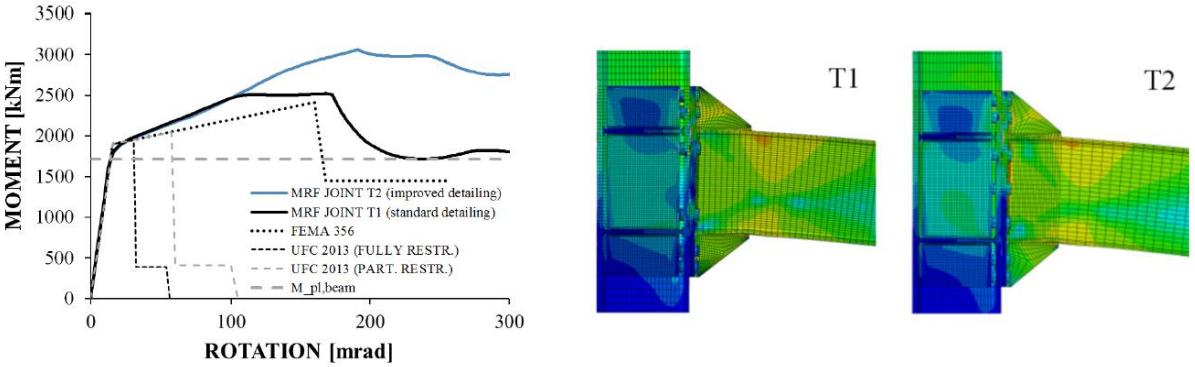

(a) Moment – chord rotation response (b) Deformed shapes (chord rotation = 100 mrad)

Figure 2.33. MRF joints under column loss action

Results showed that the assembly consisting of an IPE 600 beam and an HEB 500 column well represents the MRF, since it was characterized by the deeper beam. Hence, this assembly theoretically develops larger catenary action in the connection. Moreover, the authors emphasised that MRF beam-to-column joints are subjected to important catenary forces after a column loss scenario. Thus, they analysed two MRF joint configurations: (1) a joint with standard detailing (T1), and (2) a joint with improved detailing (T2) consisting of an additional bolt row in the middle of end plate. Figure 2.33 shows the moment – chord rotation response of the connections considered in the analysis.

These curves are compared with the plastic hinge response according to present standards – FEMA 356, UFC 2013, and the beam plastic bending moment $M_{pl,beam}$ in accordance to EN 1998-1 (CEN 2004) seen on Figure 2.33a. The deformed shapes of both joints are also shown in Figure 2.33b, with an imposed chord rotation equal to 100mrad.

Results show that both T1 and T2, being full strength joints, display satisfactory response under column loss action. It can be seen on their results that the bending strength of the joints are higher than the plastic bending moment of the beam $M_{pl,beam}$, even at large rotations. Moreover, the improved detailing of Joint T2 positively contributed on column loss scenario. The FEMA 356 results provide good compliance with the result of Joint T1, affirming the assumed behaviour for MRF. Though it is out of scope of their study, the authors recommended that improving joint detail as in Joint T2 would provide better performance of the structure in larger rotations are tested. They concluded that this will significantly improve the joint capacity under catenary action.

Lastly, the authors found on their study that seismic resistant steel MRF structures do not generally guarantee levels of robustness compatible with arresting progressive collapse. That is why joints must be able to resist to catenary actions, in which their analyses pointed out that both strength and stiffness of beams are crucial for improving robustness.

Dinu et al [3] conducted an experimental test of 3D steel frame system under column loss. To validate their results, a numerical analysis was done thereafter using the software Extreme Loading for Structures (ELS). In their experiment shown in Figure 2.34, monotonic loading is applied on top of the central column until complete failure.

For the connections, they used an extended end plate bolted connections (Figure 2.35) since that joint typology is commonly used in steel infrastructures in Europe. They were designed as fully rigid and fully

restrained connections. Their study showed that lack of the upper continuity (in real cases, when damage extends to the upper column or the lost column is in the top floor) limits the joint rotation. If the central column is prevented fully from rotation, deformation demands are equally distributed between the connecting beam ends. Therefore, the rotation demands are smaller than for the case in their study. They also emphasized that chord rotations are very useful in evaluating the structure's deformation capacity.

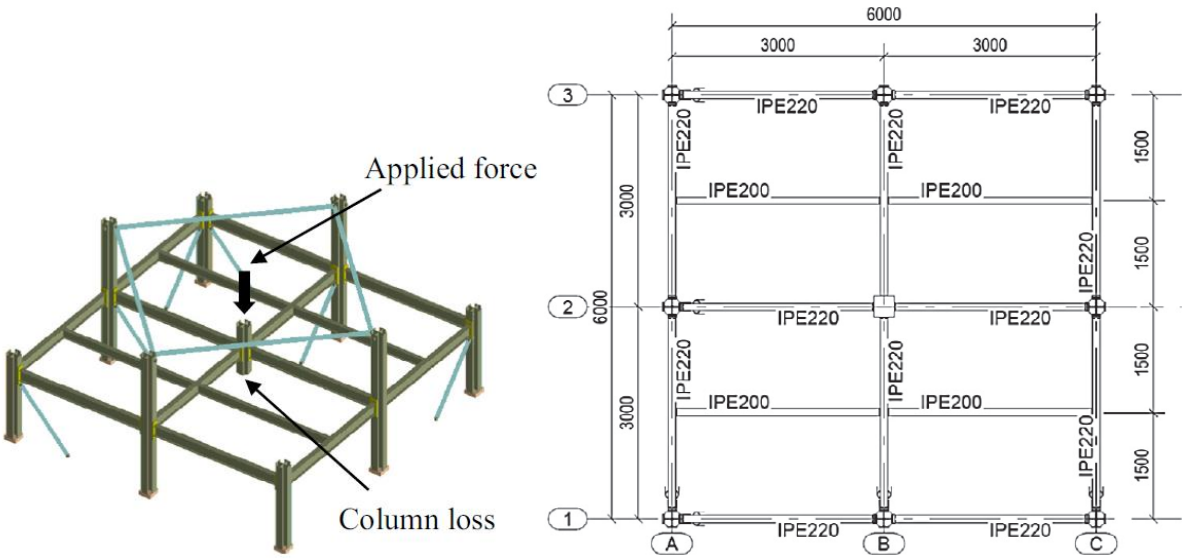

Figure 2.34. Isometric (left) and plan (right) view of the specimen in Dinu et al's experiment [3].

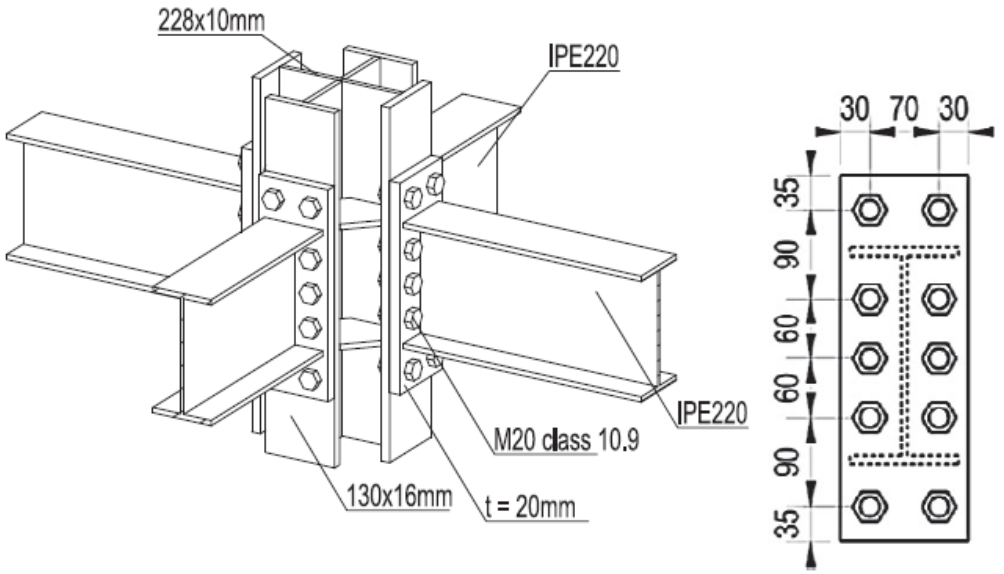

Figure 2.35. Connection detail used in the experiment [3].

Figure 2.36 shows the vertical displacement at different locations along internal beams after the test. It can be observed that a column displacement of 569mm, the bottom tension flange of the B2-B3 beam ruptured near the beam-to-column connection, with a corresponding rotation of θ = 206 mrad, even though the beam connection did not show any damages. Actual failure is shown in Figure 2.37. The obtained ultimate rotation agrees to the **US Department of Defense**'s recommendation [31], where the ultimate or fracture rotation for low level of protection LLOP is 210 mrad.

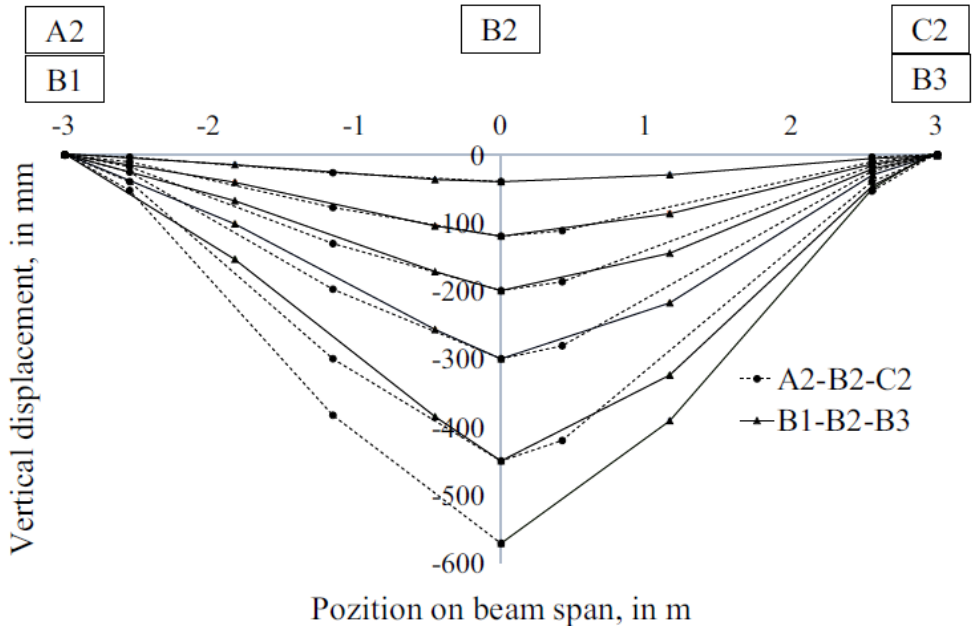

Figure 2.36. Vertical displacement at different locations along internal beams [3]

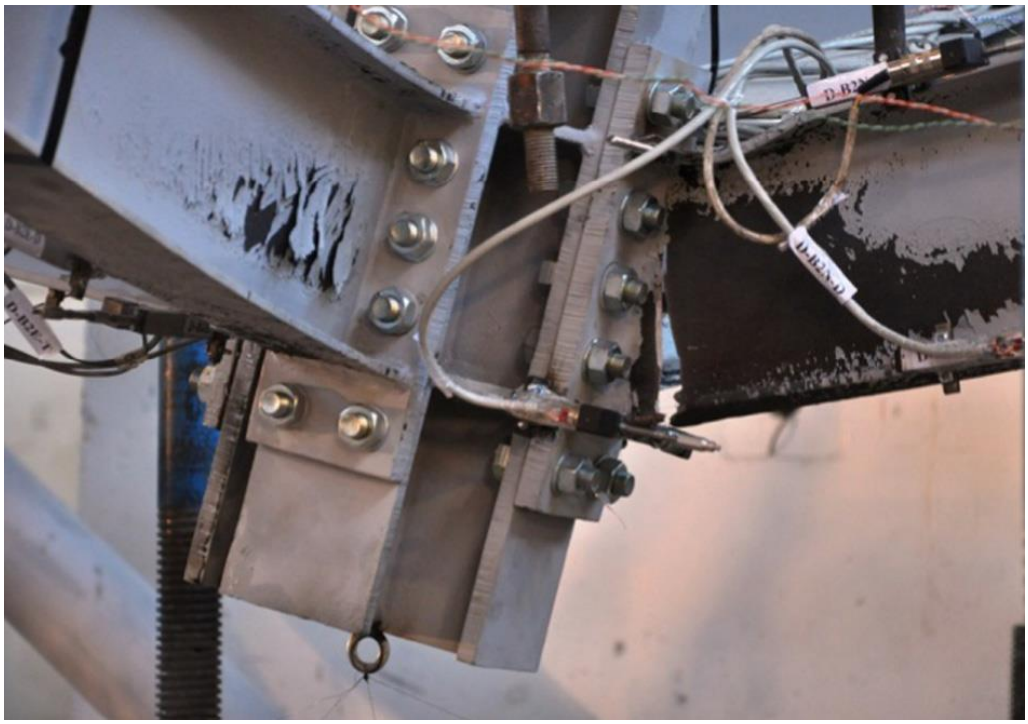

Figure 2.37. Failure of beam B2-B3 near internal end B2 [3].

However, in the requirements of Collapse Prevention Limit State (CPLS) in accordance to **ASCE 41** [32], the required rotation is 8 x θ_y, where θ_y is the yield rotation. Using this standard, the result of their test will only yield to 68 mrad. Previous studies highlighted that to utilize the catenary action in beams, rotations should be 70 mrad or more. The authors emphasized that the standards in ASCE 41 are just mainly applicable for seismic rehabilitation of buildings, assuming cyclic loading. But it is reiterated in most studies on column loss that such behaviour is monotonic. That is why in-depth study on behaviour of joints under column loss must be continually done to constitute a standard that can be adopted in a column loss scenario, where catenary action is used to increase the capacity to resist external loads. They also stated from their observations that the development of catenary forces in beams, in a sudden column loss scenario, depends on whether the adjacent structure is capable to support these forces. If the beam is

connected to a strong structure, the tying resistance of the connection must be evaluated. Otherwise, the capacity of the column to resist catenary forces must be verified.

After reaching a vertical displacement of 230 mm, the axial forces in the beams increase rapidly while the bending moment decreased. The joint then proved to behave excellently and could obtain enough strength to resist catenary forces developing in the beams. An implication of this is that the beam's tying resistance is significant in designing the column to avoid any propagation of failure to adjacent columns.

Moreover, the numerical modelling is also done by **Dinu et al** [3]. The model is shown in Figure 2.38. Results show an excellent correlation with the experimental results as shown in Figure 2.39. All stages that occurred in the experiment were seen in the numerical results as well – elastic behaviour, plasticity, initiation of catenary force, and eventually failure. The authors also emphasized that the catenary action will only be effective if the joints can sustain large actions and large axial forces.

Lastly, the authors also found that the distribution of axial forces among the bolt rows are significant in designing a joint for robustness. In their numerical study, it is found that the bolts experiencing the largest tension are from the second bolt row from the top flange for the external beam ends and the second bolt row from the bottom flange for the internal ends. However, combined effects of the tensile load and prying action could still trigger failure first of the first bolt rows.

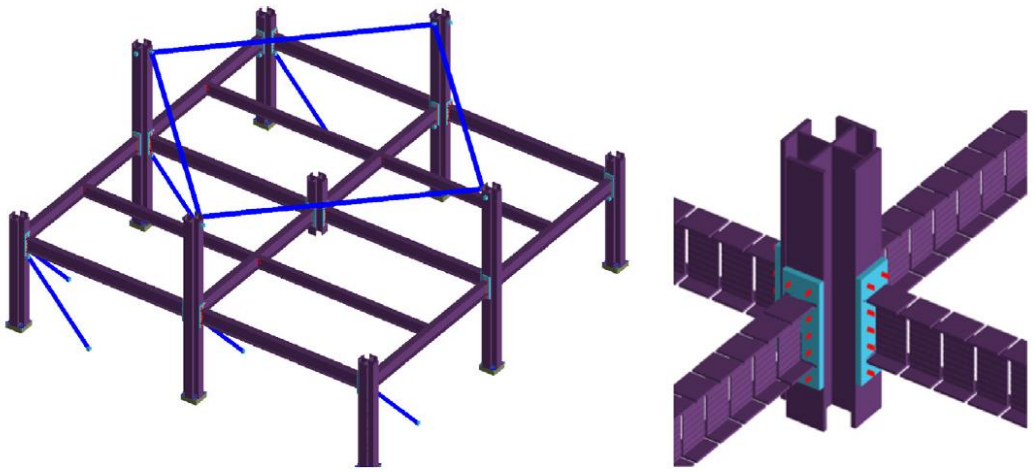

Figure 2.38. Applied element model of the experimental setup [3].

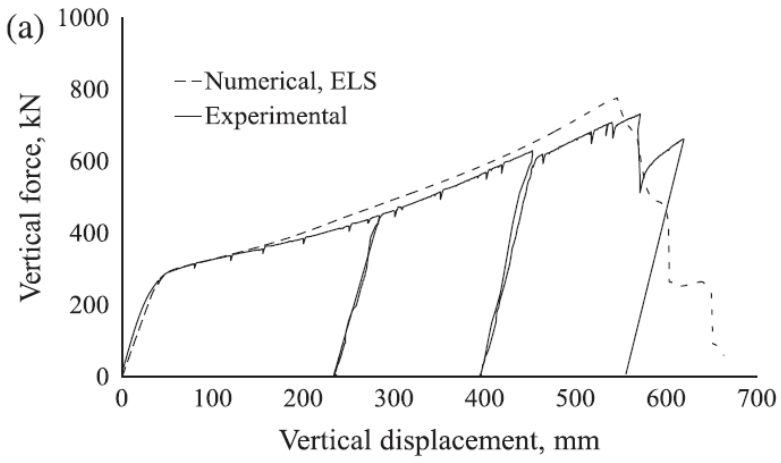

Figure 2.39. Experimental vs numerical curves (vertical force-vertical displacement) [3].

Another recent study conducted by **Tartaglia et al** [33] was done to determine the nonlinear performance of extended stiffened end plate (ESEP) bolted beam-to-column joints subjected to column removal. Their research emphasized the need to focus on robustness studies regarding ESEP since it is a widely-used type of connection both in the US and Europe. Their work showed how significant numerical analysis is in furthering our knowledge on joint detailing.

In their study, they generated numerical models of a local joint, subjecting it to a sudden column removal scenario. The numerical analysis is done on ABAQUS software where the sub-structuring and boundary conditions are shown in Figure 2.40. The results of their numerical analysis are validated from experimental tests available from literature (i.e. **Shi et al's** [24] experimental work).

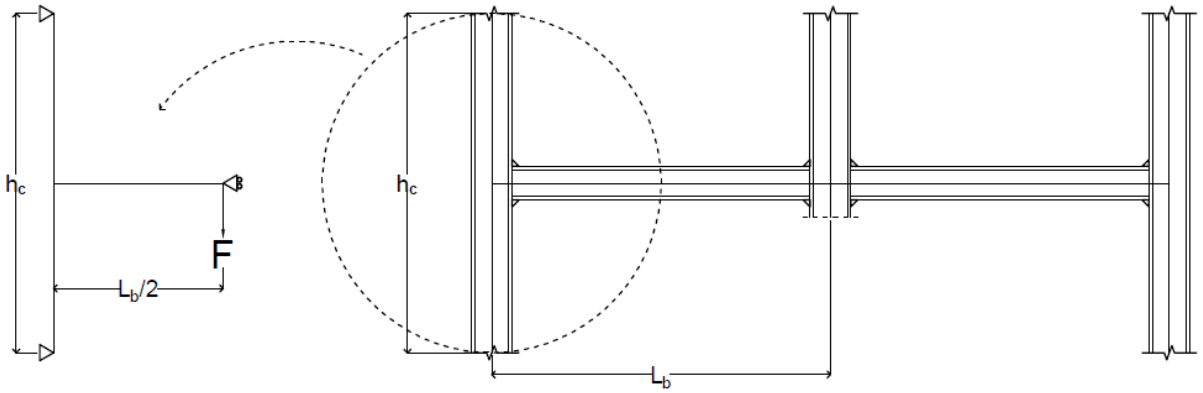

Figure 2.40. Sub-structuring of the column loss scenario [33].

Table 2.5 show the comparison of the numerical and experimental response of their work vs Shi et al's work (results shown in Table 2.4). Numerical predictions accurately match both the response curves and failure modes.

Specimen [-]	Moment Resistance		Elastic Stiffness		Failure Mode [-]
	Tests [kNm]	FEM [kNm]	Tests [kNm/rad]	FEM [kNm/rad]	
EPC-1	343.7	340.3	52276	52276	Bolts fracture
EPC-2	322.1	318.7	46094	46097	Bolts fracture
EPC-3	390.3	387.5	46066	46070	Buckling of beam flange and web in compression
EPC-4	410.8	409.3	47469	47460	Buckling of beam flange and web in compression
EPC-5	355.4	355.2	41634	41631	Bolt fracture; Buckling of end-plate rib stiffener

Table 2.5. Experimental results vs FEM predictions

Moreover, they conducted a parametric study under column loss scenario, where they investigated the effect of the bolt's steel grade and the influence of adding a bolt row in the mid end plate. As previously stated in Section 2.3.2, the addition of bolt rows was concluded to be insignificant when the structure is under pure bending actions (i.e. wind or seismic actions). However, in this study, results showed that the presence of the additional bolt row increases the tensile capacity of the joint, therefore improving both its ductility and strength. Their study of various models shows the significant increase of moment capacity when a 4BR (regular number of bolt rows) and a 5BR (additional bolt row in the middle) are compared in their study.

The steel grade, on the other hand, per Tartaglia et al, positively affected the performance of the joints under column loss scenario. Stronger bolts allow the development of prying forces, which modifies the mechanism of bolt rows in tension from failure mode 3 to 2, encapsulating the catenary action in the beam.

This is also highlighted for failure mode 1, where using stronger bolts gives way for the damage to be concentrated only on the end plate, assuring a larger rotation capacity.

Lastly, like other authors focusing on robustness action, they accentuated the importance of catenary action when designing structures. The ductility of the connection allows development of such action. Ductile response is observed when prying action takes into place. Following a column removal, catenary action modifies the forces acting on the joint.

Chen [34] conducted a numerical study to determine the performance of rigid and semi-rigid steel frame structure in progressive collapse. They also focused their study on a bolted end plate connection with one side extended (Figure 2.41). Using the software ANSYS, they generated numerical simulations, comparing rigid joints with that of semi-rigid ones. Results show that initial stiffness and ultimate bearing capacity of the rigid joint is 9.8% and 7.1% larger than the semi-rigid joint, respectively. The issue with the rigid joint, however, is the brittle fracture that occurred in the succeeding stages of the analyses. The semi-rigid joint, moreover, has better ductility than the rigid joint, which is an indication of better development of catenary mechanism.

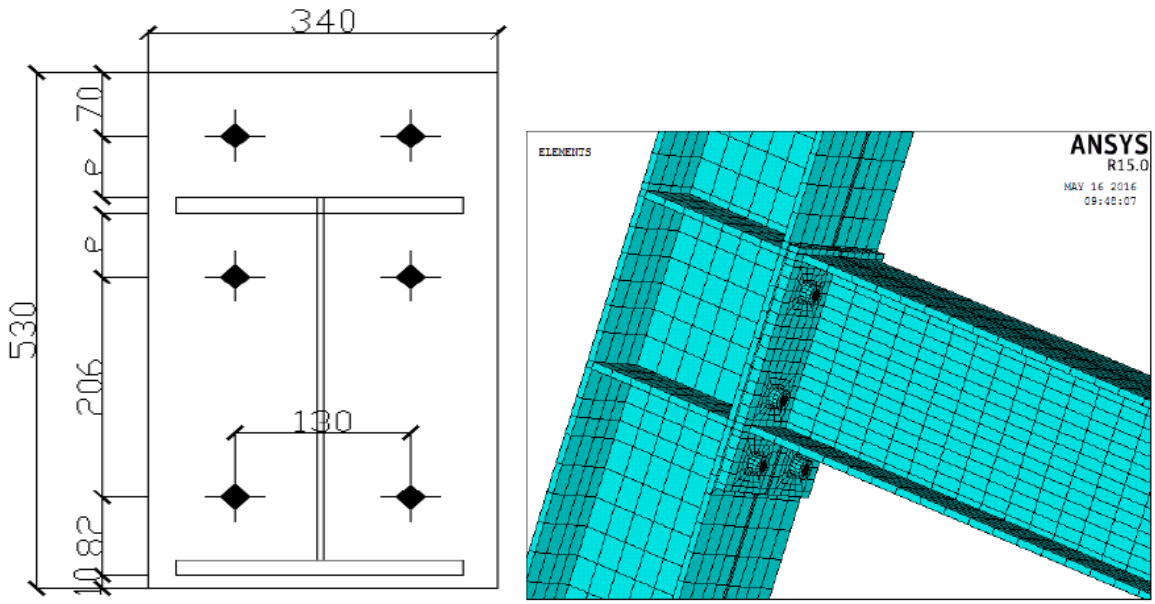

Figure 2.41. Geometry of the end plate (Left) and the finite element model in ANSYS (Right) [34].

Moreover, using SAP 2000, a comparison of the semi-rigid and rigid joints is further established by Chen. Results of the analysis show that the failure pattern of semi-rigid frame structure under collapse load is relatively more ideal than rigid joints since plastic hinges developed fully more than the other. This means that the ductility is higher and energy is more dissipated.

Chen concluded that semi-rigid joints have better capability in energy dissipation but since it is less stiff, careful design must be done since displacement could end up larger. Due to its better ductility, they have better behaviour for catenary action under progressive collapse. Rigid joints have better stiffness. It can generate effective support for the structure above the joint under collapse, making the structure enter a more stable state. However, rigid joints are more prone to brittle failure.

3. DESIGN REGULATIONS ON ROBUSTNESS

3.1 Various approach on robustness

Zdeněk [35] compiled various approaches in dealing with robustness. First is the damage control design is an approach in which each structural element is designed to withstand accidental actions, either by strengthening each element or installing protection. This is deemed a conservative approach, hence, uneconomical for most cases. Several government buildings, however, are designed in this method. This approach prevents progressive collapse, since the structural integrity of the building is designed to avoid destruction even when one member is impaired. Connections are critical on this approach since it can transfer tensile forces, providing continuity and ductility, rotational capacity wise.

The alternative load path method is a specific approach in which the redundancy of the system is utilized via Vierendeel action (Figure 3.1 a to c). The key element method, on the other hand, is an approach by which the structural integrity and general stability of the structure is provided by the key elements. This is often used in huge trusses as seen on Figure 3.1 d and e.

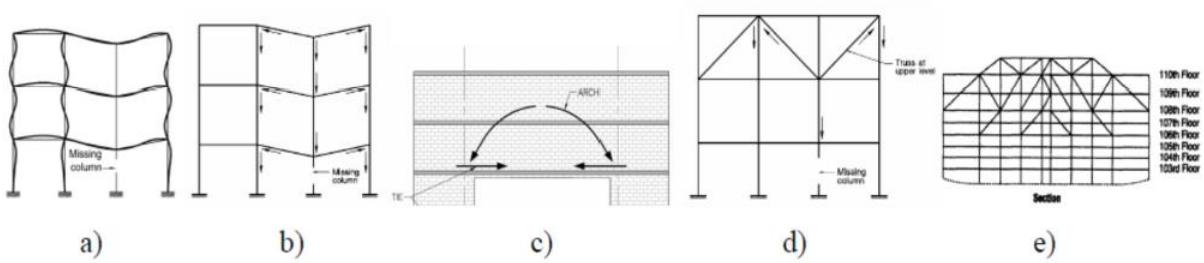

Figure 3.1. Supplementary load transfer routes [35]

3.2 British Standards [36]

After the incident of Ronan Point building, the British Standards (BS) took the initiative in designing structures under extreme load conditions, specifically against progressive collapse. BS highlighted on general tying (indirect method) of a building's several structural elements together, providing continuity and redundancy. It gave recommendations to reduce the risk of localized damage spreading. It indicated that ties provide ample enhancement on the resistance of wall panels and its debris to be sparsely scattered in the event of an explosion. It also focuses on the capability of a structure to sustain itself after loss of a support. With this approach, structural elements are considered missing one at a time. In addition, more vital structural elements must be designed as key elements (direct method), with the ability to endure accidental loads (e.g. pressure of 34 kPa). This standard became the foundation for Eurocode's take on robustness.

3.3 US Department of Defense (DoD) Unified Facilities Criteria (UFC) [37]

In this standard, design for resistance to progressive collapse is reliant on the "Levels of Protection (LOP)" assigned to the building. LOP is defined as the "degree to which an asset (e.g., a person, a piece of equipment, or an object, etc.) is protected against inquiry or damage from an attack." For example, the UFC standards provide a "Low LOP for billeting, high occupancy family housing, and primary gathering buildings and Very Low LOP for other inhabited buildings. Greater protection is provided for primary gathering buildings, billeting, and high occupancy family housing because of the higher concentration of personnel and the more attractive nature of the targets."

For lower levels of protection, the indirect design method is used by providing minimum tie forces. For higher levels, the alternate load path is applied if sufficient ties are not provided.

3.4 Eurocodes

The Eurocode EN 1990 [38] categorizes each type of infrastructure according to consequence class for accidental loading as seen on Table 3.1.

Consequences Class	Description	Examples of buildings and civil engineering works
CC3	**High** consequence for loss of human life, *or* economic, social or environmental consequences **very great**	Grandstands, public buildings where consequences of failure are high (e.g. a concert hall)
CC2	**Medium** consequence for loss of human life, economic, social or environmental consequences **considerable**	Residential and office buildings, public buildings where consequences of failure are medium (e.g. an office building)
CC1	**Low** consequence for loss of human life, *and* economic, social or environmental consequences **small or negligible**	Agricultural buildings where people do not normally enter (e.g. storage buildings), greenhouses

Table 3.1. Consequence class per Eurocode [38]

It provides strategies and rules for protecting buildings and other civil structures against both identifiable and unidentifiable accidental actions. Strategies under the Eurocode range from methods to mitigate, if not prevent, the accidental action to the structural design to resist the action. Two strategies are presented in the Eurocode with regards to accidental design condition:

1. Based on identified extreme events (e.g. internal explosions, impact, etc) which includes:
    a. design of the structure to have satisfactory robustness
    b. prevention and/or reduction of the intensity of the action (protective measures)
    c. design the structure to sustain the action'
2. Based on unspecified causes, limiting the degree of local failure:
    a. Design the structure with enhanced redundancy (alternative load paths)
    b. Design key elements
    c. Apply prescriptive design/detailing rules (integrity, ductility)

Consequence class	Example of categorisation of building type and occupancy
1	Single occupancy houses not exceeding 4 storeys. Agricultural buildings. Buildings into which people rarely go, provided no part of the building is closer to another building, or area where people do go, than a distance of $1^1/_2$ times the building height.
2a Lower Risk Group	5 storey single occupancy houses. Hotels not exceeding 4 storeys. Flats, apartments and other residential buildings not exceeding 4 storeys. Offices not exceeding 4 storeys. Industrial buildings not exceeding 3 storeys. Retailing premises not exceeding 3 storeys of less than 1 000 m^2 floor area in each storey. Single storey educational buildings All buildings not exceeding two storeys to which the public are admitted and which contain floor areas not exceeding 2000 m^2 at each storey.
2b Upper Risk Group	Hotels, flats, apartments and other residential buildings greater than 4 storeys but not exceeding 15 storeys. Educational buildings greater than single storey but not exceeding 15 storeys. Retailing premises greater than 3 storeys but not exceeding 15 storeys. Hospitals not exceeding 3 storeys. Offices greater than 4 storeys but not exceeding 15 storeys. All buildings to which the public are admitted and which contain floor areas exceeding 2000 m^2 but not exceeding 5000 m^2 at each storey. Car parking not exceeding 6 storeys.
3	All buildings defined above as Class 2 Lower and Upper Consequences Class that exceed the limits on area and number of storeys. All buildings to which members of the public are admitted in significant numbers. Stadia accommodating more than 5 000 spectators Buildings containing hazardous substances and /or processes

Table 3.2. Categorisation of consequence classes [2]

The consequence classes (CC) presented in Table 3.1 may be used as the basis on strategizing design for accidental design situations. Moreover, EN 1991-1-7 [2] presents a more specific categorisation of consequence class as seen on Table 3.2.

3.4.1 Consequence Class 1

CC1 requires no specific consideration is necessary for accidental actions except to ensure that the robustness and stability rules given in EN 1990 to EN1999, as applicable, are met;

3.4.2 Consequence Class 2

3.4.2.1 Tie-force based design methods

Tie-force methods are generally designed for low-risk structures. The idea is that in this method, the engineer is to design the detail of the structure in such a way that the members are tied together corresponding to stated requirements. As a result, it provides improved degree of ductility, load transfer, and continuity to other members of the structure.

CC2, depending upon the specific circumstances of the structure, may adopt a simplified analysis by static equivalent action models or apply a prescriptive design/detailing rules. CC2a (lower risk group), more specifically, requires effective horizontal ties or effective anchorage of suspended floors be installed. The provision differs for framed and load-bearing wall construction, as indicated in the Eurocode [2].

CC2b (lower risk group) requires effective horizontal ties (like in CC2a) together with effective vertical ties tied continuously to each column and wall from foundation to roof level. Additional provision is also different for framed and load-bearing wall construction for vertical ties. The concept of vertical tying perceived to be a method to assist with large-panel structures, but it is also proven useful for framed structures to allow vertical continuity in columns. This way, load can be reallocated in case of loss of stiffness or strength due to impairment of the structure. It is noteworthy to know that tying is generally scarce if the designer wants to provide ample resistance against progressive collapse. It just provides a minimum level of robustness.

One important thing about tying method is that it is more of a prescriptive approach, rather than deterministic or quantitative, wherein submission with the “prescribed” rules is taken to be satisfactory for the structure to meet the standards.

Another option for CC2b is to ensure that during column removal, each supporting column and each beam supporting the column, one at a time in each storey, remain stable and no local damage exceeds a certain limit.

3.4.2.2 Alternative load path methods

Aside from the prescribed methods mentioned, the alternative load path is another means for robustness design. It is a deterministic/quantitative approach rather than tying method’s more prescriptive style. The basic concept of this approach is the analytical evaluation of an impaired structure (i.e. partial or total loss of load-bearing capacity of a beam/column), assessing whether an alternative load path in structure can redistribute the additional loads. For example, in a column loss scenario, the gravitational loads the column was sustaining before will be reallocated to the floor beams and then to the still structurally intact column. If the residual capacity of such lost columns and its corresponding connections are not enough to sustain the additional loads, failure will then happen and collapse will eventually spread.

Cormie et al [39] enumerated and illustrated (Figure 3.2) five mechanism that are deemed fundamental to robustness – (1) catenary action in the structural frame, (2) shear deformation of transfer structures, (3) membrane action in structural slabs, (4) Vierendeel action, and (5) compressive arching in the beams and/or floor slabs. Structures will experience successful redistribution of load via alternative load paths if these mechanisms are mobilised.

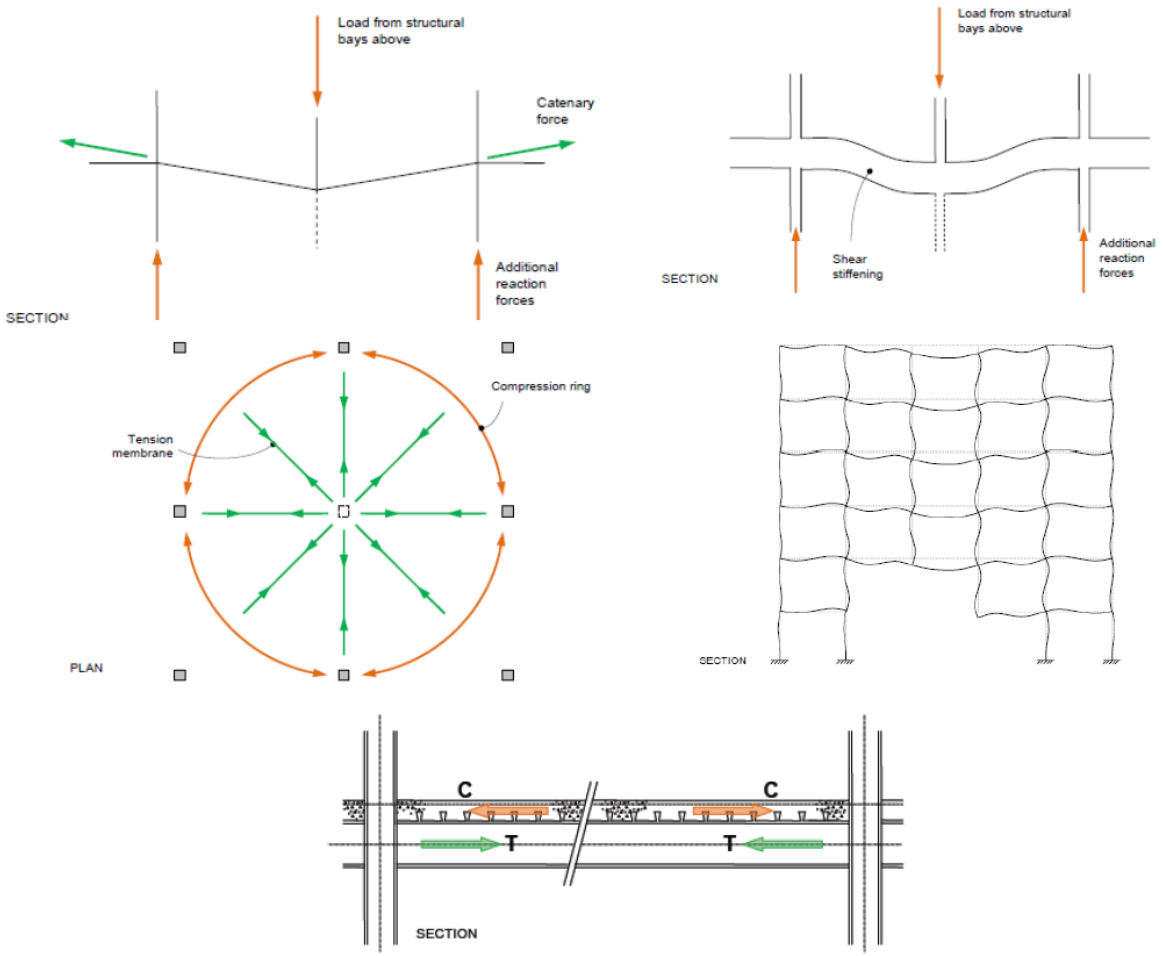

Figure 3.2. The five mechanisms fundamental to robustness problem [39]

3.4.2.3 Key element design

In cases when the notional removal of such columns and wall sections lead to a damage that is more than the agreed limit stated, these elements must be designed as a "key element". EN 1991-1-7 [2] requires that these key elements should be designed to sustain an accidental load A_d, applied in horizontal and vertical direction (one at a time). [2] recommends a value of 34kN/m^2 for A_d.

This method can be done independently for disproportionate collapse, although it is preferably used is alternative load path is not viable [40]. It is an approach that varies according to the situation, hence, scenario-specific. The element must be designed to endure the load applied without experiencing failure. According to **Kovecsi** [40], this method typically represents a cliff-edge in the capacity of a structure, that after surpassing the limit, a sudden loss in stiffness and strength is experienced, rather than a ductile response which is more gradual. In both the US and UK, this method is typically the last resort, when robustness cannot be done by other means.

3.4.3 Consequence Class 3

For CC3, a systematic risk assessment of the building must be done, accounting in the evaluation all the normal hazards that are foreseen, together with the abnormal hazards. Use of refined methods like dynamic analyses, non-linear models, and interaction between the load and the structure may be done. Hence, no specific requirement is prescribed by the code. Only the authorities and/or stakeholders (e.g. building owners, users) can initiated the assessment. General guidelines are still provided in [2] while some aspect and examples are available in ISO.

The methodology of [38] may be used as a basis on the risk assessment, comprising of three steps:

1. Assessment of the probability of occurrence of several hazards with various intensities
2. Assessment of the damage states to structure from various hazards. Evaluation of the probability of various damage states and their associated consequences
3. Assessment of the probability of insufficient performance(s) of the impaired structure together with its associated consequences

Additional measures are also proposed in the Eurocode to minimize the risk, stated as follows:

1. Prevent occurrence or decrease intensity of the hazard
2. Monitoring of the hazard to control it
3. Avoidance of collapse by changing the structural system
4. Overcoming of the hazard by enhanced strength and robustness, availability of alternative load paths by redundancies, and so on
5. Controlled failure of the structure, if the risks to human life is low.

4. THE FINITE ELEMENT MODEL

As highlighted before, joint behaviour in a structure is very vital as it provides a great impact on a structure's performance. Over the years, experimental testing is still an excellent way to investigate such behaviour. It could easily simulate the actual structure while just being in the laboratory. However, it also has its cons especially when time and cost are taken into account. When different variables are considered in an experimental setup, the investigation would require more time and cost. However, with the available technology of today's world, the numerical method via Finite Element Method software is a powerful tool that can work hand in hand with experimental work. Accurate results can be generated for as long as they are verified with the experimental one.

In this study, the same process is implemented. A structural joint is modelled in the Finite Element software ABAQUS. To achieve accuracy, the geometry and constraints simulated in the model are the same as the one used in the experimental setup by **Shi et al** [24], explained in Section 2.3.1. Similar process to the study conducted by **Tartaglia et al** [33] and **Zimbru** [14] is implemented in the present study. The **ABAQUS/CAE User's Guide** [41] was also used in further elaborating the choices done in the finite element modelling.

4.1 Model geometry

The part that is modelled in ABAQUS is just up to where the constraints are in the experimental setup (Figure 2.17). Since the focus is just the connection itself, the stiffeners at the beam and column end sections aren't defined in the model. To ease the modelling of the joint in the software, Autodesk's AUTOCAD was used first to define the whole geometry and export it afterwards to a file readable by ABAQUS. Table 4.1. Geometry of the connection implemented in ABAQUS below shows the various geometries of the beam-column connection modelled in ABAQUS. Figure 4.1 shows the general typology of the connection to be

modelled. The geometry of the ES2 models are shown in Figure 4.2 to show the difference in geometry in terms of bolt spacing of the full-strength joints with the equal and partial strength joints

Joint assembly	Joint ID	Design Criteria	End-Plate			Rib		Bolt diameter	Bolt spacing				Continuity plates		Supplementary web plate	
			H	B	t	b	a	d	e	w	p_1	p_2	b_{CP}	t_{CP}	Side	t_{swp}
			mm	mm	mm	mm	mm	mm	mm	mm	mm	mm	mm	mm	-	mm
IPE360 – HEB 340	ES1-F-C1	F	760	260	25	200	235	30	50	150	75	160	222	14	2	8
	ES1-E-C1	E	600	280	18	120	140	27	50	160	160	180	222	14	1	8
	ES1-P-C1	P	600	280	16	120	140	27	50	160	160	180	222	14	-	-
IPE450 – HEB 500	ES2-F-C1	F	870	280	25	210	250	30	50	150	75	180	234	15	2	10
	ES2-E-C1	E	770	300	20	160	190	30	55	160	200	260	234	15	1	8
	ES2-P-C1	P	770	300	18	160	190	30	55	160	200	260	234	15	-	-
IPE600 – HEB 650	ES3-F-C1	F	1100	280	30	250	295	36	55	160	95	210	232	20	2	15
	ES3-E-C1	E	1100	300	22	250	295	36	55	160	95	210	232	20	1	15
	ES3-P-C1	P	1100	300	20	250	295	36	55	160	95	210	232	20	-	-

Table 4.1. Geometry of the connection implemented in ABAQUS

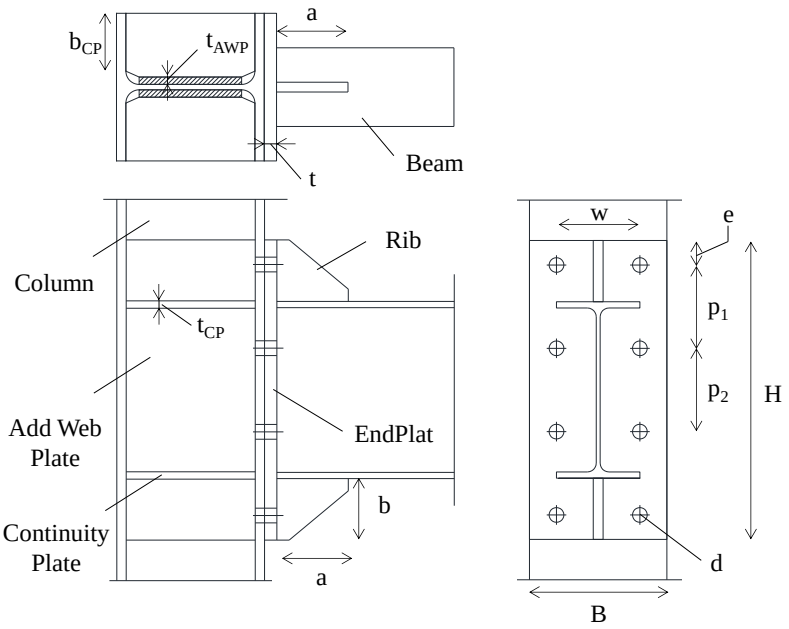

Figure 4.1. Different 2D views of the connection detail

- Rib thickness 20mm everywhere
- Column height: 3745mm
- Beam length: 3260mm (IPE 340); 3223mm (IPE 450); 3150mm (IPE 600)

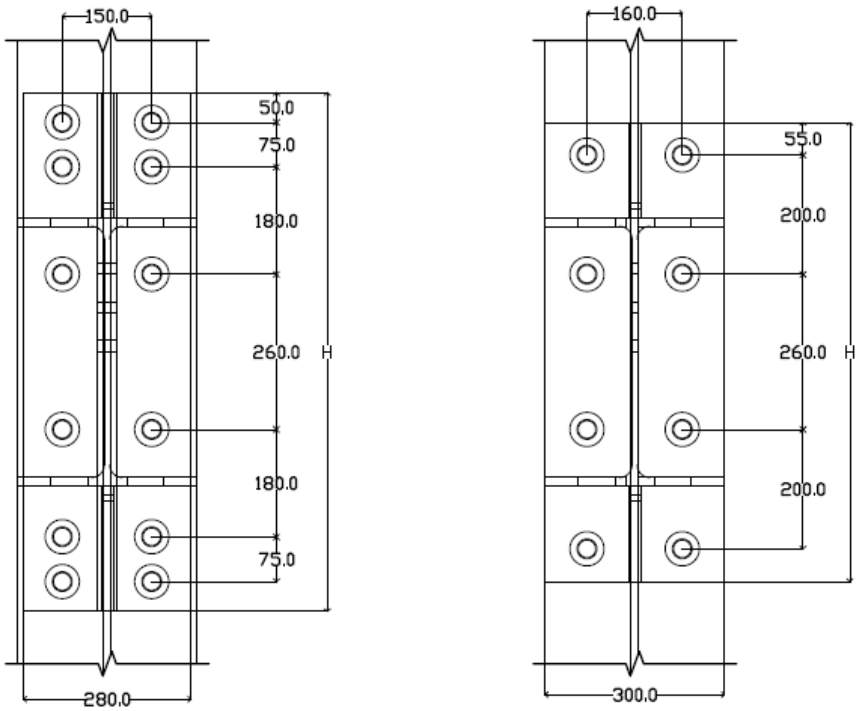

Figure 4.2. Geometry of full-strength joints (left) and partial/equal-strength joints (right)

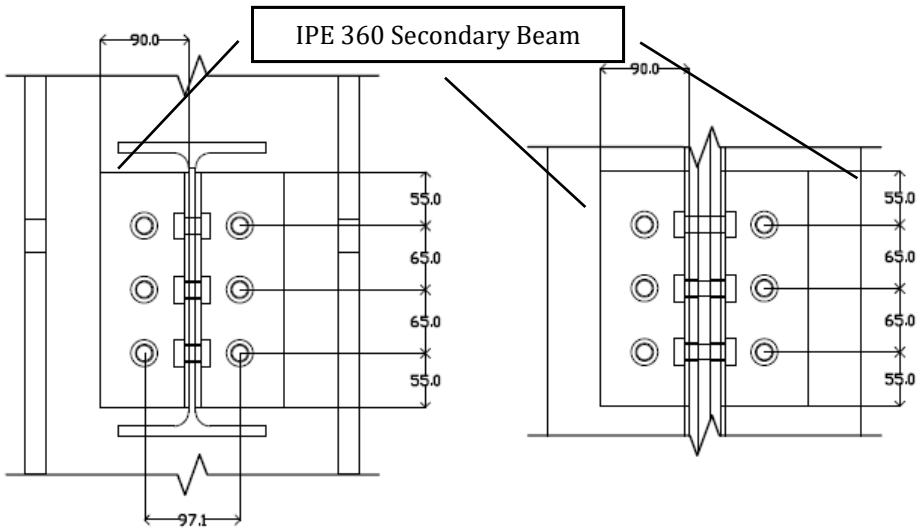

Figure 4.3. Side view (left) and front view (right) of the connection with the secondary beam and column

Figure 4.3 shows the bolt spacing used to connect the secondary beams with the column. All secondary beams in the models are IPE 360 and the angular plates are L90x90x5 (Figure 4.4). The thickness of the shank connecting the secondary beam with the angular plate is constant at 97.1mm. The bolt connecting the secondary beam with the column and the additional web plate (if applicable), is dependent on each case. Summary of the details are in Table 4.2.

Secondary Beam	IPE 360, S275
Angular Plate	L 90x90x5, S275
Bolts	M16 (110 kN pre-load force), Grade 10.9

Table 4.2. Properties on the secondary beam-column joint

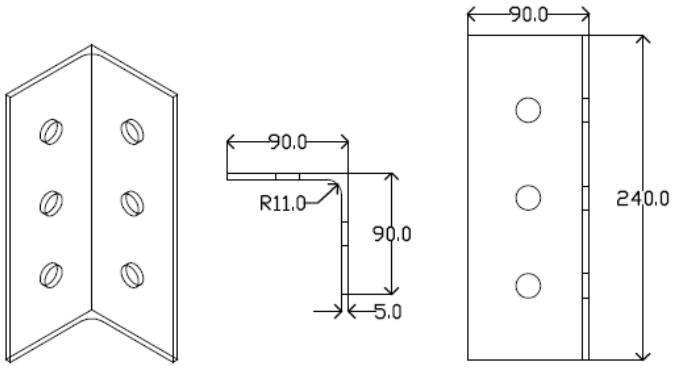

Figure 4.4. Geometry of the angular plate

It has been mentioned before that numerical analysis is an excellent tool that could lead to accurate results without compromising the results that could be gathered from experimental tests. However, due to its sophistication, a large amount of processing and running the analysis is required for 3D solid models. Welds are incorporated in the model via the Constraints interaction, which is discussed on Section 4.6.

4.2 Units

ABAQUS has no system for units of measurement. Therefore, the units must be carefully and consistently assigned since irregularities in the result could arise by just having the units mistaken along the process. Table 4.3 shows the units used in the study.

Measurement	**Length**	**Force**	**Stress**	**Density**	**Elastic Modulus**
Unit	mm	N	N/mm^2	N/mm^3	N/mm^2

Table 4.3. Units implemented in ABAQUS

4.3 Element type and other modelling assumptions

The finite element type C3D8R (8-node linear brick, reduced integration with hourglass control, solid element) was adopted for the whole model. This is the default selection of ABAQUS and was intended to be used in the model since it uses a lower-order integration to form the element stiffness. Hence, it reduces running time, especially for 3D models. Generally, it also yields more accurate results than the corresponding fully integrated elements but it would still depend on the nature of the problem. As mentioned in Section 2.4.1 in **Yang and Tan's study** [29], C3D8R elements were more advantageous since it is able to represent large deformations, geometric and material nonlinearities, and fracture simulations.

To further produce accurate results, both geometrical and mechanical nonlinearities were considered. External restraints and other boundary conditions are discussed in Section 4.7.2.

4.4 Material

4.4.1 Steel

For all elements (column, primary beam, web plate, ribs, continuity plates, and end plates), the following properties in Table 4.4 are applied. Steel grade S355 was used for the primary beams, columns, end plates, continuity plates, additional web plates, and rib stiffeners while S275 for the secondary beams and angle plates. An average yield stress approximately valued at $1.25f_y$ in accordance to EN 1998-1 is assumed.

Property	Value
Mass density	7.85 kN/m^3
Young's modulus of elasticity	210 GPa
Poisson's ratio	0.3

Table 4.4. Steel properties

Moreover, the steel's stress-strain curve used in the yielding behaviour input in ABAQUS was based on experimental tests reported in **Dutta et al's study** [42]. They replicated low-cycle fatigue (LCF), and evaluated specific fatigue parameters that is deemed viable for predicting fatigue lives on uniaxial load. Cyclic elastic-plastic stress-strain responses were utilized by means of incremental plasticity methods. Both the experimental and numerical simulations matched results, leading to a conclusion that forecasting the fatigue life is not only dependent on the typical fatigue damage models, but also on assessment of the cyclic elastic-plastic stress/strain responses. Moreover, it is modelled using von Mises yield criteria. This is to simulate a mechanical response that shows a more realistic behaviour. In the ABAQUS model, plastic hardening is characterized as nonlinear kinematic and isotropic hardening components as emphasized in Wang et al's study [43].

Table 4.5 and Table 4.6 shows the stress-strain relation of steel Grades S355 and S275, respectively, which is adopted from actual test results of their study.

Stress, MPa	Strain
443.75	0
457.25	0.02998
473.37	0.03384
489.69	0.03789
506.42	0.04249
523.88	0.04822
541.51	0.05391
561.14	0.06286
582.12	0.07358
604.80	0.08649
632.97	0.10733
665.86	0.13388
692.75	0.16399
729.69	0.21359
739.71	0.22959
747.91	0.24534
752.19	0.27989
0.00	0.28

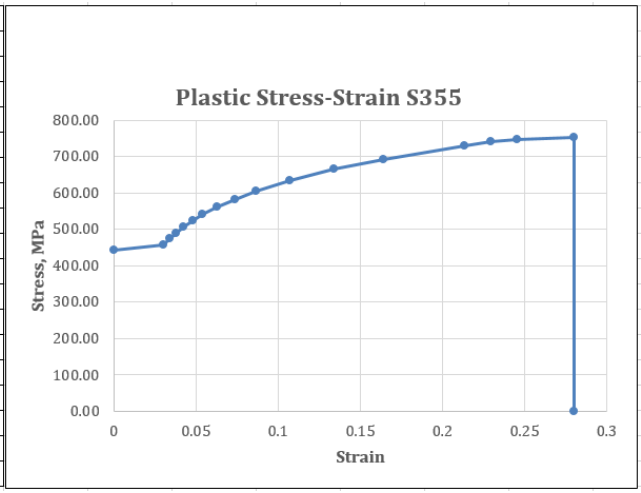

Table 4.5. Stress-strain relationship of Steel Grade S355

Stress, MPa	Strain
343.75	0
354.21	0.02998
366.70	0.03384
379.34	0.03789
392.30	0.04249
405.82	0.04822
419.48	0.05391
434.69	0.06286
450.94	0.07358
468.51	0.08649
490.33	0.10733
515.81	0.13388
536.64	0.16399
565.25	0.21359
573.01	0.22959
579.37	0.24534
582.68	0.27989
0.00	0.28

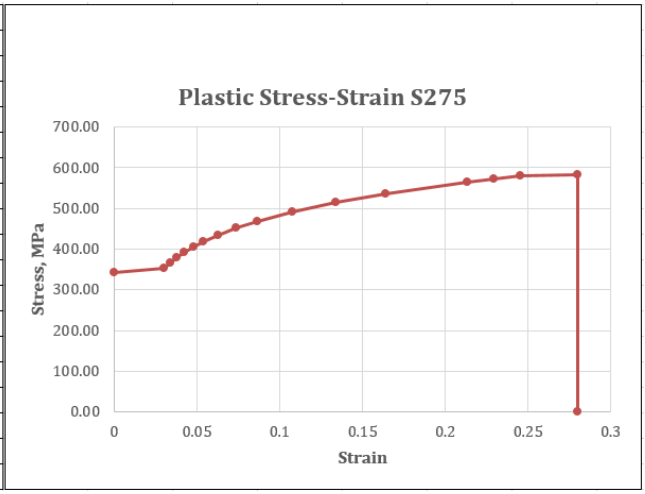

Table 4.6. Stress-strain relationship of Steel Grade S275

4.4.2 Bolt

Four bolt diameters are used on the finite element modelling, representing four classes specifically:

- M16 (bolts to connect secondary beam to the angle plate, column and additional web plate, if applicable)
- M27, M30, M36 (bolts to connect the end plate, primary beam, and column), as seen on Table 4.1

All bolts considered in the model are Grade 10.9, in continuity with the project done by D'Aniello and Tartaglia. Bolt properties are summarized in Table 4.7.

Property	Value
Mass density	7.85 kN/m^3
Young's modulus of elasticity	210 GPa
Poisson's ratio	0.3
Grade	10.9

Table 4.7. Bolt properties

The technique by which the bolts are modelled in ABAQUS is noteworthy to fully simulate its actual behaviour. Bolt shanks were taken as solid cylinder in the model, considering only the nominal diameter (i.e. 16mm, 27mm) assigned for each use. Thus, the threaded part of the shank is not physically taken into account in the model. However, it is known that the threaded part is the one that characterizes the bolt's strength, according to a study conducted by D'Aniello et al [44] on the monotonic and cyclic inelastic tensile response of preloaded Grade 10.9 bolt assemblies. The same statement could be said on the elastic stiffness of the shank with regards to its threaded area. Hence, a specific way must be done to consider them in the model, implementing the same process Tartaglia et al [33] used in their study.

To consider the threaded part of the shank in the model, the material stress was gauged according to the equation:

$$f_{effective} = f_{actual} \cdot \frac{A_{effective}}{A_{gross}}$$

where $f_{effective}$ constitutes to the effective stress to be implemented in the model, f_{actual} is the actual stress of the bolt seen on Table 4.7, $A_{effective}$ is the area of threaded part, and A_{gross} is the nominal area of the shank.

Moreover, to be able to simulate the connection's elastic behaviour, an equivalent elastic modulus must be determined based on the effective material of the shank that will be implemented in ABAQUS. This strategy will enable the analysis to match the actual stiffness of real bolts. This technique is taken from **Swanson et al's** [45] study on stiffness modelling of bolted t-stub connection components, using the equation as follows:

$$\frac{1}{k_b} = \frac{f \cdot d_b}{A_b \cdot E} + \frac{L_s}{A_b \cdot E} + \frac{L_{tg}}{A_{eb} \cdot E} + \frac{f \cdot d_b}{A_{be} \cdot E}$$

where f is the stiffness correlation factor (taken as 0.55); d_b is the nominal diameter of the bolt; A_b is the nominal area of the bolt shank; A_{be} is the effective area of the threads; L_s is the shank length; L_{tg} is the length of the threaded portion included in the bolt's grip; and E is the actual steel modulus of elasticity. The final value of the Young's modulus of the bolt implemented in the model is found to be 130GPa.

Similar to the steel model, the stress-strain relationship of the bolts for the plastic property from the same study by D'Aniello et al [44] is shown in Table 4.9. Lastly, the preload force applied for each bolt class are shown in Table 4.8:

Bolt Class	Preload Force, kN
M16	110
M27	321
M30	393
M36	572

Table 4.8. Preload force applied for each bolt class used in the model

Stress, MPa	Strain
706.929133	0
739.888901	0.00437
771.373535	0.00965
791.051431	0.01391
802.071053	0.01963
807.580864	0.02517
813.090675	0.03202
816.239138	0.04348
817.813371	0.05075
816.868831	0.05618
816.239138	0.05934
808.36798	0.06802
779.244693	0.078
724.146584	0.09
0	0.1

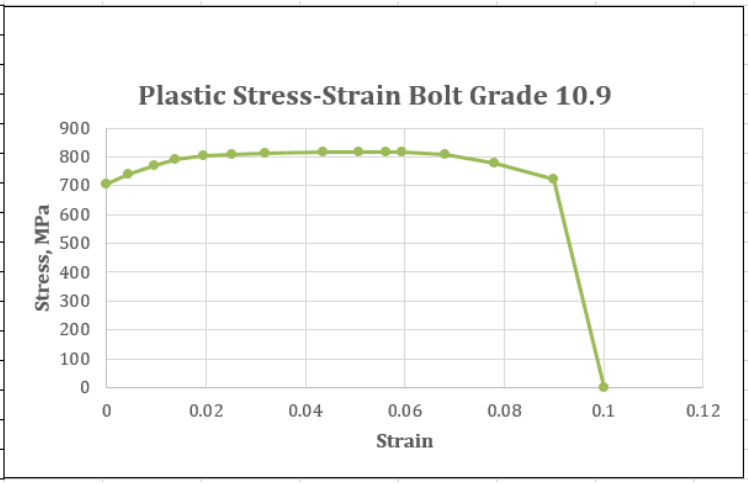

Table 4.9. Plastic stress-strain relationship of Bolt Grade 10.9

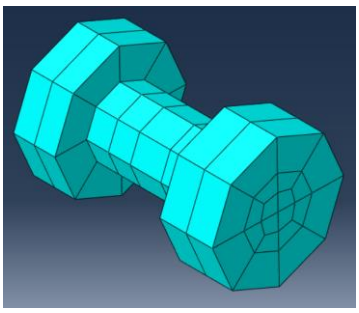

Figure 4.5. Cylindrical solid meshing implemented on the bolts

4.5 Step

A dynamic, implicit procedure was chosen as a method for creating each step in the modelling process. Dynamic, for evident reasons, is used because the load is applied in time, not instantaneously. Implicit, on the other hand, because this method provides better results assuming the modelling assumptions are sound. The NLGEOM was checked in the selection to include the nonlinear effects of large deformations and displacements in the geometry. In all steps, the load is also applied quasi-statically, which is typically used to study the rate of propagation of cracks, hierarchy of collapse and associated level of damage, etc. This is done to "introduce inertia effects primarily to regularize unstable behaviour in analyses whose focus is a final static response. Large time increments are taken when possible to minimize computational cost, and considerable numerical dissipation may be used to obtain convergence during certain stages of the loading history". An initial increment of 0.01 with a minimum value of 1E-015 was used in the steps.

The steps defined in the modelling are discussed below and the corresponding loading conditions for each step are discussed in Section 4.7.

4.5.1 Initial step

Default step at the start of all ABAQUS procedure.

4.5.2 Clamping step

This is the step assigned in ABAQUS after the initial step, where the bolts are experiencing pre-tensioning. The pre-tensioning force must only be applied for a certain amount of time prior to load application and cannot be applied instantaneously. In the modelling process, this step is applied in a 100-second interval prior to the loading step.

4.5.3 Loading step

In this step, the vertical loads applied on the secondary beam take into action. It is also applied in a 100-second interval.

4.5.4 Robustness step

This is the last step made in the modelling process, where the column removal scenario is simulated. It is applied in at 72000-second interval, which is defined to be the end of sequence time.

4.6 Interaction

In modelling the interaction of structural members in ABAQUS, the researchers used the **surface-to-surface contact** in the Interaction phase of the software. These are surfaces in the design that are may be potentially in contact. Specifically, this selection was used in all contacts between the bolt (i.e. shank, nut, head) and the corresponding surface it interacts with (i.e. hole, column flange, end plate, angle plate, etc.). Moreover, the contact between the end plate and the column, the angle plate and the column/additional web plate/secondary beam is also defined as a surface-to-surface contact. These contacts were all created in the initial step propagating to the clamping, loading, and seismic/robust action steps in ABAQUS.

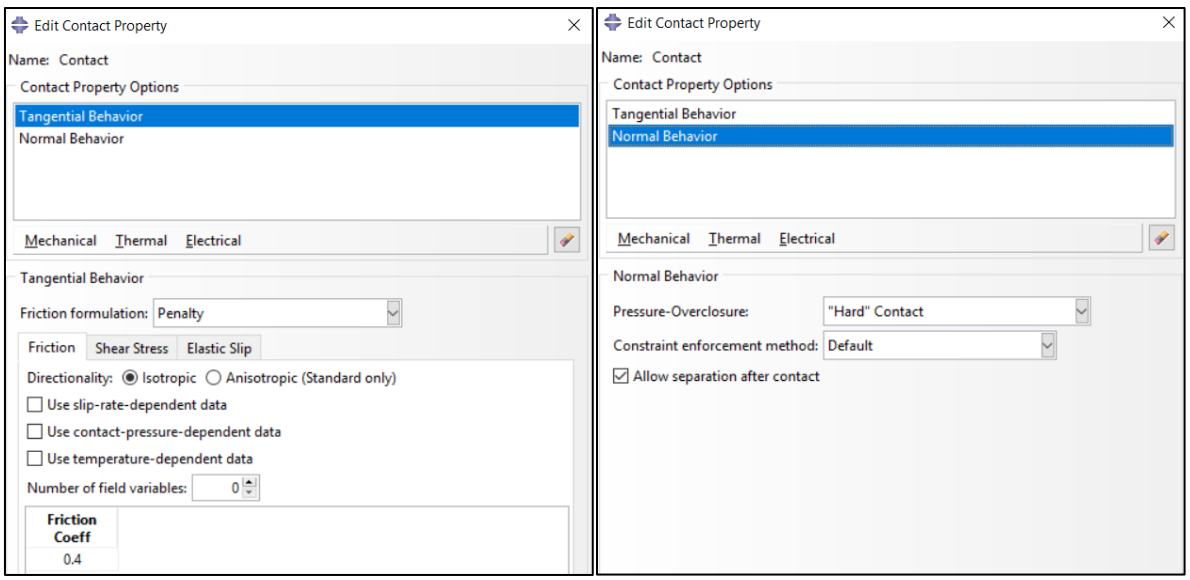

Figure 4.6. Contact property used in ABAQUS

Since we are designing the connection as realistic as possible, it is considered that the tangential contact is not frictionless, thus a friction coefficient of **0.4** is used for steel-to-steel contact by selecting the "Penalty" in the friction formulation option in ABAQUS. This is in accordance to EN 1993:1-8, corresponding to cases of surfaces cleaned by wire-brushing with loose rust removed, which is considered as the typical European practice for building unless specified otherwise. The tangential contact represents the contribution of the friction due to the shear strength of the interface, characterized using the "Coulomb Friction".

Lastly, the normal behaviour was characterized by selecting the "Hard contact" in the option for pressure overclosure. The "hard" contact relationship minimizes the penetration of the slave surface into the master surface at the constraint locations and does not allow the transfer of tensile stress across the interface. This is used to simulate the extrusion phenomenon between bolts and plates (See Figure 4.6).

Constraints partially or fully eliminate degrees of freedom of a group of nodes and couple their motion to the motion of a master node (or nodes). They are typically used for modelling adhesive connections, pinned connections, welding, etc. [40]. A tabular checklist of the interactions and the constraints in detail is shown on Section 11 (Appendices). Additional interactions were also defined in ABAQUS to define the constraints between two separate surface:

1. **Tie constraint** – It is a constraint that ties two separate surfaces together so that there is no relative motion between them (i.e. interaction between the continuity plates and the additional web plates/column, primary beams and end plates, rib stiffeners and primary beams/end plates).

2. **Rigid body constraint** – It is a constraint that allows designation of a collection of regions as a rigid body. This allows the integration of the boundary conditions in the model by selecting a reference point in selected regions.

For the surface-to-surface contact and the tie constraint in ABAQUS, a selection must be made for the master and slave surface. The ABAQUS User's guide [41] defines the differences as follow:

- Nodes on slave surface cannot penetrate the master surface
- Analytical rigid surfaces and rigid element-based surfaces must always be master surface
- A node-based surface can act only as a slave surface and always uses node-to-surface contact
- Both surfaces in a contact pair cannot be rigid surfaces with the exception of deformable surfaces defined as rigid
- Generally, if a smaller surface contacts a larger surface, it is best to choose the smaller surface as the slave surface
- Master surfaces should be smooth
- The slave surface should be more finely meshed
- For same mesh density, slave surface should be selected such that it has lower stiffness
- If the two surfaces are on structures with comparable stiffness, master surface should be selected as the surface with the coarser mesh
- The stiffness of the structure and not just the material should be considered when choosing the master and slave surface. For example, a thin sheet of metal may be less stiff than a larger block of rubber even though the steel has a larger modulus than the rubber material
- If the stiffness and mesh density are the same on both surfaces, the preferred choice is not always obvious

For example, in the model of the connection, the holes are the master surfaces and the bolt parts are the slave surfaces since the holes are the rigid-based surface while the bolts tend to "move" along the hole.

The following contact surfaces were accounted for in the study:

- contact between end plate and column flange

- contact between the bolt nuts and the bolt heads with the surfaces it's in contact with (e.g. end plate, column flange, column web (if applicable), angular plate, secondary beam web)
- contact between the bolt shank and the inner sides of the bolt holes it's in contact with (e.g. end plate, column flange, angular plate, secondary beam web, additional web plate and column web, if applicable)
- contact between the end plate and the primary beam
- contact between the rib stiffeners with the end plate and the primary beam
- contact between the additional web plate (if applicable) and the column web
- contact between the angular plate and the additional web plate and/or column web (if applicable)
- contact between the secondary beam web and the angular plate
- contact between the continuity plate and the additional web plate and/or column web (if applicable)

4.7 Loading

4.7.1 Applied load

In Section 4.5, the various steps considered in the finite element analysis are discussed. For each step, a corresponding loading condition was applied to simulate the actual load in the model. It is also worth noting that at the end of each loading step, the "fix at current length" option was selected to ensure that the current state of the structure after each step is continued to the next.

4.7.1.1 Clamping

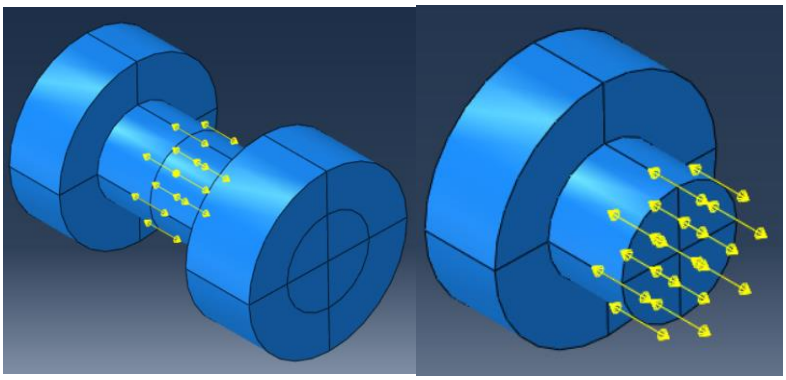

Figure 4.7. Application of the pretension force in ABAQUS

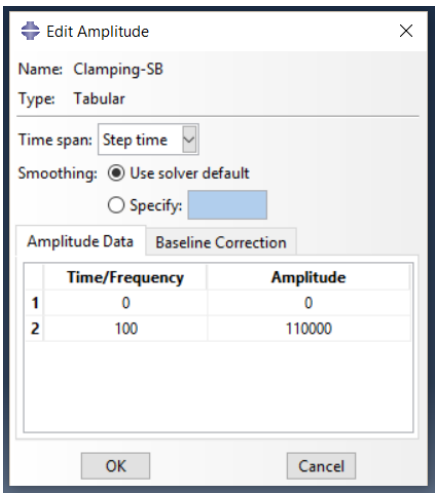

Figure 4.8. Tabular amplitude used in ABAQUS, the case for the secondary beam's bolts is shown

In the Clamping step, the mechanical, bolt load predefined option was selected. This pretension force was applied approximately in the middle section of the bolts (Figure 4.7), which uses amplitudes that linearly increases the clamping force up to the maximum in the first 100 seconds of the analysis. After that, the clamping force is constant for the rest of the steps. The values of the pretension forces of each bolt class are seen on Table 4.8.

4.7.1.2 Loading

At this step, a uniform vertical load is applied on the secondary beams to introduce the gravity loads. As seen on Figure 4.10, the pretension forces on the bolts are still active.

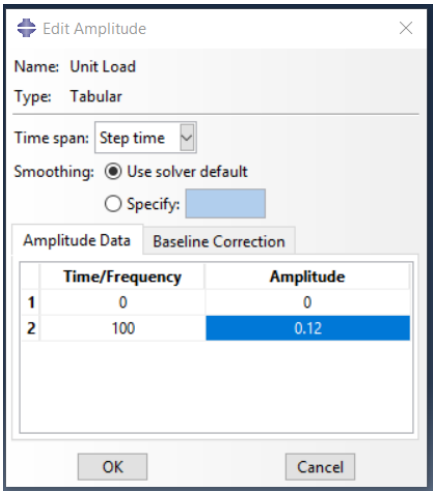

Figure 4.9.Tabular amplitude used for the loading step

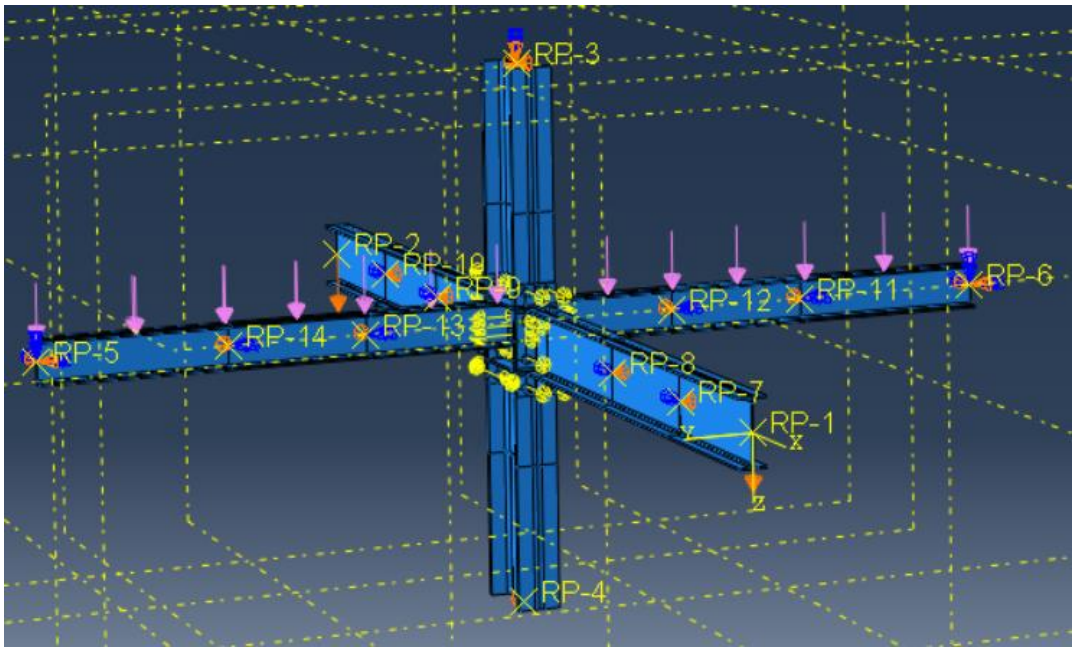

Figure 4.10. Application of the uniform load on the secondary beams

4.7.1.3 Robustness

All loads applied on the previous steps are just propagated in this final load step. In this step, the column loss scenario is taking into action. The change at this step is elaborated on the boundary conditions set in ABAQUS to simulate the seismic action and the column loss.

4.7.2 Boundary condition

The boundary conditions set in the finite element model are crucial to the analysis as this sets on how the external restraints on the local structure must behave to be able to simulate a realistic phenomenon. In ABAQUS, reference points (RP) are set on the end cross sections of both the beams and column. Reference points are also set at every one meter of the beams and the column to limit the structure against torsion. Figure 4.11 shows the RPs set in the model for the boundary conditions.

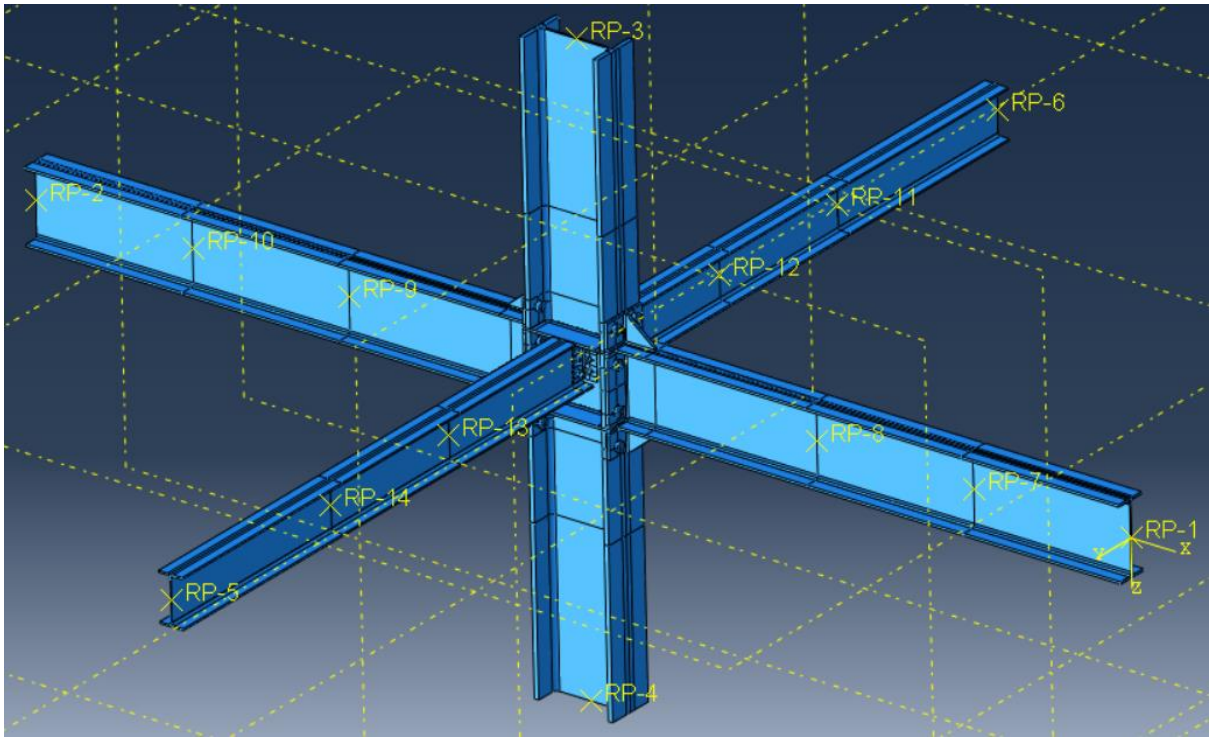

Figure 4.11. Reference points for application of boundary conditions in ABAQUS

The sub-structuring applied in the model is similar to the numerical model done by Tartaglia et al [33] as discussed in Section 2.4.2 and Figure 2.40. The difference, however, is that this study focuses more on the connection that is directly above the damaged column. Hence, the joint above the part subjected to sudden column loss. Figure 4.12 shows the subs-structuring implemented in this study. The list below shows the boundary conditions set in the model:

1. Constraints that restrict the rotations around the axis of each beam and the lateral torsional buckling
2. The ends of the primary beam all translational degrees of freedom are restrained (pinned connection).
3. All translational degrees of freedom and the rotation around the column axes are fixed before the sudden column loss (fixed connection). At the robustness step, all degrees of freedom prior are still fixed except for the translation at the z-axis, where the displacement history is imposed, to imitate the said column loss action.
4. Except for the translation at the z-axis, all translational and rotational degrees of freedom are fixed around the secondary beam ends.

To expound further, it was decided to apply a displacement instead of a force to make the bending moment increase smoothly. At the beginning of the analysis they were restrained, and in the succeeding steps, the boundary condition will vary per the imposed loading protocol.

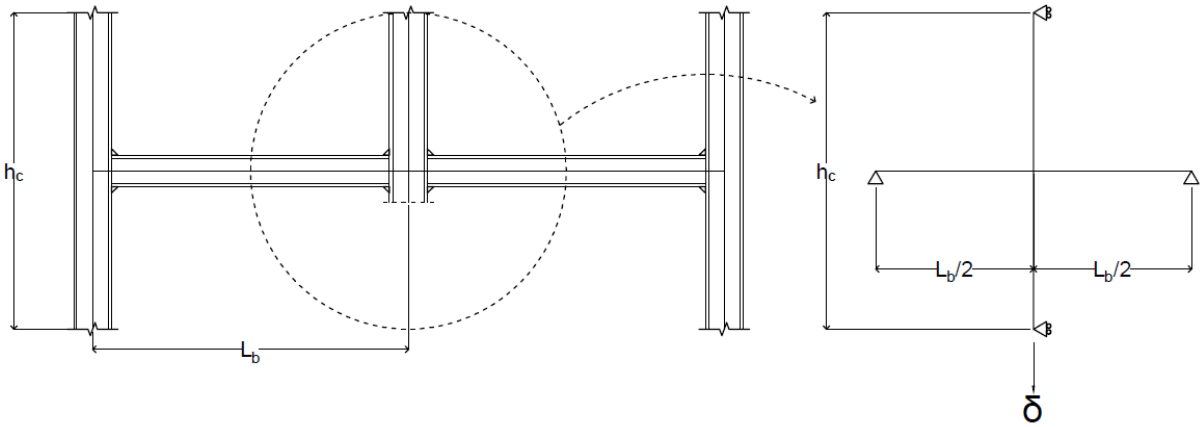

Figure 4.12. Sub-structuring and boundary conditions implemented in the finite element model

4.8 Mesh

As discussed in Section 4.3, the element type used in ABAQUS is C3D8R. Since the model is sophisticated enough and would require more time to run, the size of the mesh is varied in the model. The local joint is the focus of this study, thus, that part has finer mesh than the outward parts of the model. Figure X shows the meshing strategy implemented in ABAQUS.

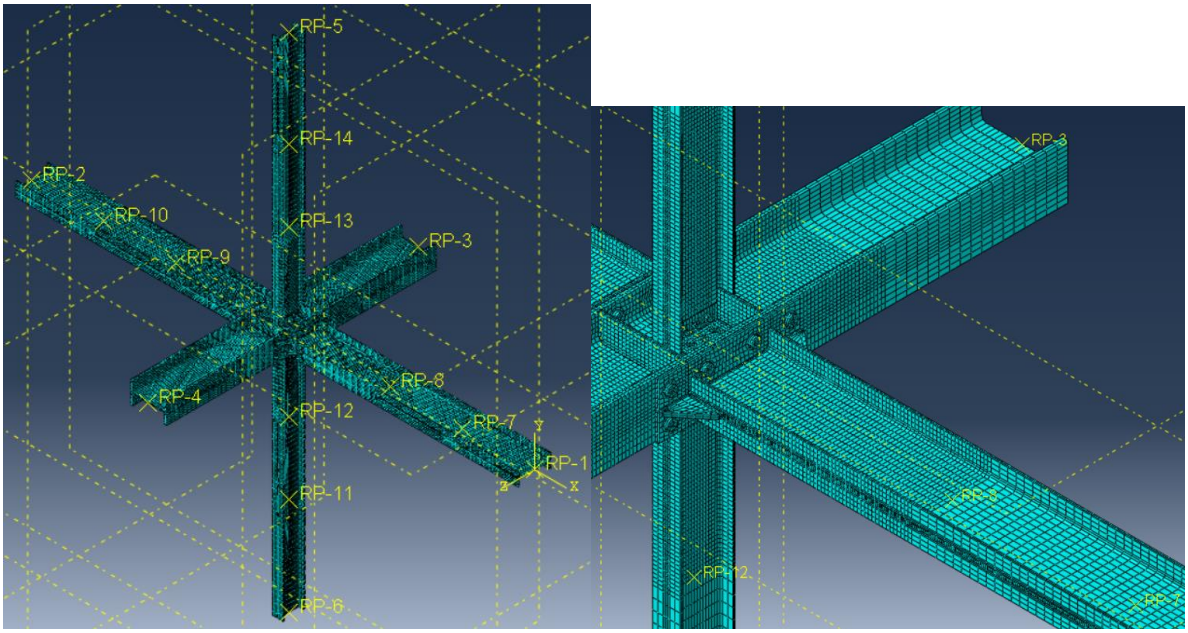

Figure 4.13. Meshing strategy implemented in ABAQUS: (left) Overall mesh, (right) Magnified view of the mesh

5. VALIDATION OF THE FINITE ELEMENT MODEL

As mentioned previously, the finite element model is only deemed useful if it is validated with experimental results – either from an experiment carried out alongside the finite element analysis or from previous tests done from other literatures. Thus, in this study, results of the FEA were calibrated from the numerical results done by Tartaglia et al [33] via the failure of the connection on two of the models. This is deemed possible since their models were validated by the monotonic experimental tests done by Shi et al [24]. They tested five stiffened extended end plates wherein they inspected the influence of geometry of the bolts and the end plate when it is subjected to pure bending. The experimental process is discussed more in detail in Section 2.3.1. Moreover, as previously mentioned, the models used in this study were the same geometrical typology studied by D'Aniello et al [44], which were also validated by their own subsequent experimental works. There are also few studies on robustness for this kind of typology where the secondary beam was also modelled, so validating it with actual experiments from previous works would be deemed difficult.

The assessment is done in terms of joint moment rotation curves and PEEQ distribution. The joint moment rotation curves consider the influence from web panel and connection only as defined by Shi et al [24] explained in Section 2.3.1. The PEEQ, on the other hand, represents the equivalent plastic strain. It displays the concentration of plastic deformation and represents a measure of local ductility and fracture tendency of the material. According to the ABAQUS User's Guide [41], PEEQ could tell if the material is currently yielding or not ("actively yielding", where the plastic strain changed during the increment). It is defined as:

$$PEEQ = \bar{\varepsilon}^{pl}\big|_0 + \int_0^t \dot{\bar{\varepsilon}}^{pl}\, dt$$

where: $\bar{\varepsilon}^{pl}\big|_0$ is the initial equivalent plastic strain and $\dot{\bar{\varepsilon}}^{pl}$ is dependent on the material model. However, for classical metal (Mises) plasticity,

$$\dot{\bar{\varepsilon}}^{pl} = \sqrt{\frac{2}{3}\dot{\varepsilon}^{pl} : \dot{\varepsilon}^{pl}}$$

To analyse the behaviour of the joint, the moment-rotation curve has to be plotted, which can be determined from the ABAQUS results via the time vs displacement curve and the time vs reaction forces curve.

5.1 Result comparison

As seen on Figure 5.1 and Figure 5.2, the numerical results are in excellent agreement with the results of the numerical behaviour [33] of the connection. EPC-3 of their study and ES2-E of the present study both showed plastic deformation on the end plate and the bolts. Similar failure is also seen on the ES1-P and EPC-5 model. It is important to note, for the sake of validation, that the orientation of the ES2-E and ES1-P in here is rotated 180° at the y-axis since the study of [33] considers the corner joint after a column loss while this study focuses on the middle column loss. In the end, the best way in validating the numerical models is through experimental models with the exact properties and typologies used in both cases. However, due to limited studies on this kind of joint for column loss scenario. As previously mentioned, for the case of this study, validation is just done through numerical models of previous studies. Lastly, to reiterate, the typologies used in this studies are the same ones used on previous experiments and numerical modelling on seismic design, which were validated with a number of studies on a seismic point of view.

The symmetry between the left and right primary beams is also a way to validate the numerical model since it would indicate that the joint behaved as expected since both sides have exactly the same properties.

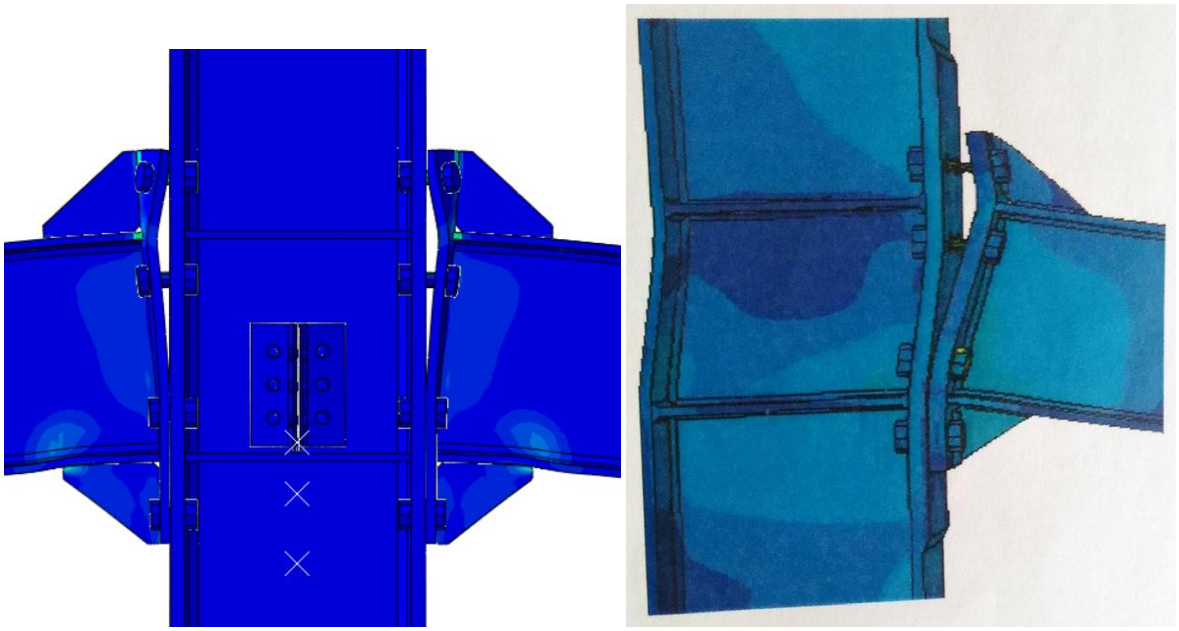

Figure 5.1. ES2-E and EPC-3 on [33]'s study

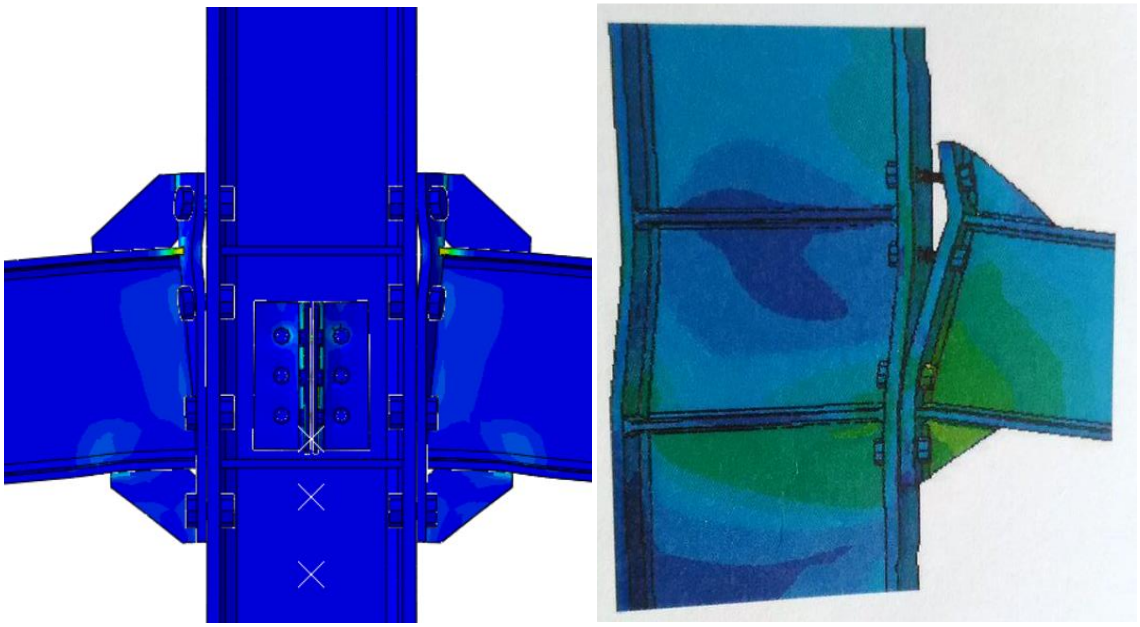

Figure 5.2. ES1-P and EPC-5 on [33]'s study

6. RESULTS

6.1 Investigated parameters

Table 6.1 shows the parameters investigated in the study. It should be noted that parametric study would need a significant number of models for complete validation of the results. However, in this study, limited models were used but for lack of better term, various parameters were checked and a numerical investigation was done. The geometry of each models investigated were shown in Table 4.1. The column size increases for each model. Moreover, for each column size, the variation of the equal, full, and partial-strength were analysed. Hence, all equal-strength joint models were compared, then all full-strength joints, and all partial-strength joints. The influence of secondary beam was taken into account in this study by comparing the ES1 models with its corresponding models when the secondary beam is absent in the typology.

Parameter Investigated	Parameter's Variation	Models Investigated
Joint typology	Effect of variating the joint typology (i.e. E, F, or P joints) were studied	a. ES1-E / ES2-E / ES3-E b. ES1-F / ES2-F / ES3-F c. ES1-P / ES2-P / ES3-P
Influence of secondary beam	Effect of secondary beam will be checked by comparing it to models with no secondary beams	a. ES1-E and ES1-E No S. Beam b. ES1-F and ES1-F No S. Beam c. ES1-P and ES1-P No S. Beam

Table 6.1. Parameters investigated in the study

6.2 Column removal scenario and the moment capacity

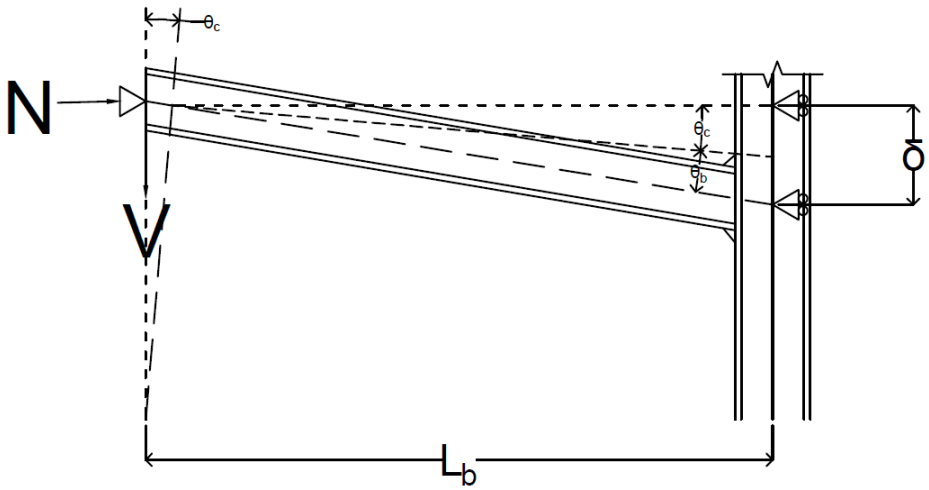

Figure 6.1. Free body diagram of incremental catenary forces

The significant factors that must be obtained to determine the behaviour of the joints in column removal situation are the displacements, reaction forces (shear *RF3* and normal *RF1* on the primary beams and shear *RF3* and normal *RF2* on the secondary beams), and plastic dissipation (*ALLPD*) on critical parts of the joint. From here, the join flexural resistance M^{II} can be derived, which is just the sum of two parts:

1. First order bending moment M^{I}

$$M^{I} = V \cdot \frac{L_b}{2}$$

2. Second order moment increase due to catenary action ΔM

$$\Delta M = N \cdot \delta$$

Both of which are clearly demonstrated in the free-body diagram in Figure 6.1. *V* is the vertical component of the applied force at the tip of the beam (normal forces *RF1* and *RF2*, for the primary beams and secondary beams, respectively) and *N* is the horizontal component of the catenary action (shear force *RF3*). L_b is the length of the beam and δ is the vertical displacement. Moreover, the rotation θ of the structure is determined by simply calculating the ratio of the vertical displacement and the total length of the beam, which is 3500mm in this case:

$$\theta = \frac{\delta}{L_b}$$

In this manner, the moment-rotation curve can be plotted and investigation can be done to verify the results for each parameter investigated.

6.3 Axial forces and the catenary action

A huge emphasis has already been established regarding the role of catenary action in improving the robustness of structures. The axial forces and the catenary action were shown in this section to consider the role of catenary action in such scenarios. As shown in Figure 6.1, development of catenary action is a key factor which modifies the internal forces distribution happening in the joint. The connection under column loss scenario is subjected to bending moment, axial and shear forces. These internal forces determine the level of catenary action every model can sustain. Since all joint typology have the same beam and column properties for ES1, ES2, and ES3 models, the analyses presented that the axial force is heavily influenced by the joint's stiffness and strength. To be more specific, the axial forces were taken in ABAQUS by obtaining an XY-plot of the *RF1* for the primary beams and *RF2* for the secondary beams, which represent the normal action at the end of each beam.

6.4 Plastic dissipation energy and the PEEQ index

As previously mentioned, the plastic dissipation energy was taken in ABAQUS by plotting a field history output of the *ALLPD* (all plastic dissipation) for the whole models and critical parts of the joint, namely—column, beam, bolts, end plates, angular plates, top ribs, continuity plates, and additional web plates (if applicable). The PD energy ratio of each critical element was represented in this study as a ratio of its plastic dissipation with the overall maximum plastic dissipation of the whole model. In this way, it is possible to know the percentage of plastic dissipated energy of each component with respect to that of the whole model. It is imperative to know as well the component which has the greatest contribution in the plasticity of the joint, which enables the author to make an analysis. The plastic dissipation energy ratio for 2%, 4%, 6%, 8% and 10% (if applicable) rotation were also shown through bar charts to clearly determine the contribution of each component at every rotation considered. Lastly, the PEEQ index, already discussed in Section 5, are also shown in the results.

6.5 ANALYSIS 1: Comparison based on each joint typology

6.5.1 Axial load and moment capacity

6.5.1.1 Equal-strength joints

Figure 6.2 shows the axial load of all equal-strength joints, with Figure 6.2d plotting all models in one graph. It can be seen on each plot the symmetrical results at the right and left primary beams, which further validates the results of the numerical investigation since it is expected that the results be symmetrical due to the same properties applied for each side of the connection. It can be noticed that behaviour of the joint

indeed depends on the strength and ductility of the connection. The arching effect is also noticeable in the graphs, where up to approximately 0.04 rad for ES1 and ES3 and 0.06 rad for ES2, the compression forces are stimulated. This transfers the lateral loads by the formation of a compression strut from the beam flange at the end of the beam to the compression centre of the connection. After these corresponding rotations (i.e. larger deformations), the beam continually elongates, which alters the axial forces from compressive to tensile loads, which represents the formation of the catenary action.

Figure 6.3, consequently, shows the moment-rotation curves of the equal-strength joints. The same type of symmetry is observed for the left and right primary beam, which is seen through the overlapping of the plots. At post-elastic range, when the structure is subjected to huge deformations because of geometric nonlinearity, the joint is under bending moments and axial forces. It can also be seen that larger columns (ES3) generated slightly larger compressive forces at smaller rotations than ES2. However, the catenary action of ES2 is activated at a slower rate (only after 0.06 rad). ES1 subsequently experiences larger tensile load (i.e. increased catenary load) at larger rotations. This is an interesting result since it can be shown that having less of the arching effect (represented by elastic behaviour) activates larger catenary actions. All models also exhibited a behaviour that under larger rotations, the normal forces become less significant and the joint experiences large tensile deformations. It can also be observed that all models have a same type of behaviour in terms of moment capacity, with similar response curves, varying only in strength as column size is increased. Images of the PEEQ index in Figure 6.3 showed a larger amount of plastic hinges on the beams for ES1 and ES2, compared to ES3.

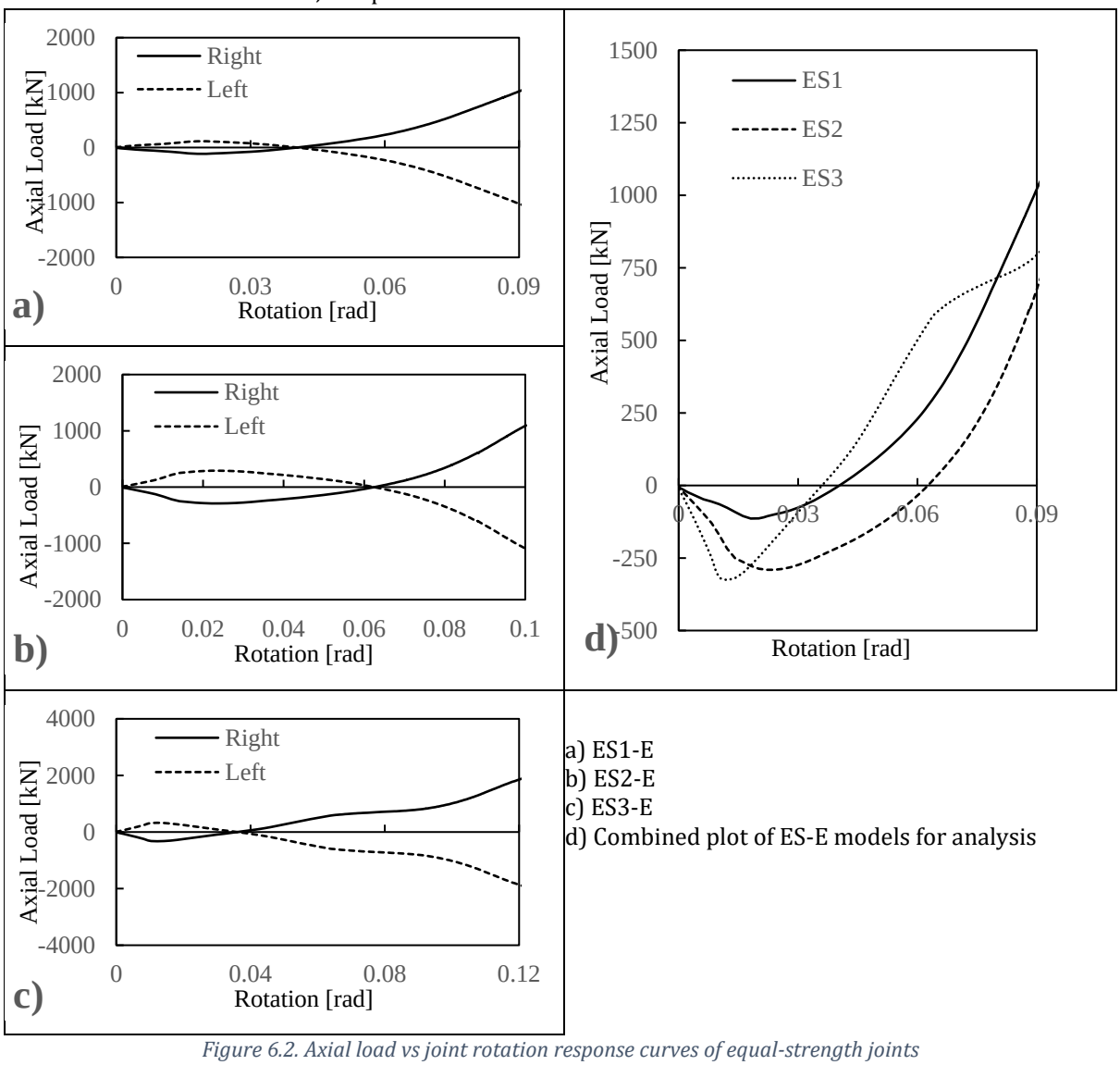

a) ES1-E
b) ES2-E
c) ES3-E
d) Combined plot of ES-E models for analysis

Figure 6.2. Axial load vs joint rotation response curves of equal-strength joints

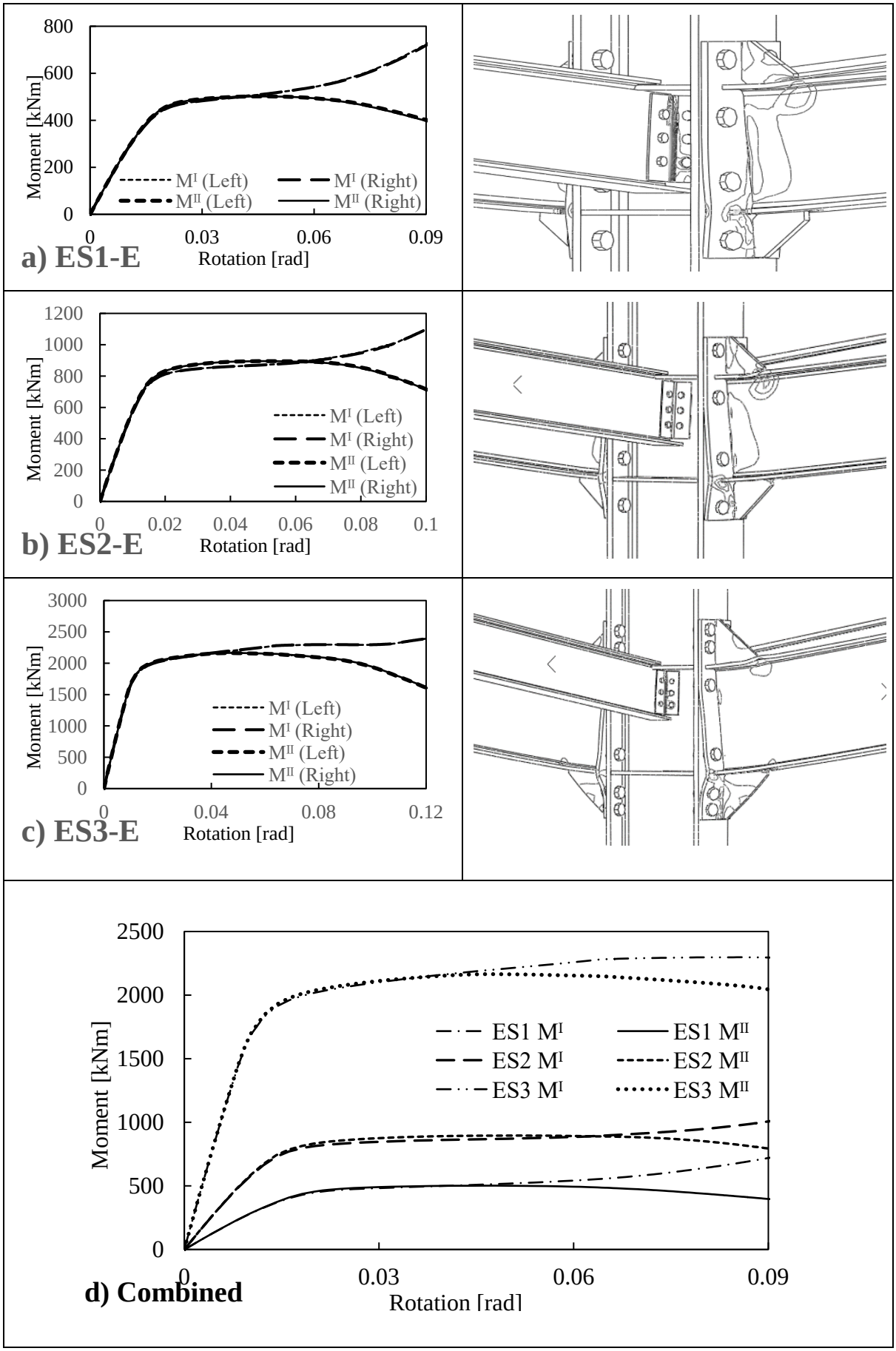

Figure 6.3. Influence of catenary action on the moment-rotation response curves on equal-strength joints.

6.5.1.2 Full-strength joints

The full-strength joints provided interesting results as well which supports the observation made on equal-strength joints. As seen on Figure 6.4, all full-strength joint models have almost zero arching effect, with ES3 having the only evident one compared with the other models. Supporting the observation made with equal joints, the arching effect opposes the development of catenary actions. From the combined plot, ES3, which has larger compressive load at small deformations, resulted to the least axial load at much larger displacements. Similar pattern was observed here as the model with the smallest column size lead to larger catenary forces.

Even the moment response curves and the PEEQ images led to similar results, as shown in Figure 6.5. However, it is also noteworthy to observe the formation of larger plasticity in the bottom ribs on full-strength joints, opposite to the equal-strength joints ES1-E and ES2-E have large plastic deformations on the ribs on top of the beam. Hence, it is also another observation that must be considered on the succeeding results that joints with larger columns tend to result with more plastic deformation on the ribs on the bottom, while joints with smaller columns has more plastic deformation on the upper ribs. Lastly, tensile forces tend to be weightier than the normal forces at larger rotations, similar to the previous analysis.

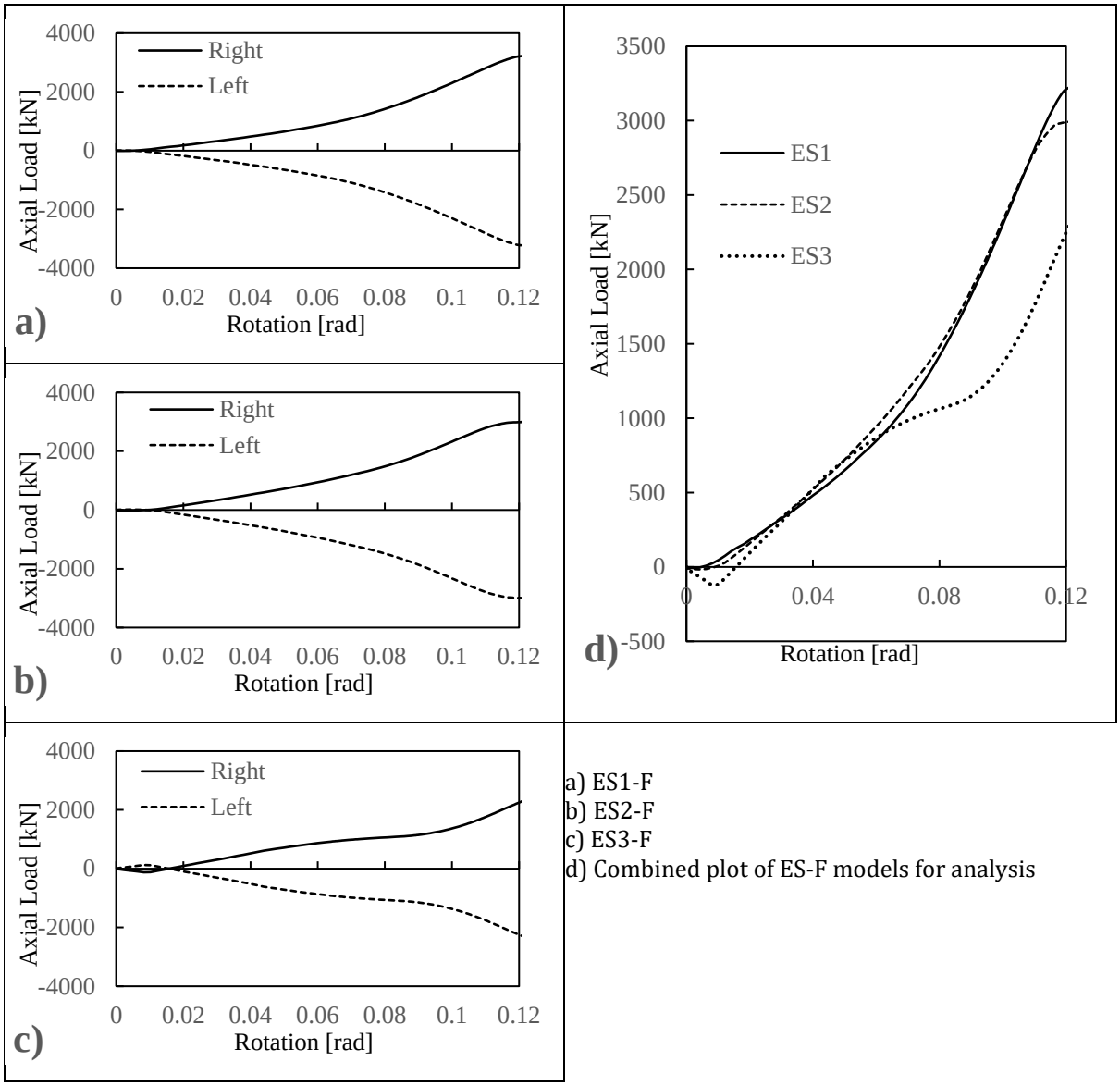

a) ES1-F
b) ES2-F
c) ES3-F
d) Combined plot of ES-F models for analysis

Figure 6.4. Axial load vs joint rotation response curves of full-strength joints

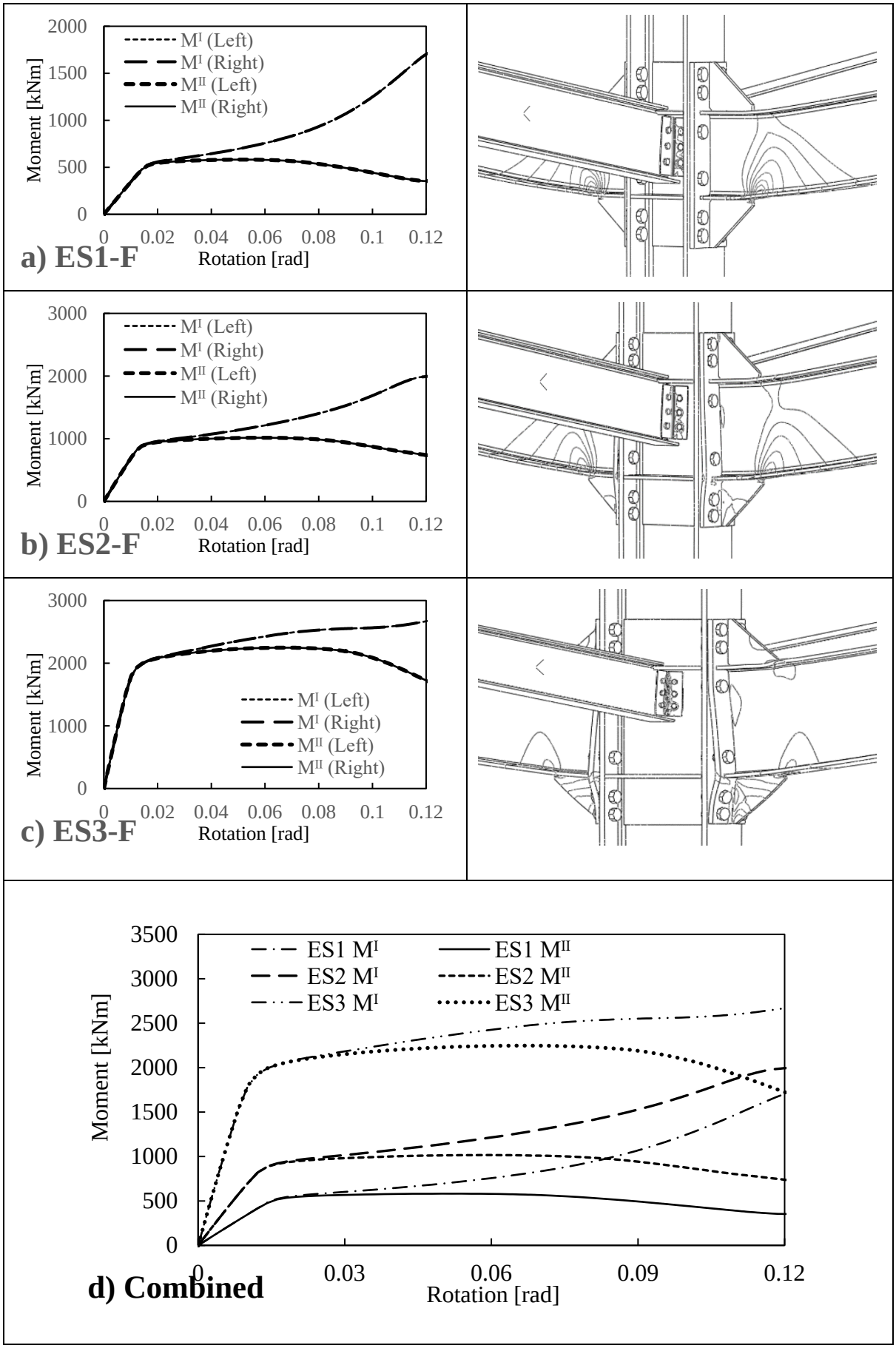

Figure 6.5. Influence of catenary action on the moment-rotation response curves on full-strength joints

6.5.1.3 Partial-strength joints

The results of the partial-strength joints in terms of axial and moment capacity are shown in Figure 6.6 and Figure 6.7, respectively. As seen on the rotation vs axial load plot, model ES3 also exhibited larger compressive forces like the previous simulations. This further justifies the previous observation on the influence of arching effect on the catenary action developing on the joints at larger displacements. As rotation becomes larger, tensile forces were also much more significant in these models while the normal action decreases. Similar behaviour is observed on their moment capacities like the previous observations on the joint flexural resistance M^{jj} of the connection, with the plot only being amplified as the column size is increased. The PEEQ index images also show that the larger columns (i.e. ES2 and ES3) have more plastic deformation on the bottom ribs, opposite to ES1, where the plastic deformation is on the top rib. Again, similar results arose from the analysis, analogous to the perceived data previously.

Convergence problems were also encountered in ES3-P model, which is an important matter to note in this study. ABAQUS finished running up to 0.08 rad of rotation only, which is why comparisons can be done up to 0.08 rad for the partial strength joints. This could be a factor that could affect the author in deriving results from this set of models. However, as similar behaviour is observed, for the sake of this study, it is safe to say that the partial strength joints validated the previous observations.

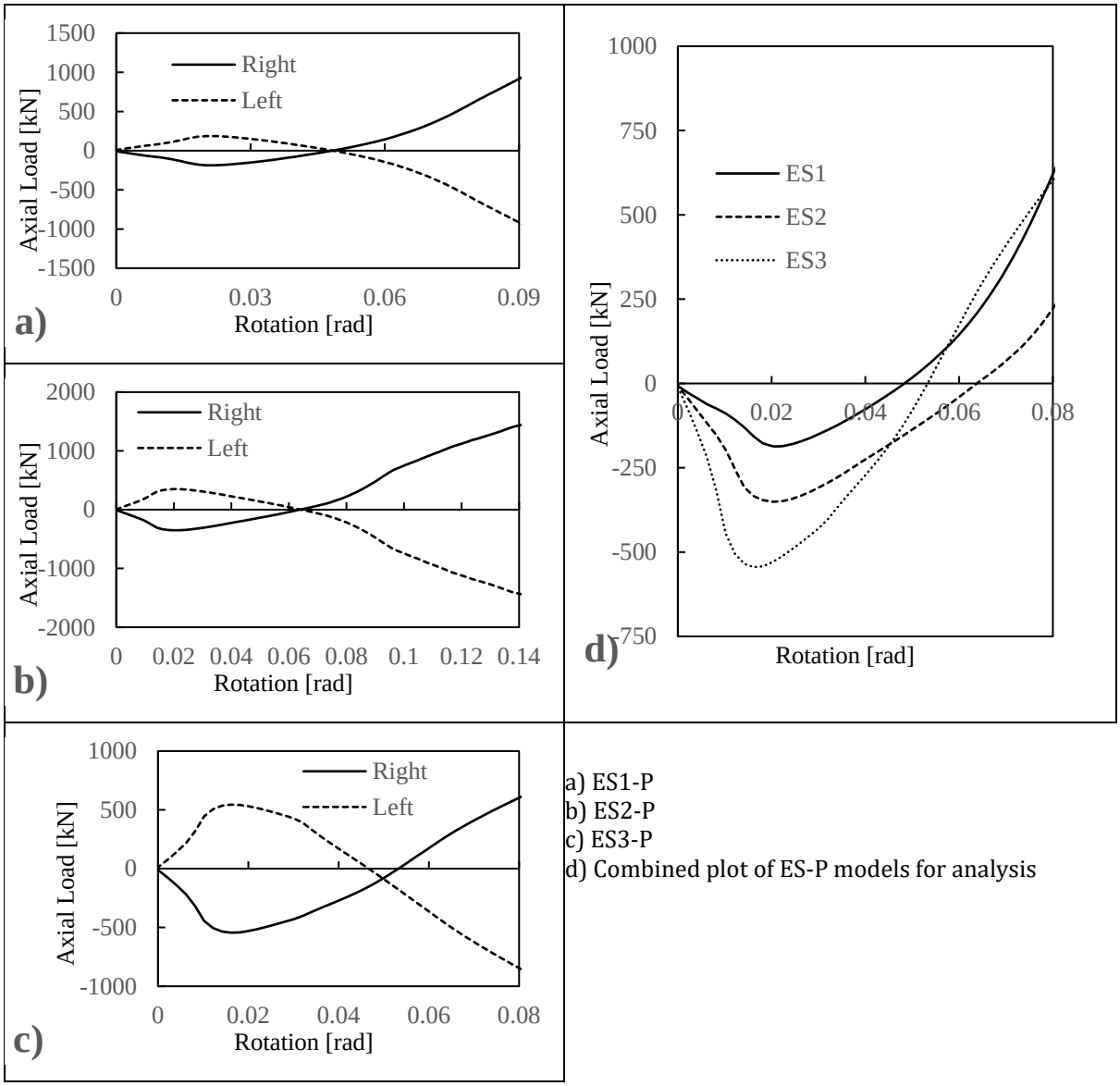

a) ES1-P
b) ES2-P
c) ES3-P
d) Combined plot of ES-P models for analysis

Figure 6.6. Axial load vs joint rotation response curves of partial-strength joints

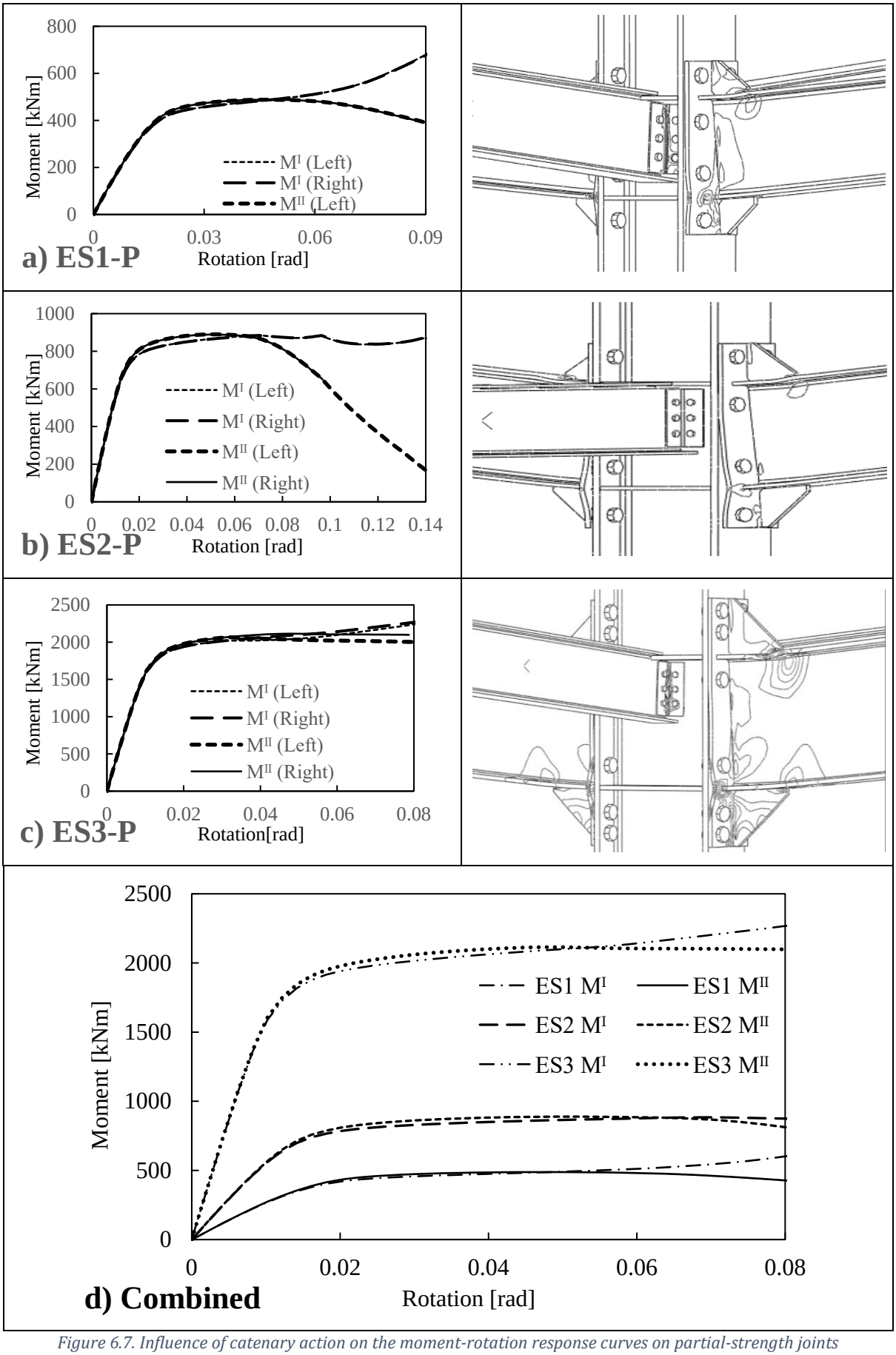

Figure 6.7. Influence of catenary action on the moment-rotation response curves on partial-strength joints

6.5.2 Plastic Dissipation Energy

6.5.2.1 Equal-strength joints

Figure 6.8 shows the rotation vs plastic dissipation energy (PD Energy) ratio curve of each component, compared with the whole model's plastic energy (also shown). A magnified figure of the components with very low plastic energy is also represented on the right figures of Figure 6.8. On the other hand, Figure 6.9 shows the PEEQ values of each component, indicating the high plasticity on the angular plates and the bolts. Figure 6.10 shows the PD energy ratio of each joint component relative to the overall plastic energy of the whole model, for 2%, 6%, 8%, and 10% (if applicable) rotations. The combined contribution of the connection is shown on Figure 6.10, showing close ratios for the beam and the connection. This is deemed desirable since equal-strength joints are designed to show a balanced contribution from the two components. Images of the PEEQ index for each rotation is shown in Figure 6.11.

The continuity plates reached no plasticity, an observation that was also seen on full and partial strength joints. The additional web plates and the secondary bolts exhibited very small PD energy ratio, where it is even almost zero for ES2-E and ES3-E. It is also worth noting that all models achieved higher plasticity of the end plate than the bolt, except for the case of ES3. ES1-E and ES2-E models exhibited higher plasticity on the top ribs than the bottom ribs, which is opposite to model ES3-E. Yielding of the angular plates were also observed especially on larger rotations, which is also visible in the PEEQ index images.

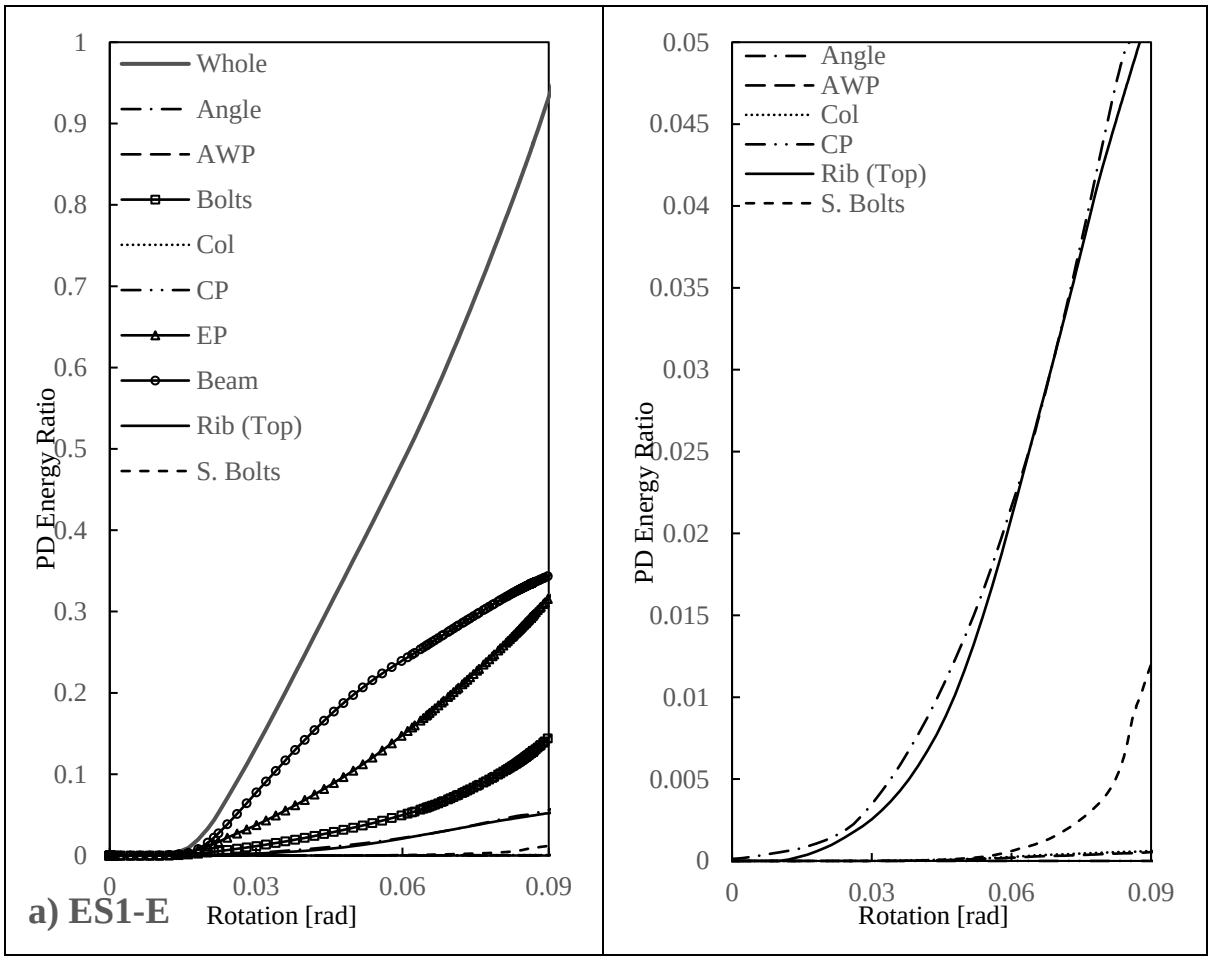

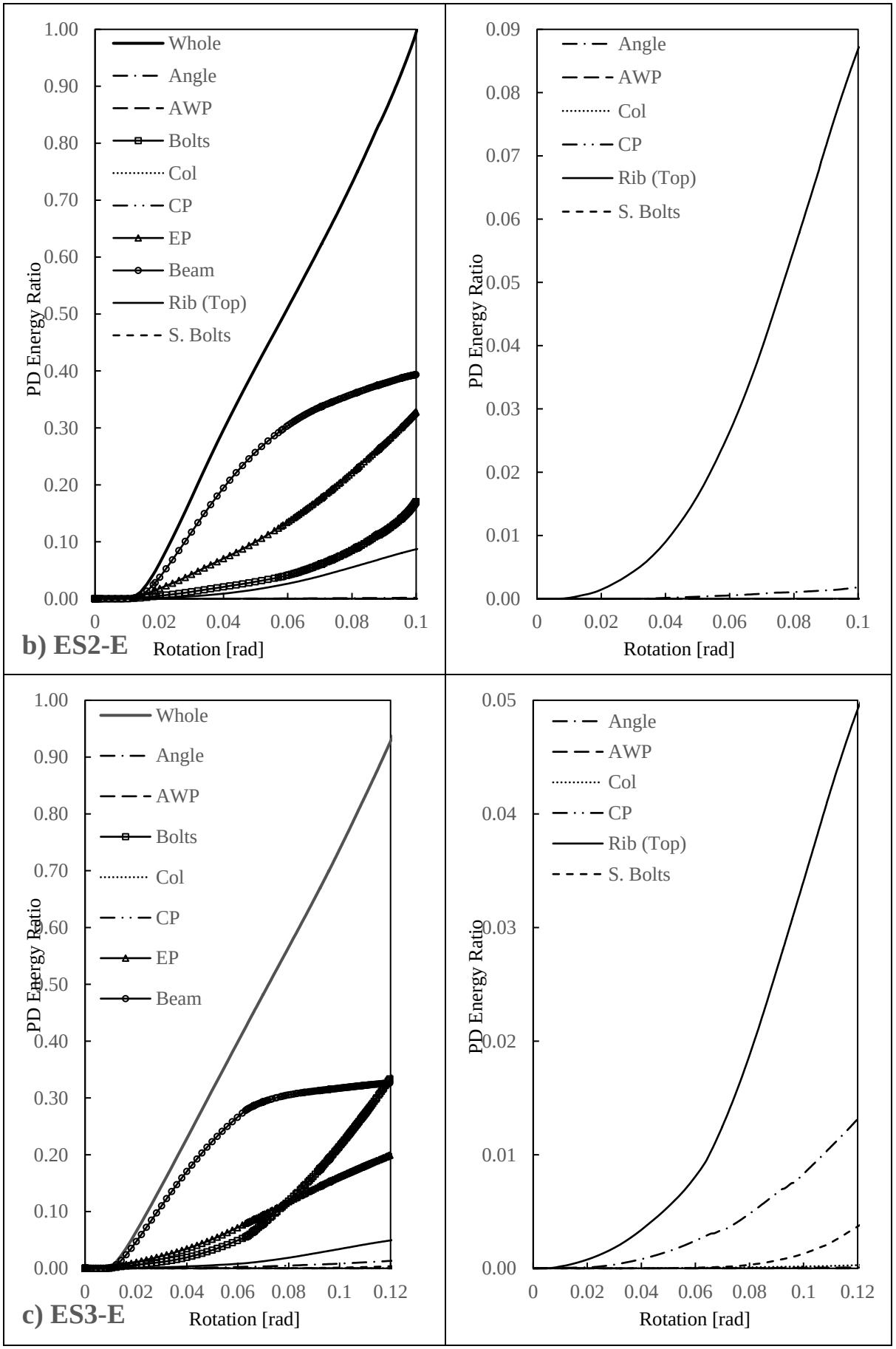

Figure 6.8. Rotation vs PD energy ratio of each connection component for equal-strength joints

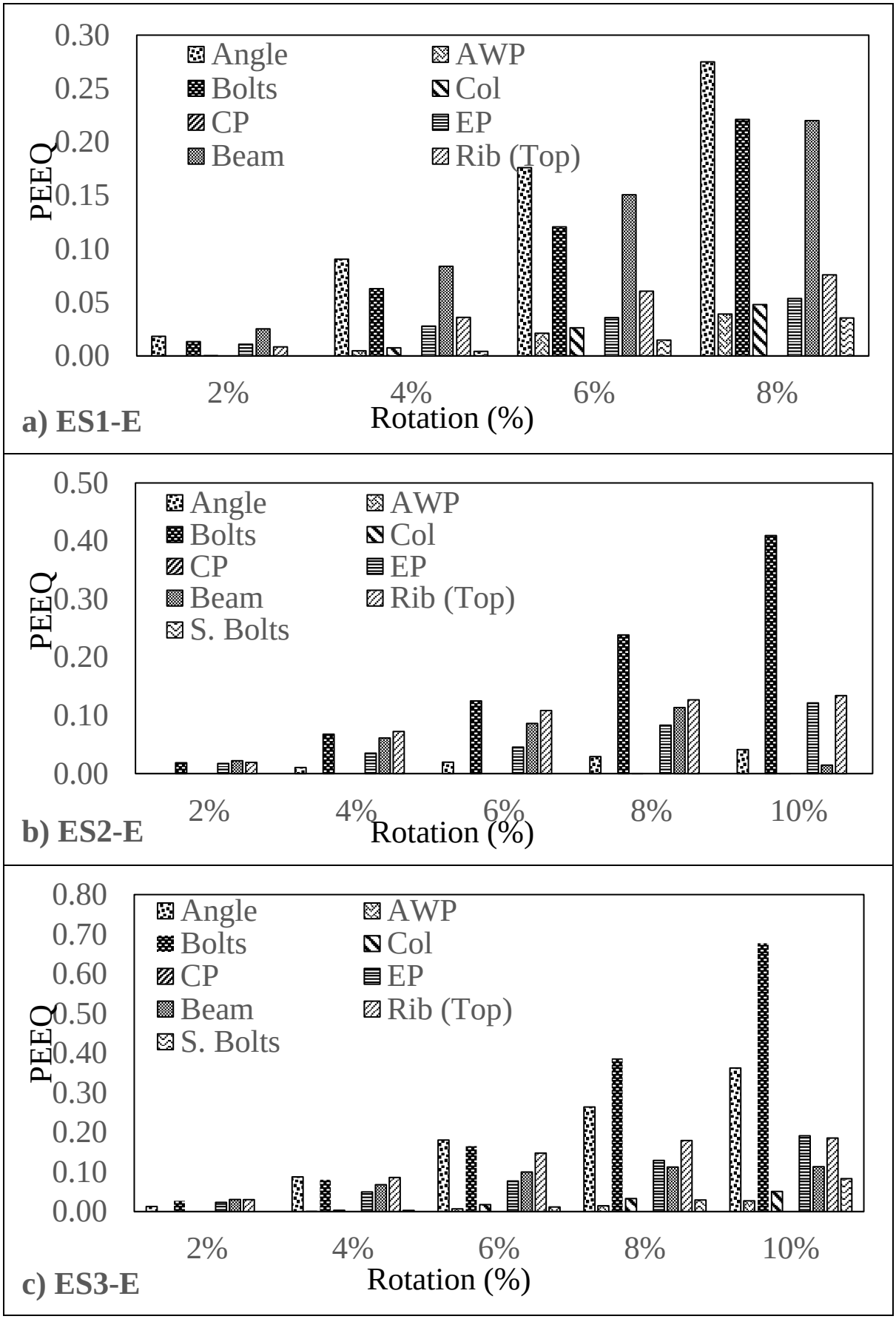

Figure 6.9. PEEQ values of each connection component for equal-strength joints

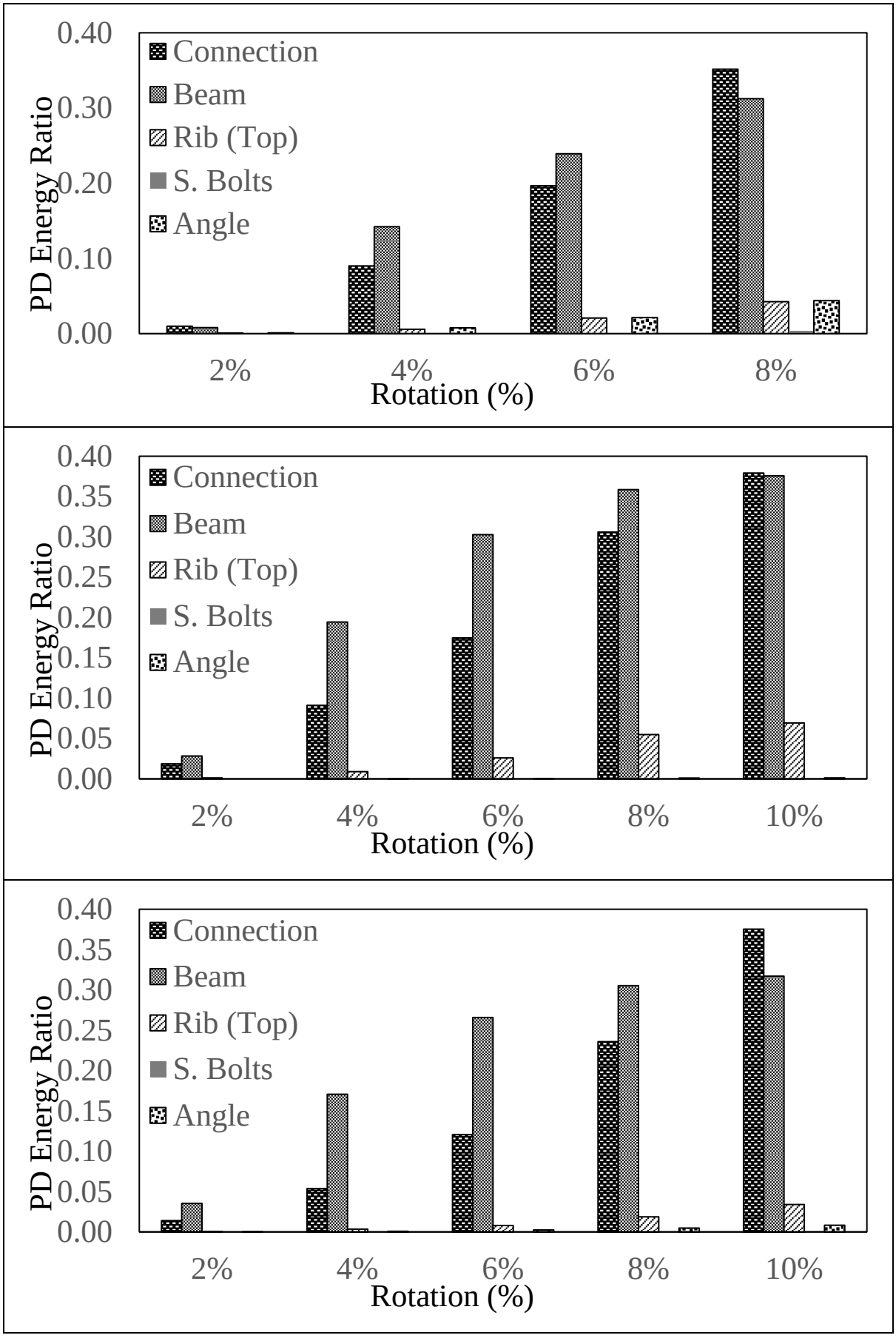

Figure 6.10. PD energy ratio of each joint component, the connection component combined (equal-strength joints)

PEEQ (%)	ES1-E	ES2-E	ES3-E
2%	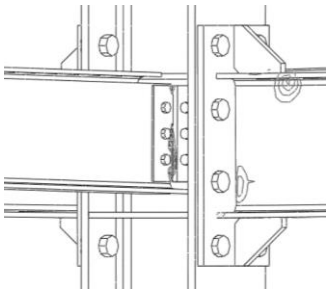	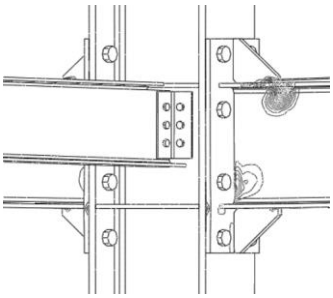	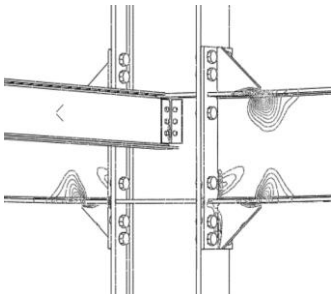
4%	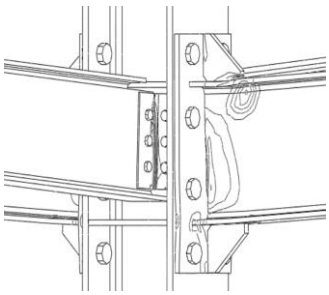	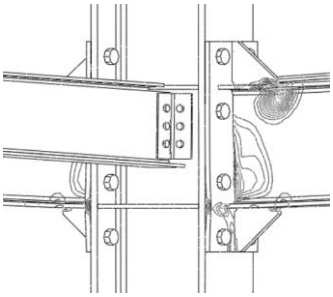	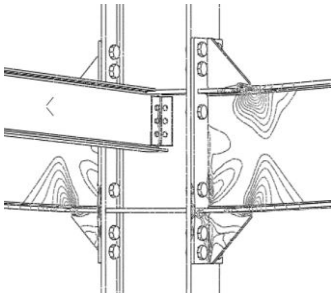
6%	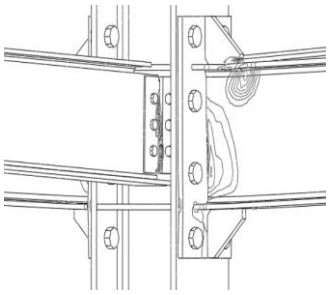	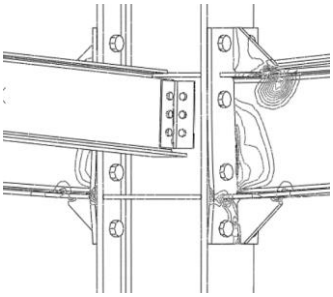	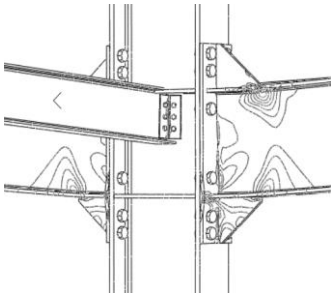
8%	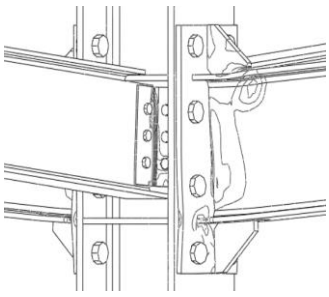	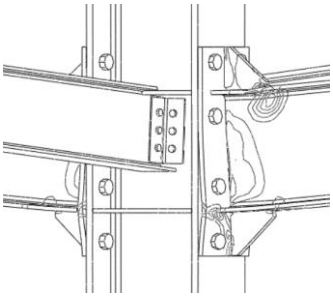	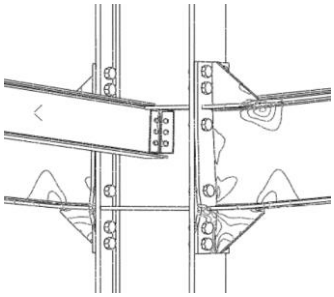
10%		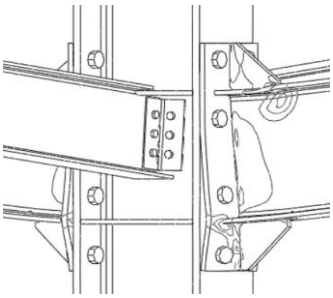	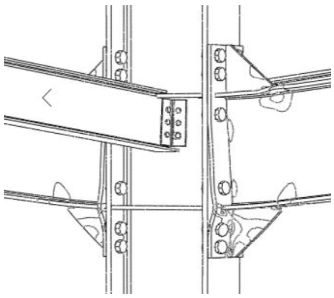

Figure 6.11. PEEQ images of the equal-strength joints

6.5.2.2 Full-strength joints

Numerical results for the full-strength joints showed an expected trend (Figure 6.14), where the beams experienced very large yielding than the other components. Full-strength joints are designed to have the plasticity concentrated on the beams. Unlike the equal-strength joints, the full-strength joints have very high plastic dissipation on the beams, taking approximately 75%, 65%, and 45% of the whole plastic deformation, respectively, for ES1, ES2, and ES3 models. This can be related to the catenary action of the joint, in which higher beam plasticity would yield to larger catenary support.

Other observations are the zero yielding of the continuity plates. The bolts have very low plastic contribution in full-strength joints, as also seen on the figures, which means that the connection does not have a huge contribution on the plastic energy of full-strength joints, compared with the equal-strength joints. This is also evident on the PEEQ index images, where a large concentration of plasticity is on the beams. Following the same trend previously, the bottom ribs exhibit larger plastic yielding on the larger columns.

Hence, from these models, an ideal behaviour was also observed since the beams have larger yielding points than the other components, leading to a more ductile behaviour.

In this set of models, it is also evident that the PEEQ values of the angular plates are much higher than other components, followed by the bolts, seen on Figure 6.13. This indicates that a huge plasticity is happening on the angular plates which could hinder its role to transfer the loads to the secondary beams.

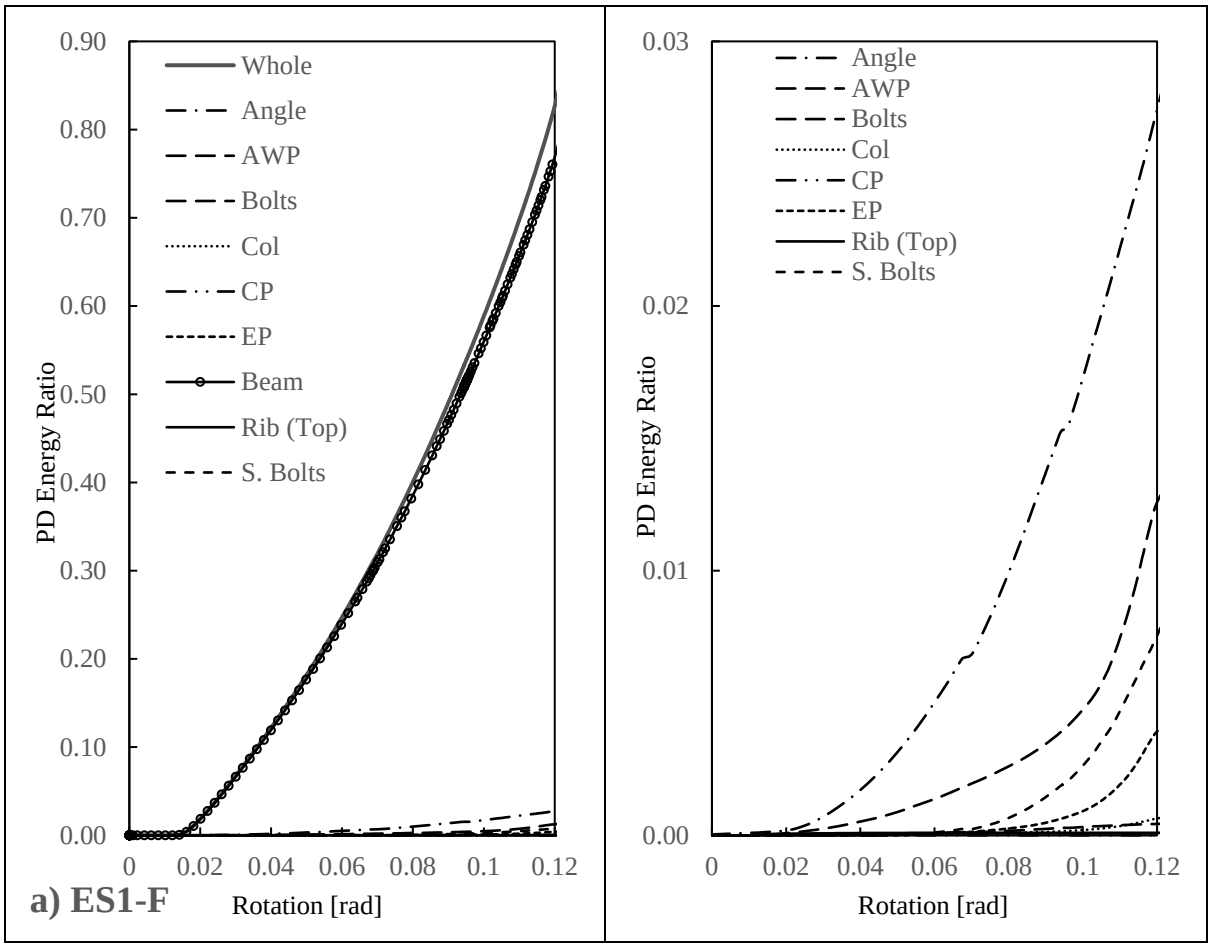

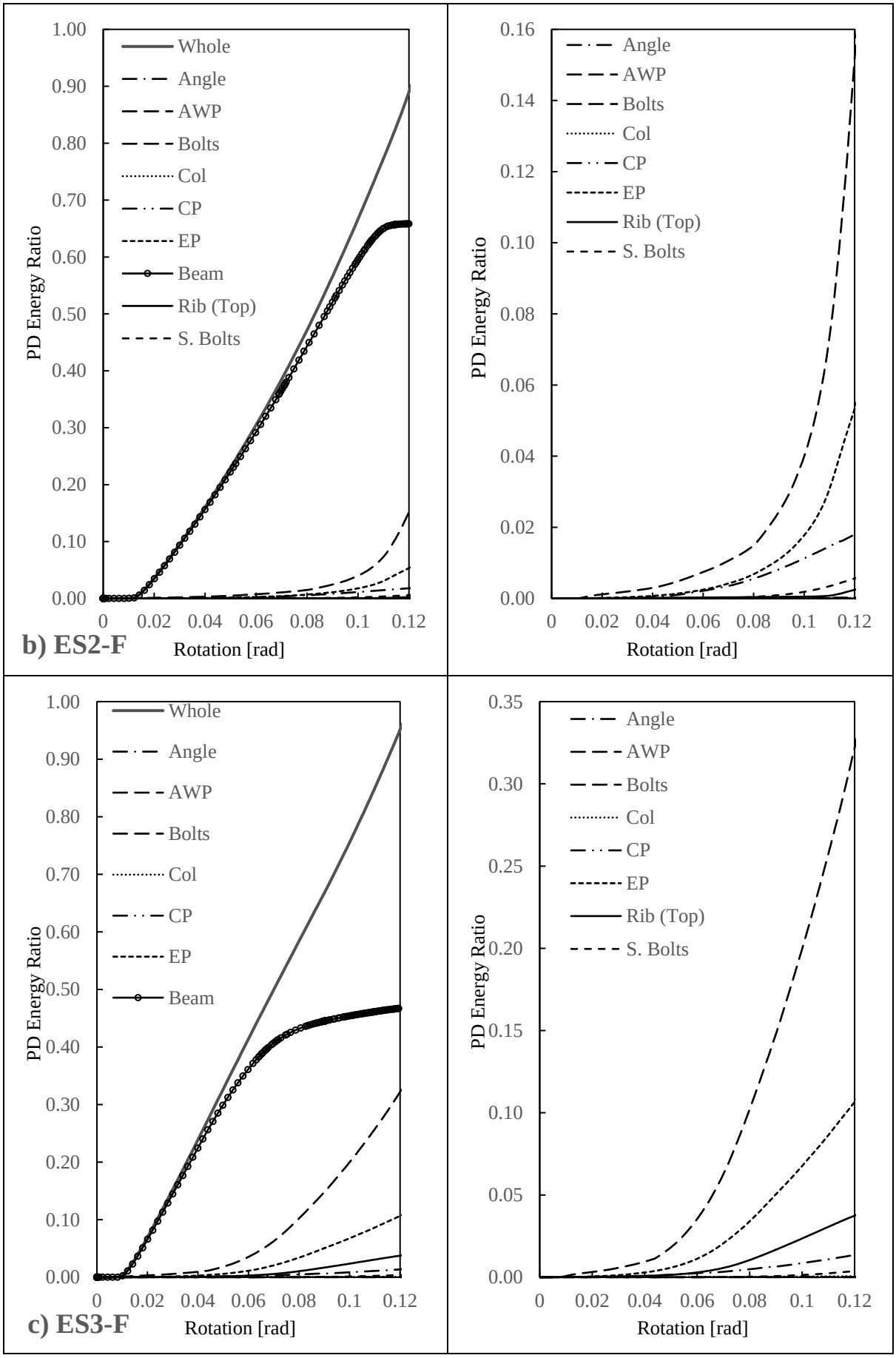

Figure 6.12. Rotation vs PD energy ratio of each connection component for full-strength joints

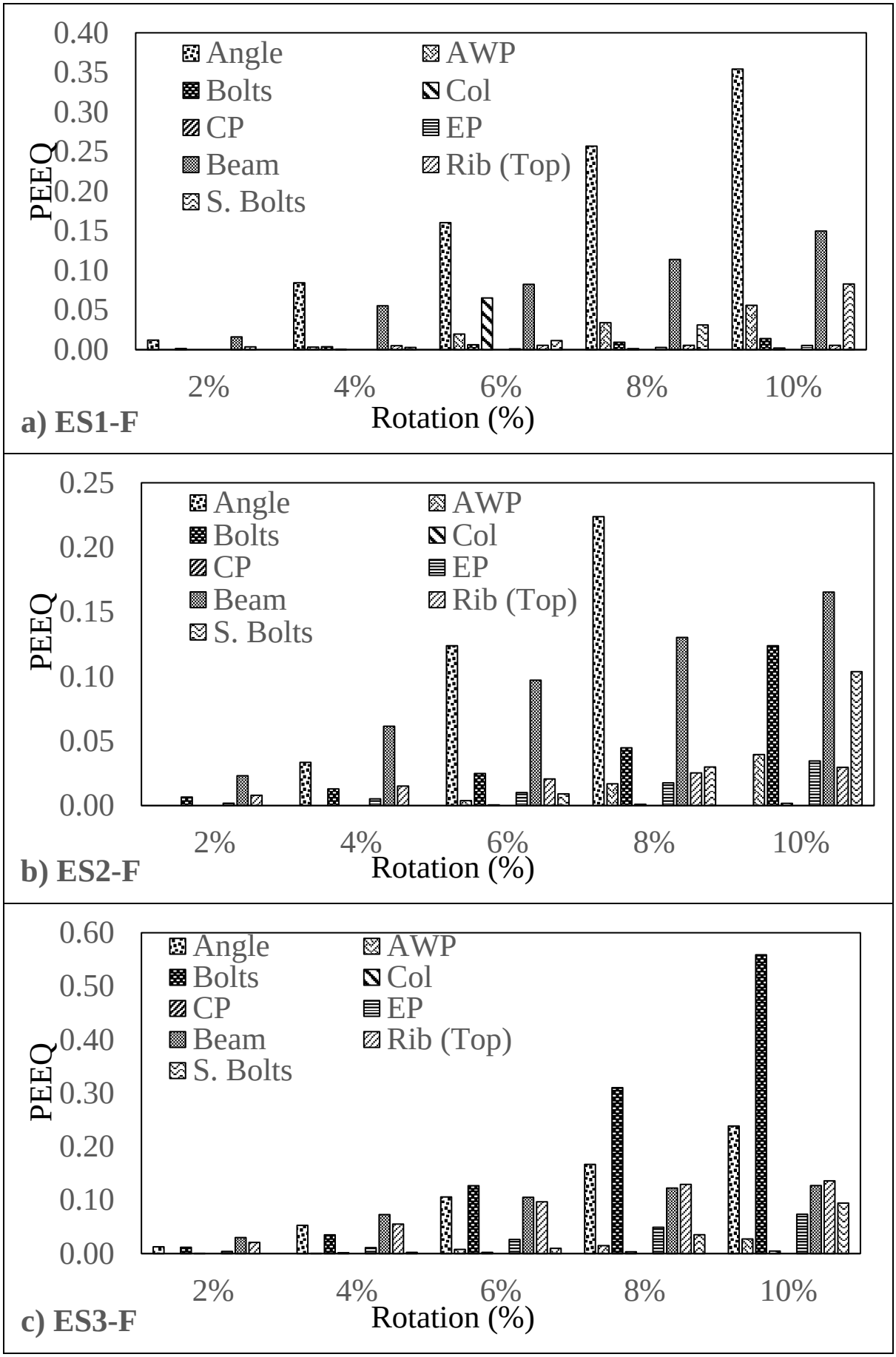

Figure 6.13. PEEQ values of each connection component for full-strength joints

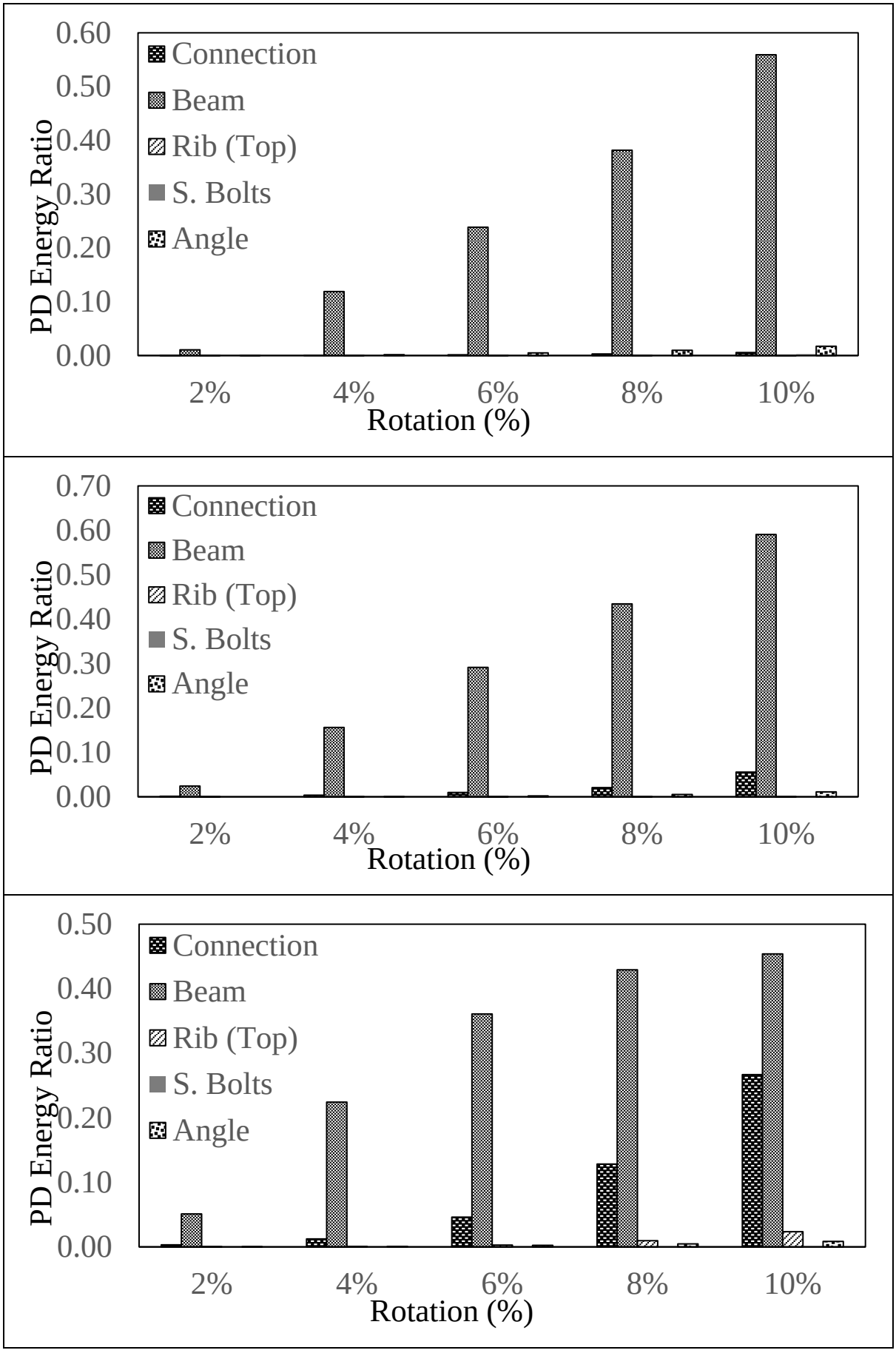

Figure 6.14. PD energy ratio of each joint component, the connection component combined (full-strength joints)

PEEQ (%)	ES1-F	ES2-F	ES3-F
2%	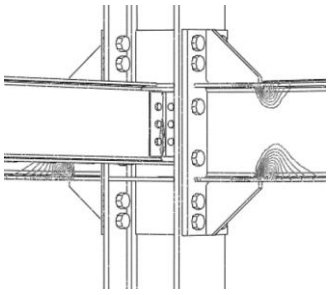	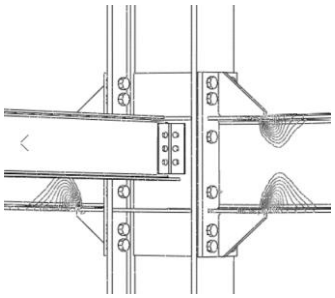	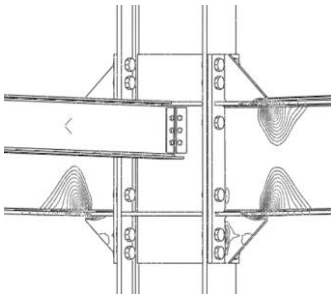
4%	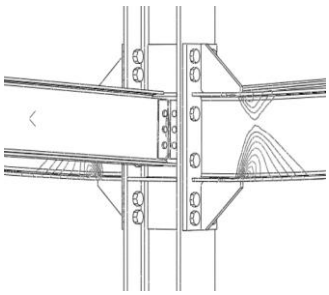	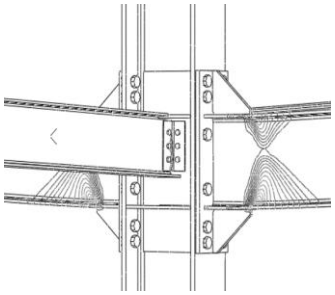	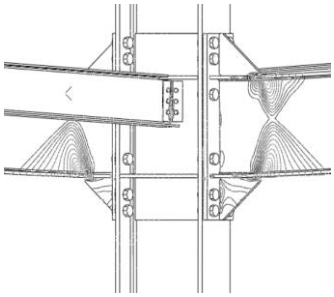
6%	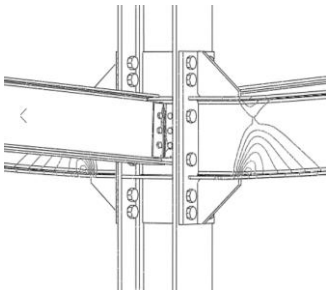	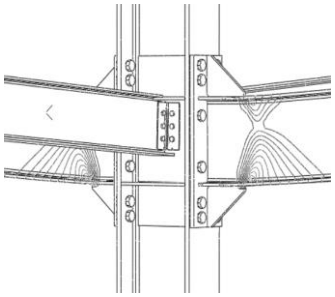	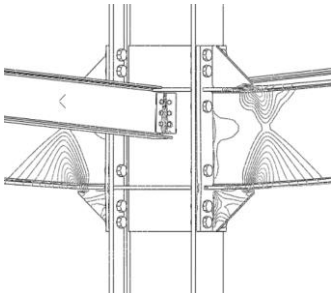
8%	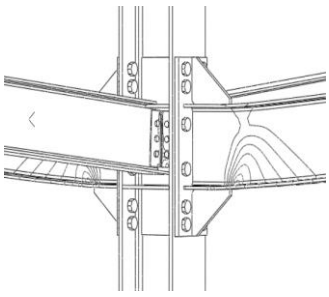	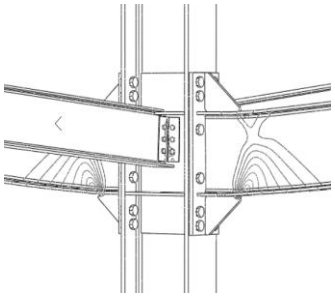	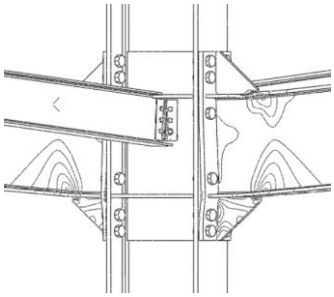
10%	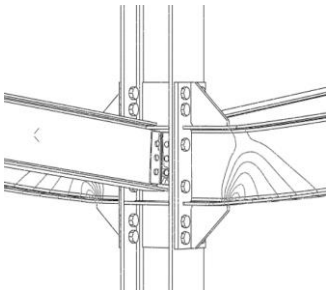	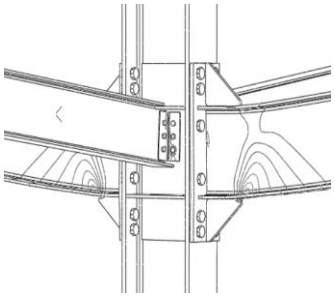	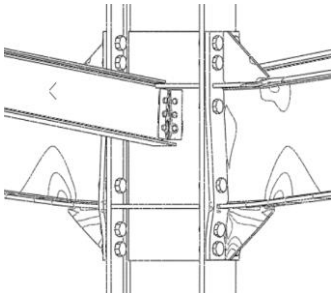

Figure 6.15. PEEQ images of the full-strength joints

6.5.2.3 Partial-strength joints

The partial-strength joints also provided expected results. As seen on Figure 6.18, the connection has the largest plasticity compared with the beams (which is expected for partial-strength joints), except for ES3-P. One reason that likely resulted with this unexpected result is the convergence problem on the ES3-P model. As you can see on Figure 6.7c, the analysis only went up to 0.08 rad, which is relatively insufficient to make any additional inference. As a recommendation, re-running and re-meshing the model would lead to a better convergence which in turn give out reasonable outcomes. Aside from that, it is also evident that the ES3-P model has the highest compressive arching effect, which also lead to a lower catenary action at larger rotations, same case as the previous models.

The high PEEQ value of the angular plates (followed by the bolts) are also observed for partial-strength joints, as seen on Figure 6.17. This indicates the same issue of the other models, wherein high plasticity at the angular plates (especially for smaller columns) would lead to inability to transfer the loads to the secondary beams, decreasing the influence of the secondary beams on the joint under column loss scenario.

Lastly, the same result was also observed with higher plasticity of the bottom ribs on larger columns where it is the opposite for the smaller ones. This is due to the size of the ribs, in which they are more proportionate in size with the smaller columns. That is why on the case of ES-3 (also for the other set of models), the ribs on the bottom are more plasticized.

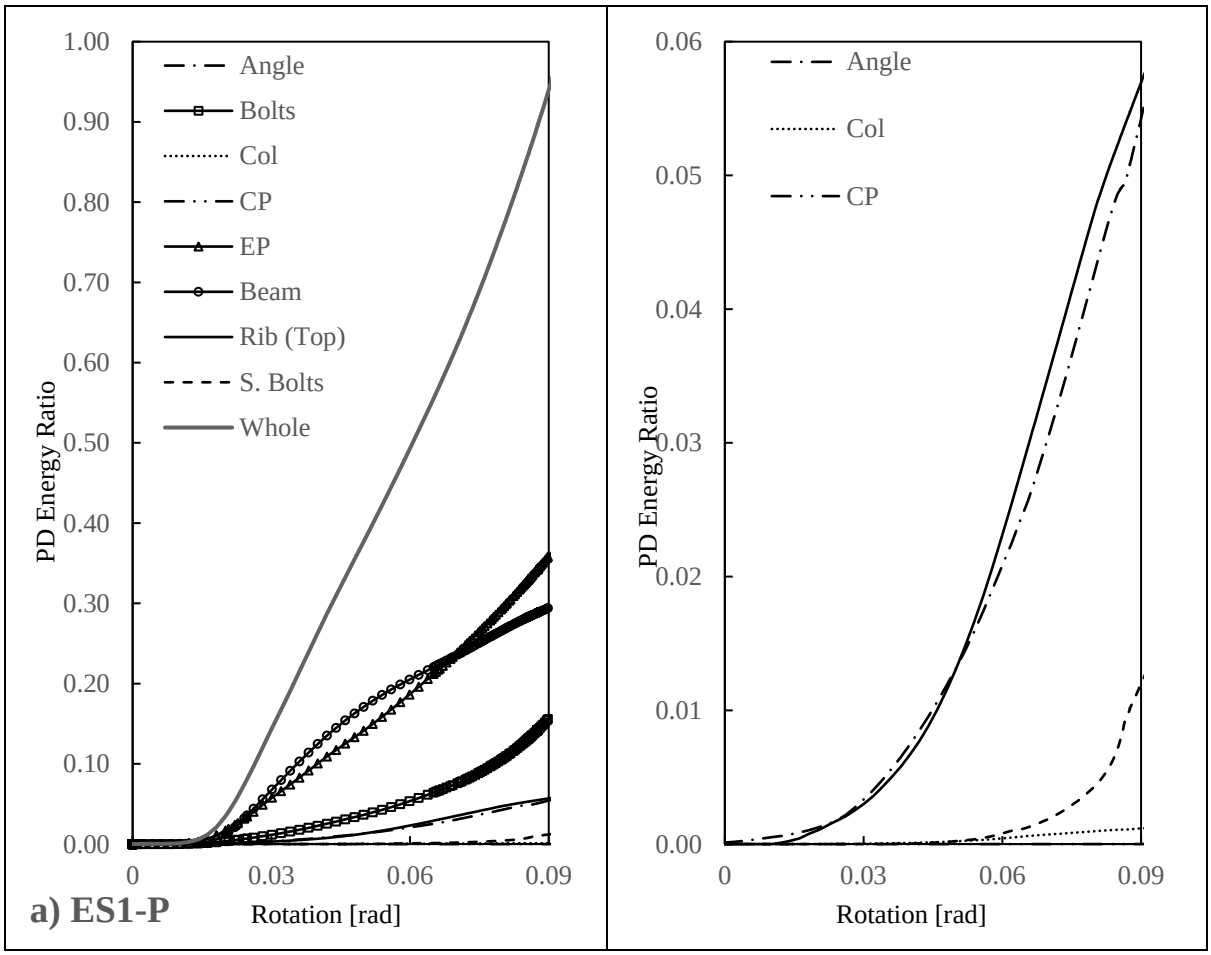

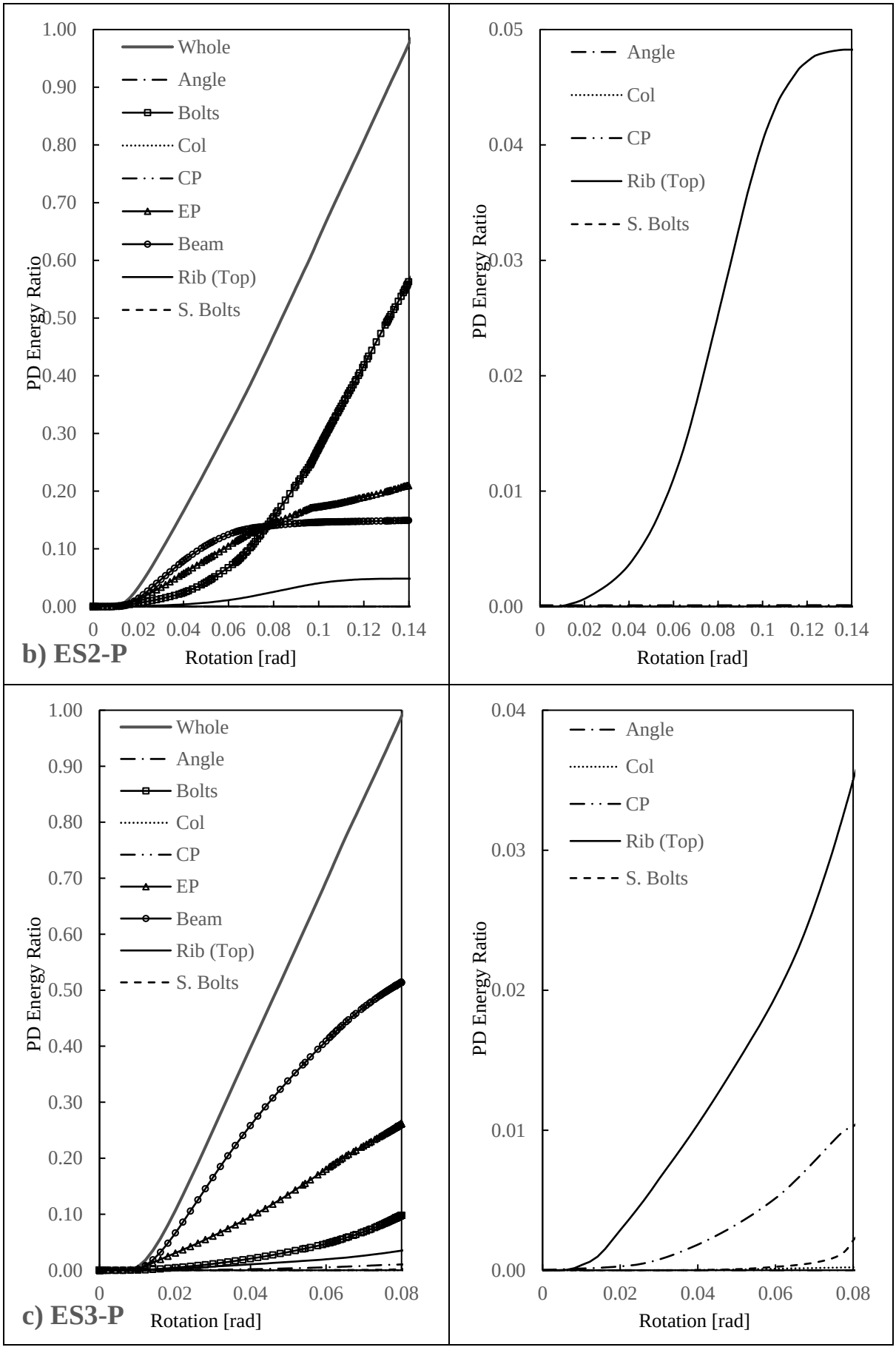

Figure 6.16. Rotation vs plastic deformation of each connection component for partial-strength joints

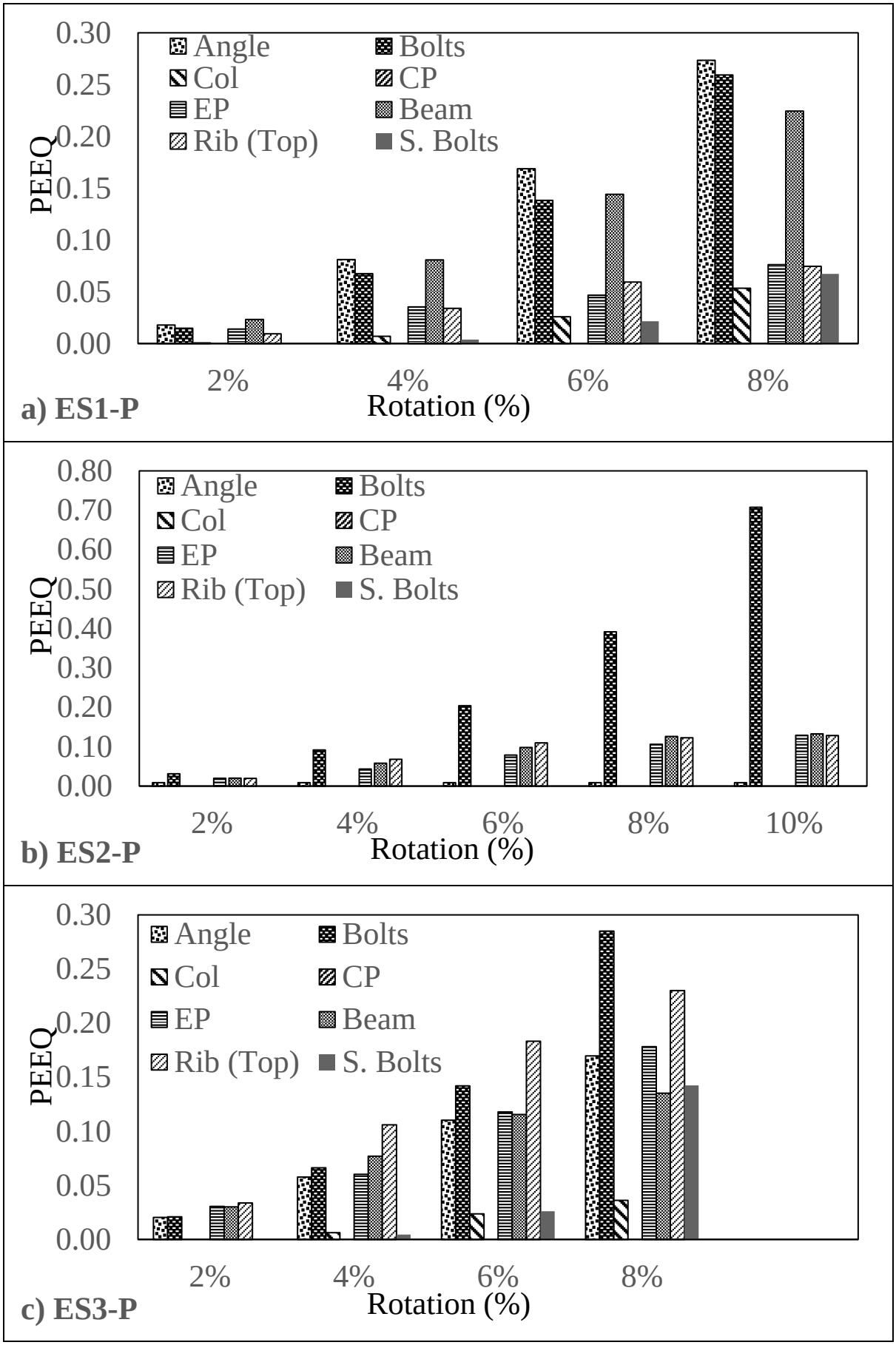

Figure 6.17. PEEQ values of each connection component for partial-strength joints

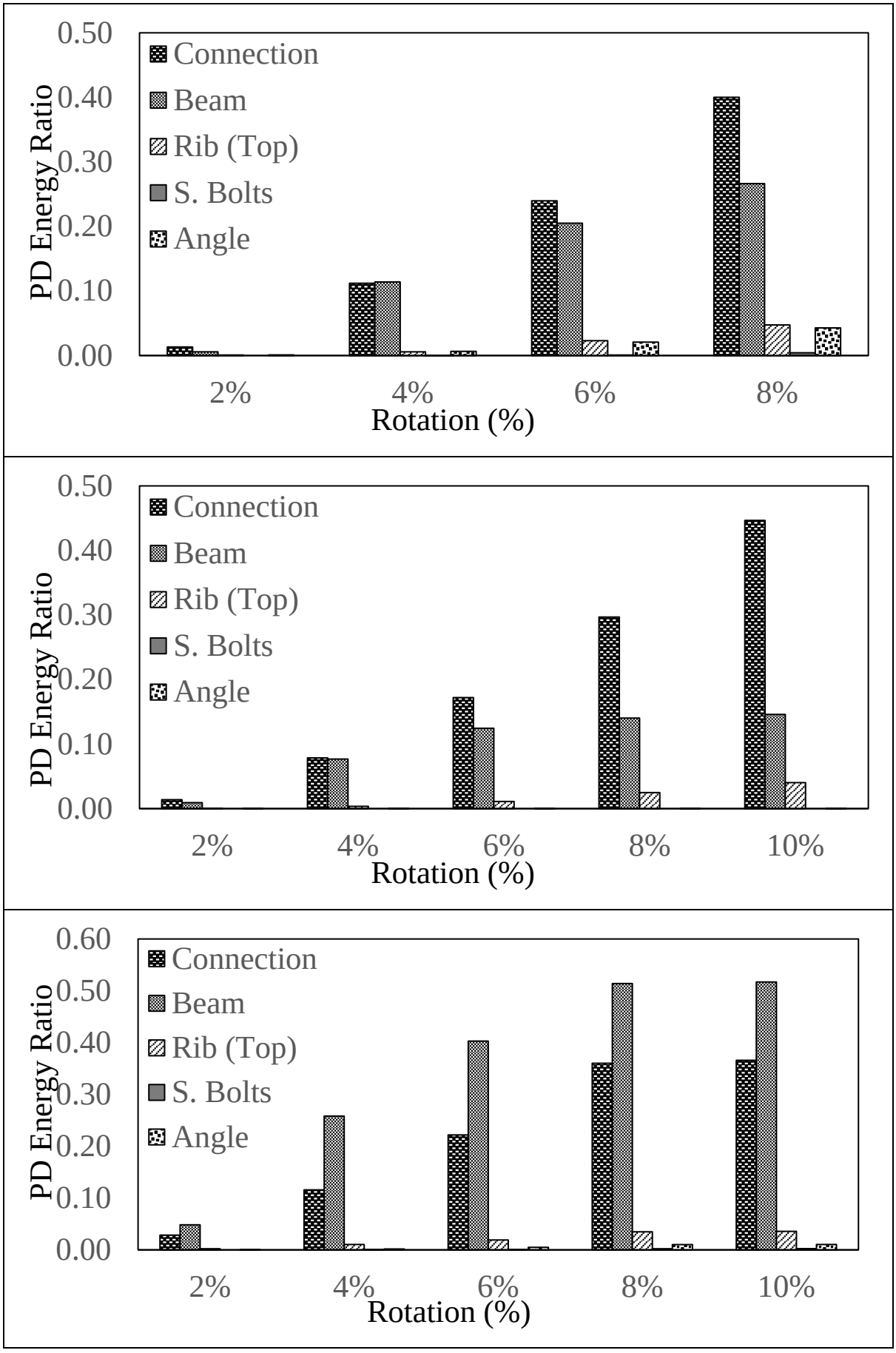

Figure 6.18. PD energy ratio of each joint component, the connection component combined (partial-strength joints)

PEEQ (%)	ES1-P	ES2-P	ES3-P
2%	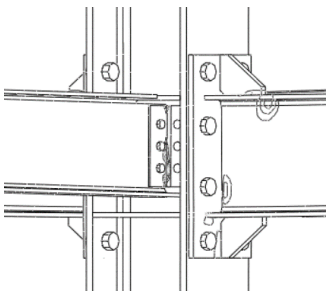	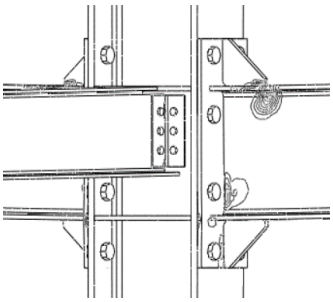	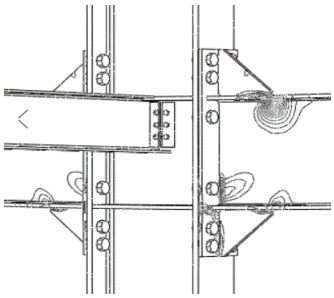
4%	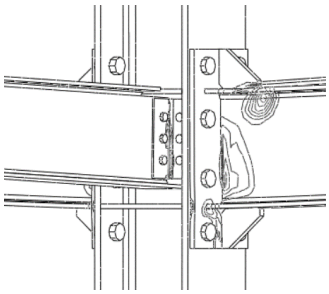	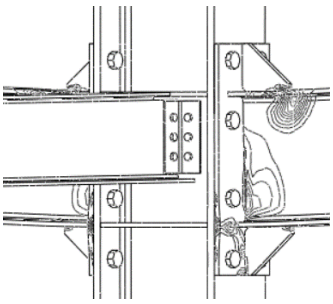	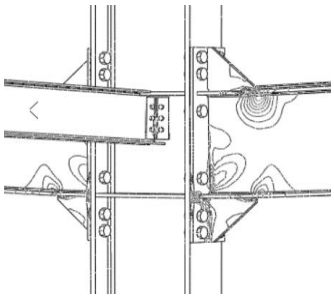
6%	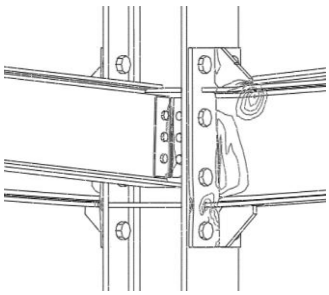	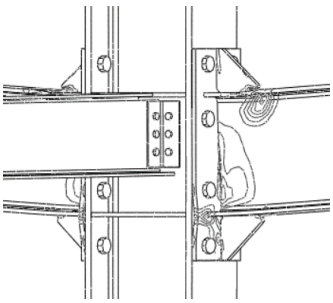	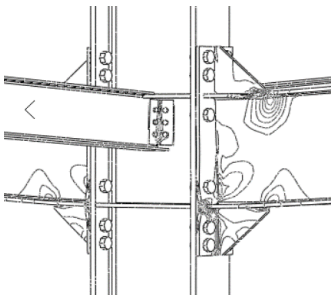
8%	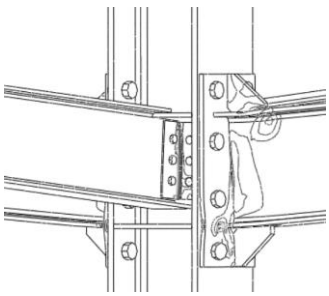	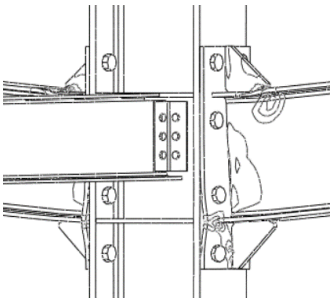	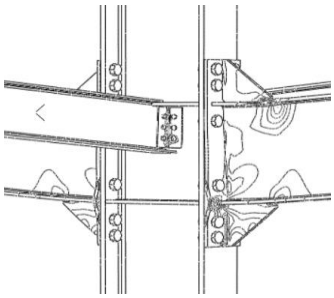
10%		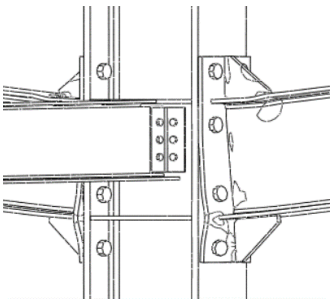	

Figure 6.19. PEEQ images of the partial-strength joints

6.6 ANALYSIS 2: Influence of the secondary beam

As indicated in the previous sections, the influence of the secondary beam was also analysed in this study. To do that, another set of models were done in ABAQUS on the same models, only deactivating the effect of the secondary beam. The results will be extracted from ABAQUS, similar to what was done in the first set of models.

Figure 6.20 shows the plot of the moment capacity curve of the joint with no secondary beams compared with the ones with secondary beams. As seen on the figure, the plots of both cases for ES1-E, ES2-E, and ES3-E are overlapping, values are almost equal, only varying by approximately around 50-300N.

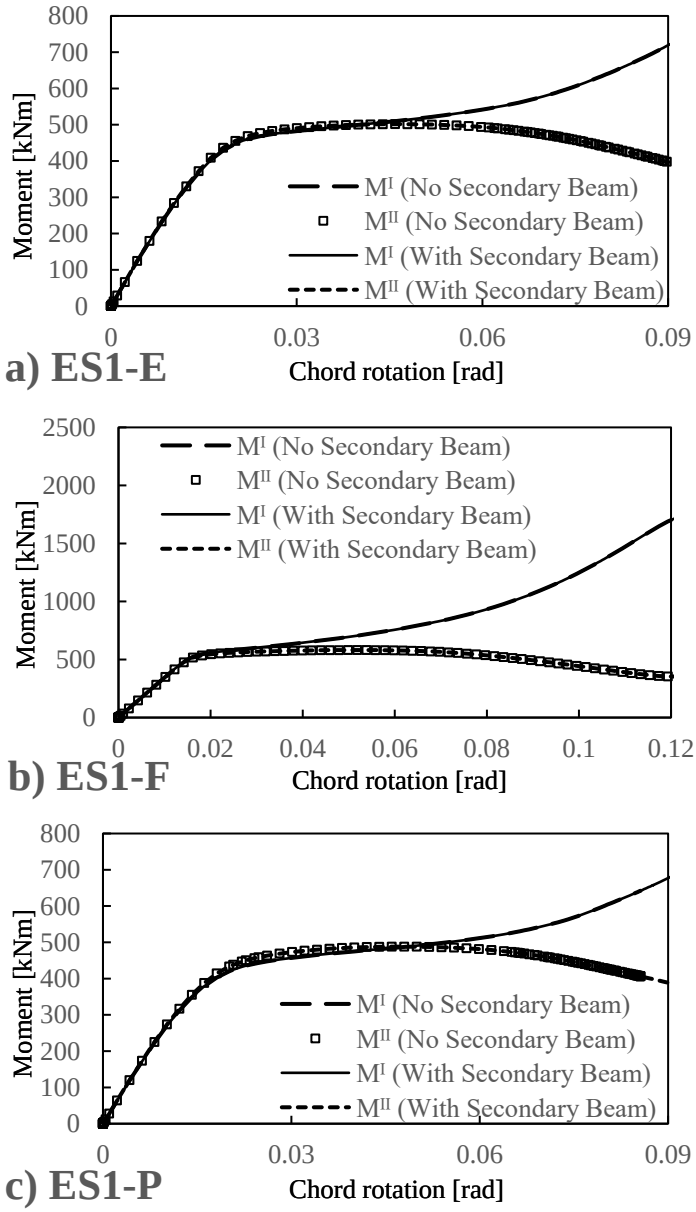

Figure 6.20. Comparison of moment capacity curves with and without secondary beams

To validate these findings, the reaction forces on the secondary beams of the original models were also obtained, the moment capacity curve is generated and finally compared with the moment capacity of the primary beams. Results are shown in Figure 6.21. As seen on the figures, all models have a contribution

from the secondary beam that are practically insignificant when compared with the contribution from the primary beam. This means that the connections of the secondary beam are much weaker than the connections on the primary beams.

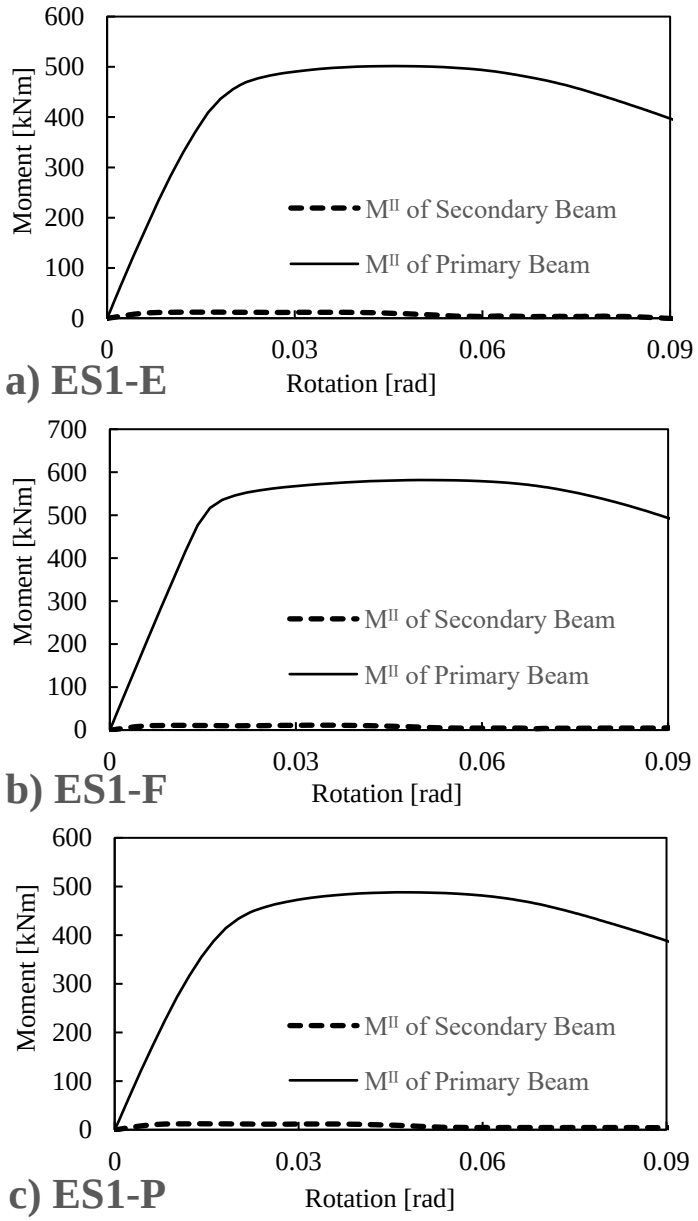

Figure 6.21. Comparison of the moment capacity curves of the primary and secondary beam

As also noticed on the PEEQ images of all models in Figure X, all angular plates received relatively larger PEEQ values. This was also discussed previously when the PEEQ values were plotted against 2%, 4%, 6%, 8%, and 10% rotation. This indicated that the angular plates failed already even before it transferred loads to the secondary beams. The strength and stiffness of these plates would be found to be adequate if they are higher, which in turn will allow proper transfer of loads to the secondary beams.

Lastly, to further investigate on the results, the shear forces acting on the angular plates and the secondary bolts are extracted from ABAQUS. The rotation vs load curve was then plotted and compared to the normal forces acting on the tip of the secondary beam. Figure 6.23 shows that for all models, the shear forces are almost equal for the three points considered in the analysis. This means that the bolts are not able to transfer the loads to the secondary beam, allowing the system to behave as shown in the figure.

Discrepancy on the bolts are taken to be from the irregularities and the movement of the bolts from the bolt holes that are larger than the nominal diameter, as prescribed by the Eurocode [46].

Further recommendations to investigate the influence of the secondary beam is to improve the strength and ductility of the connection (e.g. increasing the bolt grade, steel grade, or bolt sizes). In this way, the effect of the secondary beam will be determined since the bolts will be able to transfer the loads to the secondary beam.

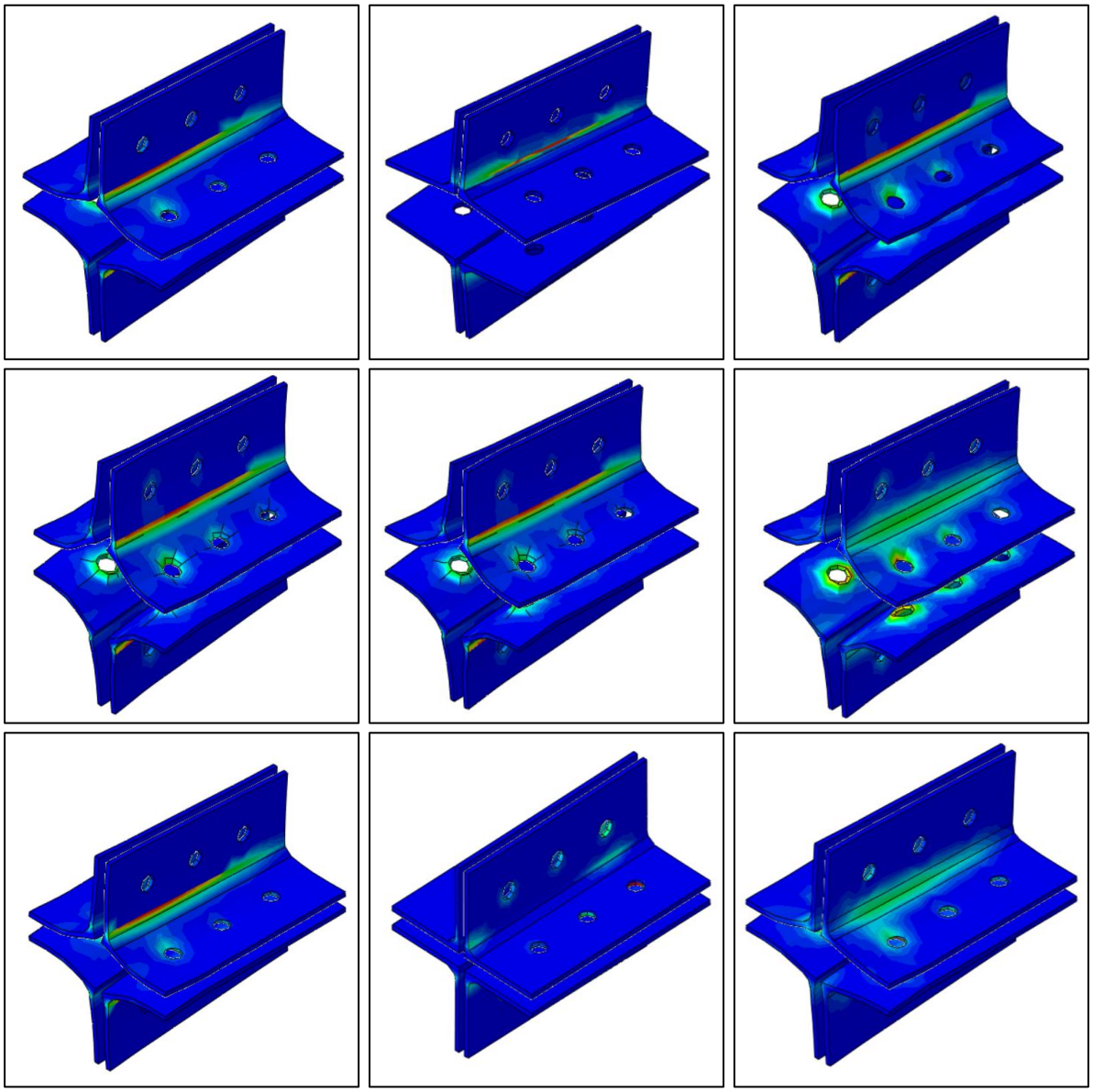

Figure 6.22. PEEQ images of the beams (top-bottom: equal-strength models, full-strength models, partial-strength models)

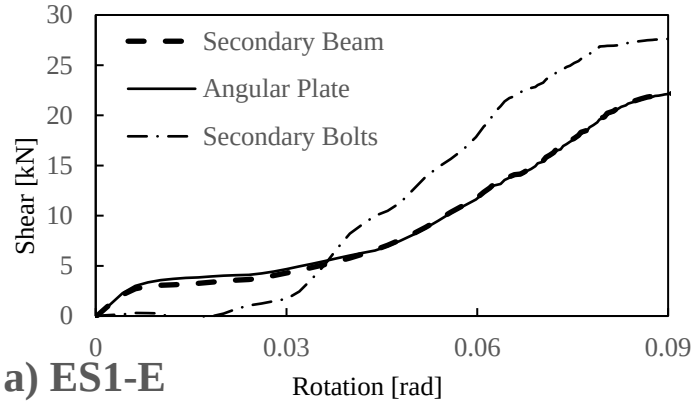

a) ES1-E

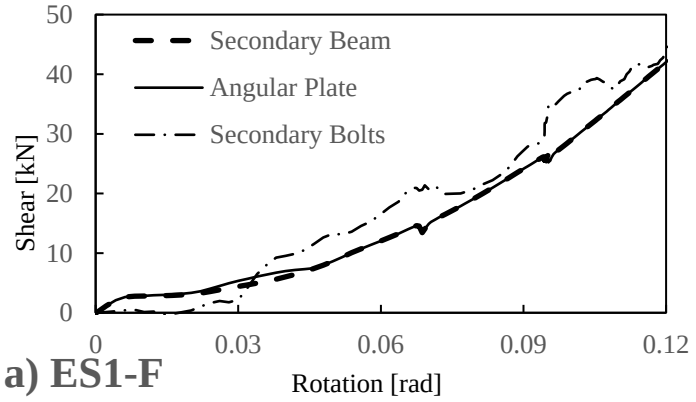

a) ES1-F

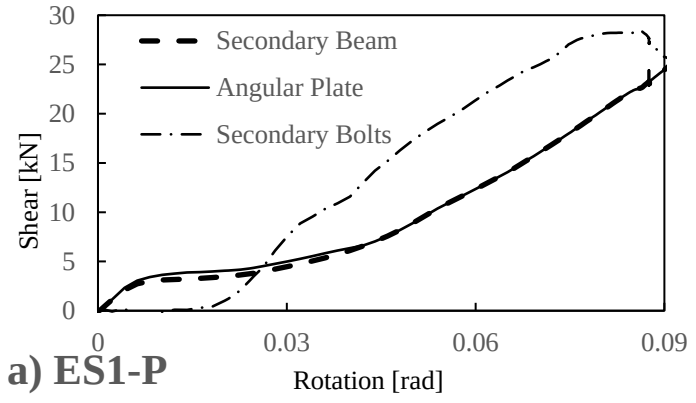

a) ES1-P

Figure 6.23. Rotation vs shear force curve of the angular plate, secondary beam tip, and the secondary bolts of the ES1 models

7. CONCLUSIONS AND RECOMMENDATIONS

It has been shown how the performance of moment-resisting steel frames under progressive collapse is greatly affected by the behaviour of its joints. A numerical investigation on stiffened extended end-plate bolted connections was presented in this study, giving light to the performance of various joint typologies recommended in seismic zones when it is also under column loss scenario. Finite element models were done to simulate such scenarios on nine typologies, which was validated on previous experimental and numerical results. Results showed symmetry on both side of the connections, allowing a desirable outcome. Based on the results discussed in this analysis, the following conclusions are presented:

1. Under column loss scenario, the arching effect in compression was the initial process that occurred on the joint. After this stage, when rotations are larger, this becomes less apparent, and tensile catenary forces are progressing on the beams, which consequently increases in length. It has been shown that the lesser this compressive arching effect, the larger the catenary action is that propagates on the beam.

2. The catenary action was investigated to modify the internal forces on the joint. Previous studies show that the internal forces are different when it is just under pure bending. Meanwhile, in this study, it was presented that large axial forces develop on the beam at larger displacements, validating the optimization of catenary action on column loss scenario.

3. All models, except for ES3-P, delivered expected results based on the plastic dissipation energy ratio with regards to the joint typology used. Equal-strength joints have close contributions from the beam and the connections, full-strength joints have way larger contribution from the beam than the connections, while partial-strength joints have contribution on the plastic energy higher on the connections than the beams.

4. The ductility of the connection is significant on the development of the catenary action.

5. The rib stiffeners on the top (tension side) are found to have larger plasticity on smaller columns (i.e. ES-1 and ES-2 models) while for larger beam (i.e. ES-3 models), the bottom stiffeners (compression side) have larger plasticity. This is due to the proportionality of the size of the beams with respect to the size of the stiffeners, wherein the smaller beam, a more proportionate size was achieved.

6. Moment capacity curves showed a similar pattern for all models under column loss scenario, only increasing in strength as the column size is increased.

7. The influence of the secondary beam is deemed insufficient in this study. Higher stiffness and strength of the secondary beam connection must be done to allow further investigations on its influence on the joint. In this study, the moment capacity of the secondary beams is almost negligible when compared to the primary beams, due to the same reason mentioned previously. PEEQ images showed that the angular plates experienced large plasticity for all models, indicating failure even before transferring the loads to the secondary beams. It was also shown that the shear forces on the angular plate, secondary beam tip, and the secondary bolts are almost equal, proving that the forces due to the column loss are not transferred in the beam.

The following recommendations, for further study, are listed below:

1. Larger displacements set on ABAQUS must be utilized when running the model since a 500-mm forced displacement only achieved rotation at around 0.09 rad for some models.

2. Re-simulating the ES3-P model where convergence problems are minimized, if not eliminated, must be done to verify its performance.

3. Investigating on the case of the typologies presented in this study under pure bending is advised to compare the performance of this type of connection under both cases.

4. Increasing the stiffness and strength of the secondary beam connection would give more light on the influence of the secondary beams under loss of the middle column scenario.

8. REFERENCES

[1] M. D'Aniello, R. Tartaglia, S. Costanzo and R. Landolfo, "Seismic design of extended stiffened end-plate joints in the framework of Eurocodes," *Journal of Construction Steel Research,* vol. 128, pp. 512-527, 2017.

[2] Eurocode EN 1991-1-7, Eurocode 1 - Actions on structures - Part 1-7: General actions - Accidental actions, 2006.

[3] F. Dinu, I. Marginean, D. Dubina and I. Petran, "Experimental testing and numerical analysis of 3D steel frame system under column loss," *Engineering Structures,* vol. 113, pp. 59-70, 2016.

[4] S. El-Tawil, H. Li and S. Kunnath, "Computational simulation of gravity-induced progressive collapse of steel-frame buildings: Current trends and future research needs," *Journal of Structural Engineering,* vol. 140, no. 8, 2014.

[5] D. Blockley, J. Agarwal, T. Pinto and N. Woodman, "Structural vulnerability, reliability and risk," *Progress in Structural Engineering and Materials,* vol. 4, no. 2, pp. 203-212, 2002.

[6] A. Formisano, R. Landolfo and F. Mazzolani, "Robustness assessment approaches for steel framed structures under catastrophic events," *Computer and Structures,* vol. 147, pp. 216-228, 2015.

[7] ASCE, Minimum design loads for buildings and other structures, American Society of Washington, D.C., 2002.

[8] Y. Yin and Y. Wang, "Analysis of catenary action in steel beams using a simplified hand calculation method, Part 1: theory and validation for uniform temperature distribution," *Journal of Constructional Steel Research,* vol. 61, pp. 183-211, 2005.

[9] J. Shen, A. Astaneh-Asl and D. McCallen, "Use of Deep Columns in Special Steel Moment Frames," Technical Information and Product Service, Structural, AISC, Chicago, Illinois, 2002.

[10] X. Zhang and J. Ricles, "Experimental Evaluation of Reduced Beam Section Connections to Deep Columns," *Journal of Structural Engineering,* vol. 132, no. 3, pp. 346-357, 2006.

[11] X. Zhang, J. Ricles, J. Fisher and L. Lu, "Analytical studies on deep column-to-beam welded steel moment connections," in *STESSA 2003 - Behaviour of Steel Structures in Seismic Areas: Proceedings of the 4th International Specialty Conference*, Naples, Italy, 2003.

[12] A. Elkady and D. Lignos, "Collapse Assessment Special Steel Moment Resisting Frames Designed with Deep Columns," in *Vienna Congress on Recent Advances in Earthquake Engineering and Structural Dynamics (VEESD)*, Vienna, Austria, 2013.

[13] C. Uang, "Seismic Design And Modeling Of "deep" Steel Columns," UC San Diego, 2017. [Online]. Available: https://structures.ucsd.edu/research/research-projects/seismic-design-and-modeling-of-deep-steel-columns. [Accessed 2017].

[14] M. Zimbru, "Numerical Investigation of Seismic Behaviour of Steel Stiffened Extended End Plate Connections (Master's Thesis)," 2015.

[15] ANSI/AISC 341-10, Seismic Provisions for Structural Steel Buildings, American Institute of Steel Construction, 2010.

[16] E. Sumner and T. Murray, "Behavior of Extended End-Plate Moment Connections Subject to Cyclic Loading," *Journal of Structural Engineering,* vol. 128, no. 4, pp. 501-508, 2002.

[17] J. Gracia, E. Bayo, F. Ferrario, O. Bursi, A. Braconi and W. Salvatore, "The seismic performance of a semi-rigid composite joint with a double-sided extended end-plate. Part I: Experimental research," *Engineering Structures,* vol. 32, pp. 385-396, 2010.

[18] B. Guo, Q. Gu and F. Liu, "Experimental Behavior of Stiffened and Unstiffened End-Plate Connections under Cyclic Loading," *Journal of Structural Engineering,* vol. 132, no. 9, pp. 1352-1357, 2006.

[19] A. Abidelah, A. Bouchaïr and D. Kerdal, "Experimental and analytical behavior of bolted end-plate connections with or without stiffeners," *Journal of Constructional Steel Research,* vol. 76, pp. 13-27, 2012.

[20] A. Ghobarah, A. Osman and R. Korol, "Behaviour of extended end-plate connections under cyclic loading," *Engineering Structures,* vol. 12, pp. 15-27, 1990.

[21] A. Girão Coelho, F. Bijlaard and L. Da Silva, "Experimental assessment of the ductility of extended end-plate connections," *Engineering Stuctures,* vol. 26, pp. 1185-1206, 2004.

[22] A. Ciutina and D. Dubina, "Column Web Stiffening of Steel Beam-to-Column Joints Subjected to Seismic Actions," *Journal of Structural Engineering,* vol. 134, no. 3, pp. 505-510, 2008.

[23] K. Tsai and E. Popov, "Cyclic behaviour of extended end-plate moment connections," *Journal of Structural Engineering,* vol. 116, no. 11, pp. 2917-29130, 1990.

[24] Y. Shi, G. Shi and Y. Wang, "Experimental and theoretical analysis of the moment-rotation behaviour of stiffened extended end-plate connections," *Journal of Constructional Steel Research,* vol. 63, pp. 1279-1293, 2007.

[25] R. Landolfo, O. Vassart, A. Elghazouli, J.-P. Jaspart, L. Simoes Da Silva, D. Dubina, L. Lucchese and V. Dehan, "European pre-QUALified steel JOINTS (EQUALJOINTS) Project: Mid-term Report (RFSR-CT-2013-00021)," 2015.

[26] U. Starossek and M. Haberland, "Approaches to measures of structural robustness," *Structure and Infrastructure Engineering,* vol. 7, no. 7-8, pp. 625-631, 2011.

[27] S. El-Tawil, "Computational Structural Simulation Laboratory (CSSL)," The Regents of the University of Michigan, 2016. [Online]. Available: http://www-personal.umich.edu/~eltawil/catenary-action.html. [Accessed November 2016].

[28] B. Yang and K. H. Tan, "Experimental tests of different types of bolted steel beam–column joints under a central-column-removal scenario," *Engineering Structures,* vol. 54, pp. 112-130, 2013.

[29] B. Yang and K. H. Tan, "Numerical analyses of steel beam-column joints subjected to catenary action," *Journal of Constructional Steel Research,* vol. 70, pp. 1-11, 2012.

[30] D. Cassiano, M. D'Aniello, C. Rebelo, R. Landolfo and L. Simoes da Silva, "Influence of seismic design rules on the robustness of steel moment resisting frames," *Steel and Composite Structures,* vol. 21, no. 3, pp. 479-500, 2016.

[31] Department of Defense DoD, Unified Facilities Criteria (UFC): design of structures to resist progressive collapse, Washington D.C., 2005.

[32] ASCE 41-13, Seismic evaluation and retrofit of existing buildings, Reston, Virginia: American Society of Civil Engineers, 2013.

[33] R. Tartaglia, M. D'Aniello and R. Landolfo, "Non-linear performance of extended stiffened end-plate bolted beam-to-column joints subjected to column removal," *The Open Civil Engineering Journal,* 2016.

[34] H. Chen, "The performance of semi-rigid steel frame structure in progressive collapse," *Vibroengineering PROCEDIA,* vol. 8, pp. 237-242, 2016.

[35] Z. Dřevěný, "Behaviour of beam-to-column joints under large vertical displacements following the loss of a column (Master's Thesis)," Timisoara, 2014.

[36] British Standards, BS5950-1, Part 1: Code of practice for design – Rolled and welded sections, British Standards Institution, 2001.

[37] Department of Defense, "Unified Facilities Criteria (UFC): design of buildings to resist progressive collapse," Washington DC, 2013.

[38] Eurocode EN 1990, Eurocode - Basis of structural design, 2005.

[39] D. Cormie, G. Mays and P. Smith, Blast Effects on Buildings 2nd Edition, Thomas Telford, 2009.

[40] T. Kovecsi, “Membrane action of slabs in framed structures in case of accidental column loss (Master's Thesis),” Timisoara, 2014.

[41] Dassault Systemes Simulia Corp., Abaqus/CAE User's Guide v. 6.14, Providence, RI, USA, 2014.

[42] A. Dutta, S. Dhar and S. Acharyya, “Material characterization of SS 316 in low-cycle fatigue loading,” *Journal of Materials Science,* vol. 45, no. 7, pp. 1782-1789, 2010.

[43] M. Wang, Y. Shi, Y. Wang and G. Shi, “Numerical study on seismic behaviors of steel frame end-plate connections,” *Journal of Constructional Steel Research,* vol. 90, pp. 140-152, 2013.

[44] M. D'Aniello, D. Cassiano and R. Landolfo, “Monotonic and cyclic inelastic tensile response of European preloadable GR10.9 bolt assemblies,” *Journal of Construction Steel Research,* vol. 124, pp. 77-90, 2016.

[45] J. Swanson, D. Kokan and R. Leon, “Advanced finite element modeling of bolted T-stub connection components,” *Journal of Constructional Steel Research,* vol. 58, pp. 1015-1031, 2002.

[46] EN 1993-1-8:2005, Eurocode 3: Design of steel structures - Part 1-8: Design of joints, 2005.

9. LIST OF TABLES

10. LIST OF FIGURES

11. APPENDICES

11.1 APPENDIX A – Surfaces defined in ABAQUS

SURFACE		F	E	P08
Col	AWP_Left			
AWP_Left	Col			
Col	AWP_Right			
AWP_Right	Col			
Col	EP_Left			
EP_Left	Col			
Col	EP_Right			
EP_Right	Col			
Col	CP_Q1			
CP_Q1	Col			
Col	CP_Q2			
CP_Q2	Col			
Col	CP_Q3			
CP_Q3	Col			
Col	CP_Q4			
CP_Q4	Col			
AWP_Left	CP_Q1			
CP_Q1	AWP_Left			
AWP_Left	CP_Q2			
CP_Q2	AWP_Left			
AWP_Right	CP_Q3			
CP_Q3	AWP_Right			
AWP_Right	CP_Q4			
CP_Q4	AWP_Right			
Pbeam_Left	EP_Left			
EP_Left	Pbeam_Left			
Pbeam_Right	EP_Right			
EP_Right	Pbeam_Right			
EP_Left	Rib_Q2			
Rib_Q2	EP_Left			
EP_Left	Rib_Q3			
Rib_Q3	EP_Left			
EP_Right	Rib_Q1			
Rib_Q1	EP_Right			
EP_Right	Rib_Q4			
Rib_Q4	EP_Right			
Pbeam_Left	Rib_Q2			
Rib_Q2	Pbeam_Left			
Pbeam_Left	Rib_Q3			
Rib_Q3	Pbeam_Left			
Pbeam_Right	Rib_Q1			
Rib_Q1	Pbeam_Right			
Pbeam_Right	Rib_Q4			
Rib_Q4	Pbeam_Right			
AWP_Left	AngleP_Q1			
AngleP_Q1	AWP_Left			
AWP_Left	AngleP_Q2			
AngleP_Q2	AWP_Left			
AWP_Right	AngleP_Q3			
AngleP_Q3	AWP_Right			
AWP_Right	AngleP_Q4			
AngleP_Q4	AWP_Right			

SURFACE		F	E	P08
AngleP_Q1	Sbeam_Left			
Sbeam_Left	AngleP_Q1			
AngleP_Q2	Sbeam_Left			
Sbeam_Left	AngleP_Q2			
AngleP_Q3	Sbeam_Right			
Sbeam_Right	AngleP_Q3			
AngleP_Q4	Sbeam_Right			
Sbeam_Right	AngleP_Q4			
Col	AngleP_Q1			
AngleP_Q1	Col			
Col	AngleP_Q2			
AngleP_Q2	Col			
Col	AngleP_Q3			
AngleP_Q3	Col			
Col	AngleP_Q4			
AngleP_Q4	Col			
Hole_L1	Col			
Hole_L2	Col			
Hole_L3	Col			
Hole_L4	Col			
Hole_L5	Col			
Hole_L6	Col			
Hole_L7	Col			
Hole_L8	Col			
Hole_L9	Col			
Hole_L10	Col			
Hole_L11	Col			
Hole_L12	Col			
Hole_R1	Col			
Hole_R2	Col			
Hole_R3	Col			
Hole_R4	Col			
Hole_R5	Col			
Hole_R6	Col			
Hole_R7	Col			
Hole_R8	Col			
Hole_R9	Col			
Hole_R10	Col			
Hole_R11	Col			
Hole_R12	Col			
Hole_L1	EP_Left			
Hole_L2	EP_Left			
Hole_L3	EP_Left			
Hole_L4	EP_Left			
Hole_L5	EP_Left			
Hole_L6	EP_Left			
Hole_L7	EP_Left			
Hole_L8	EP_Left			
Hole_L9	EP_Left			
Hole_L10	EP_Left			
Hole_L11	EP_Left			
Hole_L12	EP_Left			

SURFACE		F	E	P08
Hole_R1	EP_Right			
Hole_R2	EP_Right			
Hole_R3	EP_Right			
Hole_R4	EP_Right			
Hole_R5	EP_Right			
Hole_R6	EP_Right			
Hole_R7	EP_Right			
Hole_R8	EP_Right			
Hole_R9	EP_Right			
Hole_R10	EP_Right			
Hole_R11	EP_Right			
Hole_R12	EP_Right			
Bolt_L1	Col			
Bolt_L2	Col			
Bolt_L3	Col			
Bolt_L4	Col			
Bolt_L5	Col			
Bolt_L6	Col			
Bolt_L7	Col			
Bolt_L8	Col			
Bolt_L9	Col			
Bolt_L10	Col			
Bolt_L11	Col			
Bolt_L12	Col			
Bolt_R1	Col			
Bolt_R2	Col			
Bolt_R3	Col			
Bolt_R4	Col			
Bolt_R5	Col			
Bolt_R6	Col			
Bolt_R7	Col			
Bolt_R8	Col			
Bolt_R9	Col			
Bolt_R10	Col			
Bolt_R11	Col			
Bolt_R12	Col			
Bolt_L1	EP_Left			
Bolt_L2	EP_Left			
Bolt_L3	EP_Left			
Bolt_L4	EP_Left			
Bolt_L5	EP_Left			
Bolt_L6	EP_Left			
Bolt_L7	EP_Left			
Bolt_L8	EP_Left			
Bolt_L9	EP_Left			
Bolt_L10	EP_Left			
Bolt_L11	EP_Left			
Bolt_L12	EP_Left			

SURFACE		F	E	P08
Bolt_R1	EP_Right			
Bolt_R2	EP_Right			
Bolt_R3	EP_Right			
Bolt_R4	EP_Right			
Bolt_R5	EP_Right			
Bolt_R6	EP_Right			
Bolt_R7	EP_Right			
Bolt_R8	EP_Right			
Bolt_R9	EP_Right			
Bolt_R10	EP_Right			
Bolt_R11	EP_Right			
Bolt_R12	EP_Right			
Hole_X1	Sbeam_Left			
Hole_X2	Sbeam_Left			
Hole_X3	Sbeam_Left			
Hole_X4	Sbeam_Right			
Hole_X5	Sbeam_Right			
Hole_X6	Sbeam_Right			
Hole_X1	AngleP_Q1			
Hole_X2	AngleP_Q1			
Hole_X3	AngleP_Q1			
Hole_X4	AngleP_Q4			
Hole_X5	AngleP_Q4			
Hole_X6	AngleP_Q4			
Hole_X1	AngleP_Q2			
Hole_X2	AngleP_Q2			
Hole_X3	AngleP_Q2			
Hole_X4	AngleP_Q3			
Hole_X5	AngleP_Q3			
Hole_X6	AngleP_Q3			
SBolt_X1	AngleP_Q1			
SBolt_X2	AngleP_Q1			
SBolt_X3	AngleP_Q1			
SBolt_X4	AngleP_Q4			
SBolt_X5	AngleP_Q4			
SBolt_X6	AngleP_Q4			
SBolt_X1	AngleP_Q2			
SBolt_X2	AngleP_Q2			
SBolt_X3	AngleP_Q2			
SBolt_X4	AngleP_Q3			
SBolt_X5	AngleP_Q3			
SBolt_X6	AngleP_Q3			
SBolt_X1	Sbeam_Left			
SBolt_X2	Sbeam_Left			
SBolt_X3	Sbeam_Left			
SBolt_X4	Sbeam_Right			
SBolt_X5	Sbeam_Right			
SBolt_X6	Sbeam_Right			

SURFACE		F	E	P08
Hole_Y1	AngleP_Q2			
Hole_Y2	AngleP_Q1			
Hole_Y3	AngleP_Q2			
Hole_Y4	AngleP_Q1			
Hole_Y5	AngleP_Q2			
Hole_Y6	AngleP_Q1			
Hole_Y1	AngleP_Q3			
Hole_Y2	AngleP_Q4			
Hole_Y3	AngleP_Q3			
Hole_Y4	AngleP_Q4			
Hole_Y5	AngleP_Q3			
Hole_Y6	AngleP_Q4			
Hole_Y1	AWP_Left			
Hole_Y2	AWP_Left			
Hole_Y3	AWP_Left			
Hole_Y4	AWP_Left			
Hole_Y5	AWP_Left			
Hole_Y6	AWP_Left			
Hole_Y1	AWP_Right			
Hole_Y2	AWP_Right			
Hole_Y3	AWP_Right			
Hole_Y4	AWP_Right			
Hole_Y5	AWP_Right			
Hole_Y6	AWP_Right			
Hole_Y1	Col			
Hole_Y2	Col			
Hole_Y3	Col			
Hole_Y4	Col			
Hole_Y5	Col			
Hole_Y6	Col			
Load_L1	Seismic Load			
Load_L2	Seismic Load			
Load_L3	Seismic Load			
Load_L4	Seismic Load			
Load_L5	Seismic Load			
Load_L6	Seismic Load			
Load_L7	Seismic Load			
Load_L8	Seismic Load			
Load_L9	Seismic Load			
Load_L10	Seismic Load			
Load_L11	Seismic Load			
Load_L12	Seismic Load			
Load_X1	Seismic Load			
Load_X2	Seismic Load			
Load_X3	Seismic Load			
Load_X4	Seismic Load			
Load_X5	Seismic Load			
Load_X6	Seismic Load			
SbeamL_Top	Line Load			
SbeamR_Top	Line Load			

SURFACE		F	E	P08
SBolt_Y1	AngleP_Q2			
SBolt_Y2	AngleP_Q1			
SBolt_Y3	AngleP_Q2			
SBolt_Y4	AngleP_Q1			
SBolt_Y5	AngleP_Q2			
SBolt_Y6	AngleP_Q1			
SBolt_Y1	AngleP_Q3			
SBolt_Y2	AngleP_Q4			
SBolt_Y3	AngleP_Q3			
SBolt_Y4	AngleP_Q4			
SBolt_Y5	AngleP_Q3			
SBolt_Y6	AngleP_Q4			
SBolt_Y1	AWP_Left			
SBolt_Y2	AWP_Left			
SBolt_Y3	AWP_Left			
SBolt_Y4	AWP_Left			
SBolt_Y5	AWP_Left			
SBolt_Y6	AWP_Left			
SBolt_Y1	AWP_Right			
SBolt_Y2	AWP_Right			
SBolt_Y3	AWP_Right			
SBolt_Y4	AWP_Right			
SBolt_Y5	AWP_Right			
SBolt_Y6	AWP_Right			
SBolt_Y1	Col			
SBolt_Y2	Col			
SBolt_Y3	Col			
SBolt_Y4	Col			
SBolt_Y5	Col			
SBolt_Y6	Col			
Load_R1	Seismic Load			
Load_R2	Seismic Load			
Load_R3	Seismic Load			
Load_R4	Seismic Load			
Load_R5	Seismic Load			
Load_R6	Seismic Load			
Load_R7	Seismic Load			
Load_R8	Seismic Load			
Load_R9	Seismic Load			
Load_R10	Seismic Load			
Load_R11	Seismic Load			
Load_R12	Seismic Load			
Load_Y1	Seismic Load			
Load_Y2	Seismic Load			
Load_Y3	Seismic Load			
Load_Y4	Seismic Load			
Load_Y5	Seismic Load			
Load_Y6	Seismic Load			

11.2 APPENDIX B – Interactions introduced in ABAQUS (Master/Slave)

INTERACTIONS

MASTER	SLAVE	F	E	P08
AWP_Left	AngleP_Q1		■	■
AWP_Left	AngleP_Q2		■	■
AWP_Right	AngleP_Q3			■
AWP_Right	AngleP_Q4			■
AngleP_Q1	Col	■		
AngleP_Q2	Col	■		
AngleP_Q3	Col	■	■	
AngleP_Q4	Col	■	■	
Col	EP_Left			
Col	EP_Right			
AngleP_Q1	Sbeam_Left			
AngleP_Q2	Sbeam_Left			
AngleP_Q3	Sbeam_Right			
AngleP_Q4	Sbeam_Right			
Hole_L1-Col	Bolt_L1-Col			
Hole_L2-Col	Bolt_L2-Col			
Hole_L3-Col	Bolt_L3-Col			
Hole_L4-Col	Bolt_L4-Col			
Hole_L5-Col	Bolt_L5-Col			
Hole_L6-Col	Bolt_L6-Col			
Hole_L7-Col	Bolt_L7-Col			
Hole_L8-Col	Bolt_L8-Col			
Hole_L9-Col	Bolt_L9-Col		■	■
Hole_L10-Col	Bolt_L10-Col		■	■
Hole_L11-Col	Bolt_L11-Col		■	■
Hole_L12-Col	Bolt_L12-Col		■	■
Hole_R1-Col	Bolt_R1-Col			
Hole_R2-Col	Bolt_R2-Col			
Hole_R3-Col	Bolt_R3-Col			
Hole_R4-Col	Bolt_R4-Col			
Hole_R5-Col	Bolt_R5-Col			
Hole_R6-Col	Bolt_R6-Col			
Hole_R7-Col	Bolt_R7-Col			
Hole_R8-Col	Bolt_R8-Col			
Hole_R9-Col	Bolt_R9-Col		■	■
Hole_R10-Col	Bolt_R10-Col		■	■
Hole_R11-Col	Bolt_R11-Col		■	■
Hole_R12-Col	Bolt_R12-Col		■	■
Hole_L1-EP_Left	Bolt_L1-EP_Left			
Hole_L2-EP_Left	Bolt_L2-EP_Left			
Hole_L3-EP_Left	Bolt_L3-EP_Left			
Hole_L4-EP_Left	Bolt_L4-EP_Left			
Hole_L5-EP_Left	Bolt_L5-EP_Left			
Hole_L6-EP_Left	Bolt_L6-EP_Left			
Hole_L7-EP_Left	Bolt_L7-EP_Left			
Hole_L8-EP_Left	Bolt_L8-EP_Left			
Hole_L9-EP_Left	Bolt_L9-EP_Left		■	■
Hole_L10-EP_Left	Bolt_L10-EP_Left		■	■
Hole_L11-EP_Left	Bolt_L11-EP_Left		■	■
Hole_L12-EP_Left	Bolt_L12-EP_Left		■	■

MASTER	SLAVE	F	E	P08
Hole_R1-EP_Right	Bolt_R1-EP_Right			
Hole_R2-EP_Right	Bolt_R2-EP_Right			
Hole_R3-EP_Right	Bolt_R3-EP_Right			
Hole_R4-EP_Right	Bolt_R4-EP_Right			
Hole_R5-EP_Right	Bolt_R5-EP_Right			
Hole_R6-EP_Right	Bolt_R6-EP_Right			
Hole_R7-EP_Right	Bolt_R7-EP_Right			
Hole_R8-EP_Right	Bolt_R8-EP_Right			
Hole_R9-EP_Right	Bolt_R9-EP_Right		■	■
Hole_R10-EP_Right	Bolt_R10-EP_Right		■	■
Hole_R11-EP_Right	Bolt_R11-EP_Right		■	■
Hole_R12-EP_Right	Bolt_R12-EP_Right		■	■
Hole_X1-AngleP_Q1	SBolt_X1-AngleP_Q1			
Hole_X1-AngleP_Q2	SBolt_X1-AngleP_Q2			
Hole_X1-Sbeam_Left	SBolt_X1-Sbeam_Left			
Hole_X2-AngleP_Q1	SBolt_X2-AngleP_Q1			
Hole_X2-AngleP_Q2	SBolt_X2-AngleP_Q2			
Hole_X2-Sbeam_Left	SBolt_X2-Sbeam_Left			
Hole_X3-AngleP_Q1	SBolt_X3-AngleP_Q1			
Hole_X3-AngleP_Q2	SBolt_X3-AngleP_Q2			
Hole_X3-Sbeam_Left	SBolt_X3-Sbeam_Left			
Hole_X4-AngleP_Q3	SBolt_X4-AngleP_Q3			
Hole_X4-AngleP_Q4	SBolt_X4-AngleP_Q4			
Hole_X4-Sbeam_Right	SBolt_X4-Sbeam_Right			
Hole_X5-AngleP_Q3	SBolt_X5-AngleP_Q3			
Hole_X5-AngleP_Q4	SBolt_X5-AngleP_Q4			
Hole_X5-Sbeam_Right	SBolt_X5-Sbeam_Right			
Hole_X6-AngleP_Q3	SBolt_X6-AngleP_Q3			
Hole_X6-AngleP_Q4	SBolt_X6-AngleP_Q4			
Hole_X6-Sbeam_Right	SBolt_X6-Sbeam_Right			
Hole_Y1-AWP_Left	SBolt_Y1-AWP_Left		■	■
Hole_Y1-AWP_Right	SBolt_Y1-AWP_Right			■
Hole_Y1-AngleP_Q2	SBolt_Y1-AngleP_Q2			
Hole_Y1-AngleP_Q3	SBolt_Y1-AngleP_Q3			
Hole_Y1-Col	SBolt_Y1-Col			
Hole_Y2-AWP_Left	SBolt_Y2-AWP_Left		■	■
Hole_Y2-AWP_Right	SBolt_Y2-AWP_Right			■
Hole_Y2-AngleP_Q1	SBolt_Y2-AngleP_Q1			
Hole_Y2-AngleP_Q4	SBolt_Y2-AngleP_Q4			
Hole_Y2-Col	SBolt_Y2-Col			
Hole_Y3-AWP_Left	SBolt_Y3-AWP_Left		■	■
Hole_Y3-AWP_Right	SBolt_Y3-AWP_Right			■
Hole_Y3-AngleP_Q2	SBolt_Y3-AngleP_Q2			
Hole_Y3-AngleP_Q3	SBolt_Y3-AngleP_Q3			
Hole_Y3-Col	SBolt_Y3-Col			
Hole_Y4-AWP_Left	SBolt_Y4-AWP_Left		■	■
Hole_Y4-AWP_Right	SBolt_Y4-AWP_Right			■
Hole_Y4-AngleP_Q1	SBolt_Y4-AngleP_Q1			
Hole_Y4-AngleP_Q4	SBolt_Y4-AngleP_Q4			
Hole_Y4-Col	SBolt_Y4-Col			

MASTER	SLAVE	F	E	P08
Hole_Y5-AWP_Left	SBolt_Y5-AWP_Left			
Hole_Y5-AWP_Right	SBolt_Y5-AWP_Right			
Hole_Y5-AngleP_Q2	SBolt_Y5-AngleP_Q2			
Hole_Y5-AngleP_Q3	SBolt_Y5-AngleP_Q3			
Hole_Y5-Col	SBolt_Y5-Col			
Hole_Y6-AWP_Left	SBolt_Y6-AWP_Left			
Hole_Y6-AWP_Right	SBolt_Y6-AWP_Right			
Hole_Y6-AngleP_Q1	SBolt_Y6-AngleP_Q1			
Hole_Y6-AngleP_Q4	SBolt_Y6-AngleP_Q4			
Hole_Y6-Col	SBolt_Y6-Col			

11.3 APPENDIX C – Constraints and sets assigned in ABAQUS

CONSTRAINTS				
MASTER	SLAVE	F	E	P08
AWP_Left	CP_Q1			
Col	CP_Q1			
AWP_Left	CP_Q2			
Col	CP_Q2			
AWP_Right	CP_Q3			
Col	CP_Q3			
AWP_Right	CP_Q4			
Col	CP_Q4			
Col	AWP_Left			
Col	AWP_Right			
Rib_Q2	EP_Left			
Rib_Q3	EP_Left			
Rib_Q1	EP_Right			
Rib_Q4	EP_Right			
Pbeam_Left	EP_Left			
Rib_Q2	Pbeam_Left			
Rib_Q3	Pbeam_Left			
Pbeam_Right	EP_Right			
Rib_Q1	Pbeam_Right			
Rib_Q4	Pbeam_Right			

SETS			
	F	E	P08
AWP			
Angle			
Bolt			
CP			
Col			
EP			
Pbeam			
Rib_Top			
Sbolts			
Actuator_Left			
Actuator_Right			
Col-Bot			
Col-Up			
Sbeam_Left			
Sbeam_Right			
Tors-7			
Tors-8			
Tors-9			
Tors-10			
Tors-11			
Tors-12			
Tors-13			
Tors-14			
RP-1			
RP-2			
RP-3			
RP-4			
RP-5			
RP-6			
RP-7			
RP-8			
RP-9			
RP-10			
RP-11			
RP-12			
RP-13			
RP-14			